Propulsion through Wake Synchronization using a Flapping Foil

by

David Nelson Beal

B.S., Cornell University (1995)
S.M., Massachusetts Institute of Technology (1997)

Submitted to the Department of Mechanical Engineering
in partial fulfillment of the requirements for the degree of

Doctor of Philosophy

at the

MASSACHUSETTS INSTITUTE OF TECHNOLOGY

June 2003

Author .....
Department of Mechanical Engineering
May 23, 2003

Certified by .....
Michael S. Triantafyllou
Professor of Ocean Engineering
Thesis Supervisor

Certified by .....
Kamal Youcef-Toumi
Professor of Mechanical Engineering
Committee Chairperson

Accepted by .....
Ain Sonin
Chairman, Department Committee on Graduate Students

Propulsion through Wake Synchronization using a Flapping Foil

by

David Nelson Beal

Submitted to the Department of Mechanical Engineering
on May 23, 2003, in partial fulfillment of the
requirements for the degree of
Doctor of Philosophy

Abstract

The design issues associated with underwater vehicles operating in the surf zone or other high-energy environments are likely to have viable biomimetic solutions. The flapping fin is capable of producing high instantaneous forces, giving fish the ability to turn and accelerate rapidly, and fish are capable of sensing the flow characteristics in their environment using the lateral line, aiding obstacle entrainment, schooling, rheotaxis, and prey detection. A highly maneuverable vehicle that is capable of sensing the changing flows in its environment would have a considerably higher survival rate in dangerous currents. As an initial foray into the sensory and control methods that could be used by a biomimetic vehicle, we studied energy extraction through synchronization with an incoming Kármán wake for both fish and mechanical flapping foils.

Rainbow trout (*Oncorhynchus mykiss*) swimming within a flow channel voluntarily positioned themselves $4D$ downstream from a 2" D-section cylinder, and synchronized with the cylinder wake in both frequency and phase. The phase of the trout's lateral position relative to the wake, described through a Wake Function $W(x,t)$ defined as the lateral-sum of vorticity at a point downstream from the cylinder, was 100° for the head, 160° for the center-of-mass, and 240° for the tail, implying that the trout's mass was moving laterally with the flow in a low-power swimming mode, but that its head and tail had flow across them. A euthanized trout passively synchronized with the wake and accelerated forward towards the cylinder, through fluid-excited motion only, proving that trout benefit not only from drafting in the velocity deficit behind the cylinder, but also through interaction with the vortices in the wake.

The thrust and efficiency of a heaving and pitching foil depends on how the foil interacts with the wake of an upstream cylinder. A systematic set of tests varying foil motion within the wake revealed that thrust was considerably more sensitive to wake interaction then efficiency, with the coefficient of thrust varying by 0.4, and the efficiency by 0.1, depending on the phase between foil and cylinder heave motions. Thrust and power input was always highest when the foil leading-edge motion opposed the lateral velocities in the wake, likely due to an increase in the angle-of-attack across

the foil. When thrust production was high ($C_T \approx 1$), the foil was most efficient when it led the wake by 30° for the leading-edge and 120° for the trailing-edge, but when thrust was low ($C_T \approx 0.3$), efficiency was highest for interactions similar to that of the trout, leading the wake by 125° for the leading-edge and 215° for the trailing-edge. Since the trout's coefficient of thrust was also low, these results were in agreement despite the many differences between the fluid-mechanical systems.

I designed and tested an algorithm that could synchronize the foil with an unknown wake using simple sensors and calculations. Additionally, I studied the foil moving passively in the wake using force-feedback to model the foil supports as a spring-mass-damper. The foil produced 0.27 N of thrust at a negative mean power input of 90 mW (energy extraction), a feat impossible for a passive device within a uniform stream.

Thesis Supervisor: Michael S. Triantafyllou
Title: Professor of Ocean Engineering

Committee Chairperson: Kamal Youcef-Toumi
Title: Professor of Mechanical Engineering

Acknowledgments

I would like to start by thanking the members of my committee for their suggestions, comments, and investment in time. Dr. Franz Hover has given me a great deal of advice over the years, and Professor Michael Triantafyllou kept me focused on the big picture throughout, where my tendency was to get bogged down in the day-to-day details. Many thanks are well deserved by Professors Kamal Youcef-Toumi and Dick Yue.

I'd like to thank my family for creating such a supportive environment throughout my life. I certainly could not have done any of this without you behind me.

I'd like to thank all of my many colleagues at the Towing Tank over the years, including (now) Professor Alexandra Techet, Doug Read, Michael Sachinis, Mike Jakuba, Karl Magnus McLetchie, Craig Martin, Josh Davis, Andrin Landolt, Øyvind Haugsdal, Anna Michel, Øyvind Smogeli, Victor Polidoro, Stephen Licht, Pradya Prempraneerach, Jeff Stettler, and Jason Dahl for making work more fun and for putting up with me.

I'd like to thank Professor George Lauder for the generous use of his facilities and all of the help given with the biological side of things, which really helped to 'spark' this thesis. Additionally, I'd like to thank Jimmy Liao for making the work with the live fish some of the most interesting, and most fun, in my time here.

Finally, and most importantly, I'd like to thank my Carolyn for being the rock upon which I could stand throughout this long process. You have been most supportive and understanding, and we share in this milestone together.

This research was supported by MIT Sea Grant Program Grant NA86RG0074.

Contents

1 Introduction **17**

1.1 Overall Review 19

1.2 Background 20

1.3 Nomenclature 25

2 Rainbow Trout Entraining within Vortex Wakes **27**

2.1 Review of Literature 28

2.2 Trout Synchronizing with Cylinder Wakes 29

2.2.1 Experimental Setup 30

2.2.2 Results and Discussion 34

2.3 Flow Visualization of Wake Interaction 36

2.3.1 PIV Setup 36

2.3.2 Results and Discussion 41

2.3.3 Summary 46

2.4 Dead Fish within Wakes 47

2.4.1 Methods 48

2.4.2 Results and Discussion 48

2.4.3 Summary 53

3 Performance of a Flapping Foil within a Vortex Wake **55**

3.1 Review of Literature 55

3.2 Motion Trajectories 57

3.3 Apparatus 61

3.4 Foil Performance within Varying Wakes 65
3.4.1 Results 66
3.4.2 Discussion 68
3.5 Wake Interaction and Combined Wake Modes 69
3.5.1 Dye Visualization 70
3.5.2 Anemometry 72
3.6 Variation of Foil Motion Parameters 78
3.7 Comparison of Trout and Foil Motion 82
3.8 Summary 87

4 Active Wake Synchronization **89**
4.1 Wake Synchronization 89
4.1.1 Experimental Setup 90
4.1.2 The Synchronization Algorithm 92
4.1.3 Results 99
4.1.4 Robustness to Wake Variation 103
4.1.5 Discussion 104
4.2 Wake Centering 105
4.2.1 Methods 106
4.2.2 Results and Discussion 108
4.3 Summary 109

5 Passive Energy Recovery in Wakes **111**
5.1 Methods 112
5.2 Results and Discussion 116

6 Conclusions **123**
6.1 Summary of Main Results 123
6.2 Recommended Future Work 125

A Additional Foil Plots **129**
A.1 Foil Performance within Varying Wakes 129

A.2 Dye Visualization 131
A.3 Combined Wake 133
A.4 Varying Foil Parameters Within a Wake 136
A.5 Additional Passive Energy Recovery Runs 140

List of Figures

1-1 Foil Thrust Wake Diagram 21

1-2 Fish Thrust Wake Diagram 21

2-1 Trout Kinematics Setup 31

2-2 Body Waves with Time 32

2-3 Measuring Phase Speed and Frequency 33

2-4 Summary Diagram of Fish within Wakes 35

2-5 PIV Setup Diagram 38

2-6 Wake Function Diagram 40

2-7 Lateral Velocity Diagram 41

2-8 Trout within Vorticity Flood Plot 42

2-9 Trout within U-velocity Flood Plot 43

2-10 Phase Between Motion and Wake Function 44

2-11 Amplitudes of Lateral velocity and Flow Velocity 45

2-12 Phase between Lateral Velocity and Lateral Flow 46

2-13 Average and Minimum U-velocities Encountered 49

2-14 Dead Fish Towed within Wakes 50

2-15 Upstream Velocity of a Dead Trout 51

3-1 Stylized Diagram of Foil within the Cylinder Wake 58

3-2 Foil Opposing Lateral Flow 60

3-3 Foil Moving with Lateral Flow 60

3-4 Carriage Diagram 62

3-5 Relative Positions of Foil and Cylinder 63

3-6 Foil and Cylinder Photograph 64
3-7 Signals Diagram 65
3-8 Forces and Positions 67
3-9 Thrust and Efficiency: $St_c = .20$ 68
3-10 Picture Illustrating Interception 71
3-11 Picture Illustrating Slaloming 71
3-12 Picture Illustrating Inline Combined Wake 72
3-13 Cylinder Anemometer Rake Setup Diagram 74
3-14 Relation between ϕ and Interaction Phase 75
3-15 Interaction Phase for High and Low Performance 76
3-16 Combined Wake Anemometry Setup Diagram 77
3-17 Mean Velocity Profiles Within Combined Wake 78
3-18 Range of Velocity Profiles in Combined Wake 79
3-19 Combined Wakes - Interception and Slaloming 79
3-20 Varying Foil Parameters in Wake - $\psi = 90$, Thrust 81
3-21 Varying Foil Parameters in Wake - $\psi = 90$, Efficiency 82
3-22 Comparison of S(x,t) with W(x,t) 85
3-23 Trout Phase Relative to Foil 86

4-1 Synchronization Setup Diagram 91
4-2 Control Algorithm Diagram 93
4-3 Low-Pass Filter 94
4-4 Normalized Signal 96
4-5 SRF Closed-Loop Pole-Zero Map 98
4-6 Ermentrout Startup Transient 100
4-7 SRF Startup Transient 101
4-8 Synchronized Motion Thrust, Efficiency, and Phase 102
4-9 Output Frequencies and Phase Error 103
4-10 Ermentrout's Response to Sudden Frequency Switch 104
4-11 SRF Response to Sudden Frequency Switch 105

4-12 Instantaneous Frequencies Reacting to Sudden Switch in Input 106
4-13 Wake Centering Setup Diagram 107
4-14 Wake Centering Algorithm Diagram 108
4-15 Wake Centering Results 109
4-16 Wake Centering Signals 110

5-1 Force Feedback Setup 113
5-2 Calibration Linearity 115
5-3 Force Feedback Output Signals 117
5-4 Force Feedback Comparisons 119

A-1 Thrust and Efficiency: $St_c = .30$ 129
A-2 Thrust and Efficiency: $St_c = .33$ 130
A-3 Dye Visualization: $H_c = 0.75D$, $St_c = .30$, $\phi = 70°$ and $250°$ 131
A-4 Dye Visualization: $H_c = 0.75D$, $St_c = .33$, $\phi = 110°$ and $290°$ 132
A-5 Dye Visualization: $H_c = 0.75D$, $St_c = .30$ and $.33$, $\phi = 150°$ and $180°$ 132
A-6 Mean and Range of Velocity Profiles Within Combined Wake: $H_c = 0.75D$, $St_c = .30$ 133
A-7 Mean and Range of Velocity Profiles Within Combined Wake: $H_c = 0.75D$, $St_c = .33$ 133
A-8 Mean Centerline Velocity vs. C_T and η: $H_c = 0.50D$, $St_c = .20$ 134
A-9 Mean Centerline Velocity vs. C_T and η: $H_c = 0.75D$, $St_c = .30$ 134
A-10 Mean Centerline Velocity vs. C_T and η: $H_c = 0.75D$, $St_c = .33$ 135
A-11 Varying Foil Parameters in Wake - $\psi = 80$, Thrust 136
A-12 Varying Foil Parameters in Wake - $\psi = 80$, Power 137
A-13 Varying Foil Parameters in Wake - $\psi = 80$, Efficiency 137
A-14 Varying Foil Parameters in Wake - $\psi = 90$, Power 138
A-15 Varying Foil Parameters in Wake - $\psi = 100$, Thrust 138
A-16 Varying Foil Parameters in Wake - $\psi = 100$, Power 139
A-17 Varying Foil Parameters in Wake - $\psi = 100$, Efficiency 139
A-18 Force Feedback Output Signals: run1 140

A-19 Force Feedback Output Signals: run2 141
A-20 Force Feedback Output Signals: run3 142
A-21 Force Feedback Output Signals: run4 143

List of Tables

1.1 Chapter Summary 19

2.1 Fish Swimming behind Cylinder vs. Free-stream 35
2.2 Comparison between Dead and Live Trout 52

3.1 Baseline Drafting Data 69
3.2 Average Sensitivities to Foil Motion Parameters 80
3.3 Highest Performance with Thrust Production 83

5.1 Force-Feedback Parameters 115

Chapter 1

Introduction

Throughout history, humans have marveled at the relative ease with which fish and marine mammals can swim and maneuver. Fish combine awesome physical abilities with specialized sensors in order to swim in prohibitively dangerous environments — at least relative to humans or human-developed vehicles — such as leaping up waterfalls and swimming in surf, as well as to glean energy savings from structures in the flow. Capable of high maneuverability, pike can accelerate at $15g$ and have a turning radius of just a tenth of a body length [14]. Salmonids have been shown to position themselves within turbulent streams in order to maximize net energy gain [18], and dolphins have been observed to surf the bow wakes of ships in order to utilize the high-pressure zone for energy savings while swimming [19].

The littoral zone is a dangerous place for a vehicle to roam, requiring both high maneuverability and the ability to produce high instantaneous forces. The need for high maneuvering forces has led to a push to investigate biomimetic foil-based propulsion in many forms. Barrett built and tested an experimental robot mimicking the shape and motion of a bluefin tuna [8]. Anderson developed an autonomous, hydraulically-powered robotic fish [6]. Nekton has built several prototype foil-powered vehicles, utilizing a relatively high-frequency pitch motion to create a vectored thrust [33]. Colleagues at the MIT Towing Tank Laboratory are currently building and testing a 4-fin vehicle for high-energy output — in acceleration and maneuverability — with each fin moving in roll and pitch [41].

Flapping foils have been studied extensively within uniform incoming flows [43]. However, in the surf zone the vehicle is likely to encounter powerful and quickly-changing cross-flows and turbulence. Optimally, the vehicle control systems would be capable of detecting and adjusting to environmental conditions in order to prevent collision or catastrophic damage. Again, biology yields inspiration: aside from standard human-like senses such as vision and hearing, fish have a lateral line consisting of millions of hair-like sensors (neuromasts) located within channels just beneath the skin, which are used by fish for schooling [40], prey detection [12], rheotaxis [34, 36], and obstacle entrainment [49].

Considerable gains in thrust and efficiency can be achieved when an unsteady, two-dimensional hydrofoil is controlled in such a manner as to manipulate existing vorticity, such as that shed from an upstream cylinder [23, 47]. If the flow signals from a man-made 'lateral line' are used to estimate the external vorticity field, then it would be likely that a flapping foil mechanism could manipulate that vorticity with its fins in a similar fashion, with a corresponding increase in performance.

A flapping foil was studied within the wake of an upstream D-section cylinder, and the relationship between performance and wake interaction was identified. Similarly, rainbow trout were observed to swim within a cylinder wake, consistently synchronizing their frequency and phase to that of the wake. These simple, controlled scenarios can be seen as a subset of the study of foil propellors within unsteady flows in general, taking the first steps towards developing the strategies to be used by a vehicle that is not only maneuverable, but is also capable of using information about the local flow conditions in order to use that agility in an optimal fashion. Combining fish-like locomotion with sensors like the lateral line will enable manufacturers to build AUV's that are efficient as well as maneuverable and reactive enough to survive in dangerous currents or surf. These studies may also be applicable to energy generation and fish schooling energetics work.

1.1 Overall Review

The basic overall goal of the thesis is to map the mechanism of interaction between an actively controlled body or fin with an incoming vortex wake, using both live fish and mechanical hydrofoils. This study of foils within cylinder wakes breaks down into three basic regimes in a range from high to low thrust production. At one extreme, the foil is required to produce high thrust (C_T on the order of 1), perhaps as a propellor for a large or bluff vehicle. In the center of the range, the foil needs to produce only low thrust (C_T on the order of 0.2), but do so with low power output, such as that needed to propel a streamlined body like a fish. At the opposite extreme, the foil is only required to overcome its own drag, while extracting as much power from the oscillating flow in the wake as possible. A low-power sensor in a stream would be an example application for an oscillating wake energy-extractor such as this. Table 1.1 summarizes the appearance of these cases in the chapters which follow.

High Thrust	Mechanical hydrofoil	Chapter 3
Low Thrust, Low Power	Mechanical hydrofoil Rainbow trout	Chapter 3 Chapter 2
Near-zero Thrust, Power Generation	Mechanical hydrofoil Euthanized trout	Chapter 5 Section 2.4

Table 1.1: Chapter Summary

Chapter 2 describes the study of how live fish will voluntarily synchronize with a cylinder wake in both frequency and phase, using Particle Image Velocimetry to quantify the vorticity field around a rainbow trout swimming freely in a Kármán wake. Additionally, through tests showing passive upstream 'swimming' with a euthanized trout, where the oscillating flow in the wake is the only possible source of energy for the trout, fish were shown to benefit not just from drafting in the velocity deficit but also from synchronizing with the alternating vorticity in a cylinder wake.

Chapter 3 describes tests performed using a biomimetic, two-dimensional flapping foil apparatus within the wake of a heaving cylinder. The correlation between the foil's thrust and efficiency and its interaction with the cylinder wake was quantified.

Since the frequency and phase of an incoming vortex wake will not generally be known, Chapter 4 describes a system designed to synchronize the mechanical foil with the incoming wake using simple sensors.

Chapter 5 will show that it is possible to passively recover energy as well as produce thrust within a cylinder wake, using force-feedback to model the mechanical foil support as a passive spring-mass-damper.

The appendices show results for several test cases not shown in the relevant chapters for reasons of brevity and redundancy.

1.2 Background

Gray [24] did ground-breaking research regarding the capabilities of fish swimming and performance. He described the motion of a variety of fishes and began exploring the method of fish propulsion. Lighthill [32] did considerable theoretical work regarding the swimming of fish, proposing a parametric description of fish body motion and performance.

Koochesfahani [27] and Freymuth [21] described the vortex wake behind unsteady foils, which were found to produce thrust through the creation of an alternating street of vortices, of a reverse-sign from those seen in the Kármán wake of a cylinder. The vortices shed by the foil are oriented to create a jet of fluid within the wake, directed away from the foil, resulting in the production of thrust, as seen in Figure 1-1. In fish, this wake would take the form of vortex rings [15], as shown in Figure 1-2.

Triantafyllou *et al* identified the Strouhal number, based on tail-beat frequency, wake width, and flow velocity, as a primary determinant of swimming efficiency, finding that most fish swim with a Strouhal number between 0.25 and 0.35, a range which has been associated with wake stability [50, 51].

Anderson [5], Lauder [29], and Muller *et al* [35] more recently used quantitative flow visualization in the proximity of swimming fish in order to describe the means of propulsion. Anderson found that the body-bound vorticity created by the undulation of the body passes down the body and interacts with the tail.

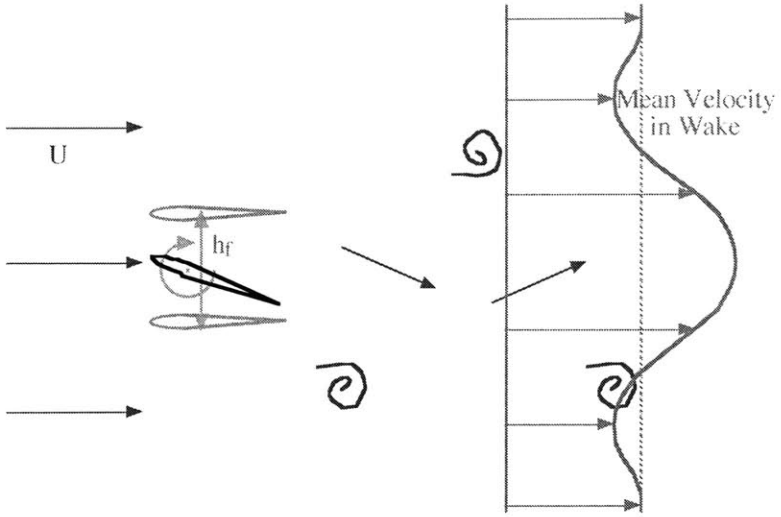

Figure 1-1: A thrust jet is formed behind a two-dimensional flapping foil through the creation of an alternating wake of vortices

Triantafyllou *et al* [50], Streitlien *et al* [47], and Read *et al* [43] explored the flapping foil as a method for underwater propulsion. Read explored a range of foil motions, varying the Strouhal number, maximum angle-of-attack, and heave amplitude, and found that flapping foils are capable of efficiencies greater than 70% and thrust coefficients of 2.4 in steady motion, albeit within different motion regimes. Additionally, experiments performed in order to quantify the foil's potential for maneuvering forces and thrust vectoring exhibited mean lift coefficients of 4.

Koochesfahani and Dimotakis [28], Streitlien *et al* [47], Gopalkrishnan *et al* [23],

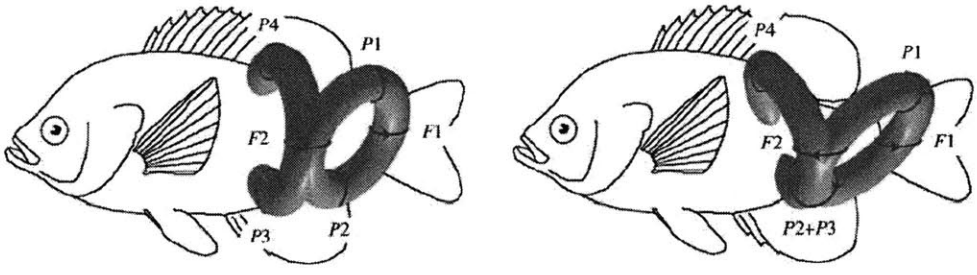

Figure 1-2: A thrust jet is formed behind a fish through the creation of an alternating wake of vortex rings (from [15])

Anderson *et al* [7], and So *et al* [45] explored foil/vortex interaction and the effect of oncoming vorticity on the foil performance. Koochesfahani found, through dye injected into the flow, that the vortex wake produced by a pitching foil can be exactly cancelled by a downstream foil pitching at the proper phase.

When a flapping foil actuator operates within the Kármán wake of a cylinder, the performance has been seen to vary considerably depending on the mode of interaction with the incoming wake. Streitlien [47] numerically evaluated two-dimensional potential flow for a Joukowski foil within a vortex field, and found that, generally, when the foil moved such that it closely encountered the oncoming vortices it would have significantly higher thrust and efficiency then when the foil avoided the oncoming vortices.

Using a foil and cylinder heaving in tandem within a uniform stream, with the interaction between the foil and cylinder wake controlled by the separation distance between the foil and cylinder, Gopalkrishnan found that efficiency can vary by 0.20 through the combination of effects from interaction and the distance of the foil from the cylinder [23].

Anderson identified the heaving D-section cylinder as an excellent vortex generator, identifying the regimes in which it would produce a strong 2-S wake and noting that the shedding was relatively robust to the presence of objects placed downstream, such as a foil [5].

For foil-propelled vehicles in general, the dragonfly can be used as an interesting source of inspiration, for the dragonfly has a relatively simple wing-beat motion — compared with other insect species [11] — utilizing two pairs of wings to produce a wide variety of forces, including those needed for gliding, high speed flying, fast maneuvering, and hovering, while remaining in a similar Reynolds number regime ($> 10^4$). Dragonflies have been observed accelerate at 9g and turn 180° within 3 wing-beats [2, 3], with an estimated aerodynamic efficiency of 54% for steady flight [53].

A situation similar to foil/cylinder wake interaction is the interaction between the aft wing of the dragonfly with the wake of the fore-wing. During steady flight, the aft

wing is seen to lead the fore-wing motion by 90° [46]. However, while accelerating or turning the wings are seen to beat in-phase [2], implying that the optimum interaction for the production of large maneuvering forces may be different than that for efficient flying.

Wu led the investigation into heaving and pitching foils within a wavy stream [57, 58], focusing, as a test case, on foils near a wavy surface. Pointing out that it was simple to see, if one is at a vantage moving with a uniform stream, that "flow energy resulting from any unsteady body motion must be at the expense of the body or its power supply" [57], he realized that this was no longer true if the incoming stream had a wavy component. Theoretically modeling a foil moving in heave and pitch synchronously near a wavy surface, he identified three important regimes. In some test cases, the wavy stream increased the efficiency of the foil by a combination of increasing thrust and/or decreasing power input. In other cases, the foil was producing thrust with an efficiency greater than 100%, implying that it was recovering energy from the flow, while still requiring a power input to maintain motion. In yet other cases, he found that the foil was capable of producing thrust and extracting energy in a fluid-excited motion, meaning that no power input from the foil was required.

Although his test cases involved a foil near surface waves, he realized that his results were not limited, as follows

> Although the simple water wave is chosen as a concrete example, it makes little difference to the subsequent discussion if other kinds of wavy streams are considered as long as the transverse velocity of the basic flow can be represented by ... $V_o(x,t) = iA_o e^{i(\omega_o t - kx)}$ [57].

In order to make his theoretical equations tenable, however, he was required to assume that there was no separation from the leading edge of the foil, that the lateral flow velocities were much less than the forward velocities, and that the wavelength of the surface waves were long relative to the foil chord, none of which apply to any of the experimental cases which follow in this work.

Isshiki experimentally verified Wu's earlier work, showing that a foil, passively attached with springs for heave and pitch motion, can produce thrust during fluid-induced motions from surface waves [26].

The flukes of a whale have the proper orientation to take advantage of surface waves. It has been estimated that, if the tail-foil is moving synchronously with the wavy stream, and if the body-length of the whale is not much smaller than the wavelength of the surface waves, a whale could "absorb up to 25% of its required propulsive power in head seas and 33% of propulsive power in following seas" [10]. Anecdotal stories from whalers tell of dead whales coasting at approximately 1 knot indefinitely, implying that fluid-excited motion and thrust production can occur for a dead whale in surface waves.

1.3 Nomenclature

$\alpha(t)$	Angle-of-attack to uniform incoming flow
α_{max}	Maximum angle-of-attack
c	Foil chord length
D	Cylinder diameter
$h_c(t)$	Cylinder heave position
H_c	Cylinder heave amplitude
$h_f(t)$	Foil heave position
H_f	Foil heave amplitude
λ_f	Wavelength of foil or fish motion
λ_w	Wavelength of incoming wake
L_f	Fish body-length
ϕ	Phase between foil and cylinder heave motions
ψ	Phase between foil heave and pitch motions
s	Foil span
$S(x,t)$	Wake signal defined in Section 3.5
St_c	Strouhal number of cylinder defined using $2H_c$
St_f	Strouhal number of foil defined using $2H_f$
$\theta(t)$	Pitch position
θ_o	Pitch amplitude
U	Velocity of incoming uniform flow
U_c	Velocity taking into account constriction
ω	Motion frequency in radians per second
W	Width of flow channel
$W(x,t)$	Wake function defined in Section 2.3
x	Cartesian coordinate in the upstream-downstream direction
y	Cartesian coordinate transverse to both the uniform flow and the cylinder axis
z	Cartesian coordinate in the direction of the cylinder axis

Chapter 2

Rainbow Trout Entraining within Vortex Wakes

While it is clear that stream-dwelling fish, like the rainbow trout studied here, would be expected to take advantage of the velocity deficit behind a cylinder, it is desired to investigate whether they also benefit from the vortices and oscillating lateral flows in the wake through the creation of beneficial angles-of-attack across the trout's body and tail. If the trout do not synchronize their tail-beat frequency to the shedding frequency of the wake then there is little chance that they utilize the vorticity in any special way, other than for the lower downstream velocities present in a cylinder wake. As such, the initial experiments compared the kinematics of the trout swimming in the presence of cylinders relative to the same fish swimming in a uniform incoming flow, and showed that the trout voluntarily synchronize to the vortex wake in frequency. Subsequent tests using particle image velocimetry (PIV) quantitatively illustrated the interaction between the trout and the incoming Kármán wake, showing that the trout synchronize with the wake in phase as well as frequency. Additionally, these tests show how the interaction with the wake varies along the trout's body and tail.

Synchronization with the wake in frequency and phase does not necessarily mean that the fish are capable of taking advantage of those oscillating flows, as the fish could still just be drafting in the velocity deficit with motion forced upon them by the strong lateral flows in the wake. In order to prove that the fish were entraining

not just to take advantage of the wake's velocity deficit, but to gain further energy benefit from the unsteady flows and large-scale vorticity, a euthanized fish was shown to be able to passively swim within the wake, against its own drag, using only the oscillating flows in the wake as energy input.

Note that all experiments in this chapter were performed in conjunction with J. Liao and G. Lauder of Harvard University, who generously provided laboratory space, fish, and live animal care, and responded most warmly when the author approached them regarding this research. The author wrote most of the MATLAB analysis software and shared equally in the experimental setup, testing, and analysis tasks.

2.1 Review of Literature

Fish are capable of surviving and thriving within high-energy environments, such as rivers, streams, or surf. It should be expected that an animal which has evolved to live in such an environment would be capable of finding and utilizing any possible method to reduce its energy expenditure, including entraining behind obstacles and locating semi-permanent eddies or roughness near the banks or bottom. Indeed, salmon and trout have been found to position themselves within streams in order to optimize their net energy gain [18], a function of local currents and the availability of food. The lateral line enables fish to choose an optimal hydrodynamic location in the flow, through the detection of "flow or pressure discontinuities" [49].

Fish propel themselves using a wide variety of methods, from the pectoral fins of bluegill sunfish to the caudal fins of tuna [52]. An oscillating fin produces thrust through the formation of a staggered array of vortex rings, where the mean flow within the ring forms a jet away from the fin [15].

Thunniform swimmers, such as tuna, create the majority of thrust with their caudal fins. As the body undulates with a wave passing from the head to tail, body-bound vortices are formed and pass down the body with the wave. The tail, rather than cutting through a uniform incoming flow, interacts with this body-bound vorticity

[5]. Additionally, the tail has been found to interact with vortices shed by the anal and dorsal fins in a beneficial way [56, 16].

In addition to interaction with self-induced vorticity, there are many cases in which fin-based swimmers can benefit from interacting with environmental vorticity. For instance, it has been hypothesized that schooling can serve a hydrodynamic benefit, with fish in the second rank, swimming between the thrust wakes created by those in the first rank, seeing a 40-50% reduction in incoming velocity [20]. Dolphins have been observed to surf in the bow wakes of ships [19], and whales can see significant thrust benefits from swimming near surface waves, due to the oscillating flow over the tail fluke [10].

Webb studied how river chub and smallmouth bass align themselves with obstacles in a flow channel. Using cylinders mounted both vertically and horizontally, he found that the fish tended to hold position with their nose or head up against the obstacle, without showing any synchronization with the cylinder wake [55].

The following describes a set of experiments performed with rainbow trout (*Oncorhynchus mykiss*) within a flow channel containing a vertically-mounted cylinder. The experiments differ from previous work, other than the species of fish, in that the ratio in sizes between the cylinder and the fish are considerably larger than those studied by Webb.

Being a lotic (stream-dwelling) fish, it is expected that rainbow trout should be well-evolved to take advantage of the obstacles presented to it in an optimal way. The following studies how rainbow trout located themselves, voluntarily, at a relatively constant distance downstream from the cylinder, and synchronized with the cylinder wake for energy benefit.

2.2 Trout Synchronizing with Cylinder Wakes

As a motivation for further study of foils within vortex wakes, we first desired to see whether a lotic fish was capable of taking advantage of the vorticity within a cylinder wake, rather than simply drafting within the cylinder's velocity deficit. The

first and easiest test of this was to show that fish will synchronize with the incoming vorticity; although synchronization does not necessarily imply benefit, if they do not show such behavior then there is little likelihood that they use the vorticity in any special manner and little point in studying them further.

2.2.1 Experimental Setup

We performed a set of experiments studying the strategies and motions of rainbow trout, a fish well adapted to turbulent stream environments, swimming in the presence of a vertically-mounted D-section cylinder in a water channel located in the Lauder Laboratory at Harvard University. The experimental setup and results are discussed in detail in [31], and are summarized here with a different emphasis.

A batch of rainbow trout were purchased from a hatchery, and kept in a temperature-controlled recirculating tank. Since we desired to use fish of similar size for all the tests, fish were chosen whose length was close to 10 cm. In all, eight fish were used, averaging 10.3 ± 0.3 cm in length, and 10.0 ± 0.5 g in mass, where ranges given are standard error. One fish was run through all of the tests, and then euthanized with MS-222 and stored in a freezer for posterity, before testing began with the next fish.

The flow channel's test section was 80 cm long with a 28x28 cm cross-section. A variable-speed pump was used to set the flow velocity in the channel, and the pump speeds were calibrated to flow speed using PIV. A baffle of flow-straighteners was placed at the upstream end of the test section in order to reduce the turbulence of the incoming flow. An additional screen was placed at the downstream end of the test section, to prevent any fish from introducing themselves to the pump rotor.

A high-speed digital video camera (the RedLake Motionscope PCI-500) was set up to record the silhouette of the fish within the flow channel at 250 frames per second, with a backlit ventral view, as seen in Figure 2-1. Luckily, the fish were found to maintain a fairly constant position within the cylinder wakes, meaning that once set up, the camera and mirror were not moved for the duration of the experiments.

The cylinders were clamped into place, with the lower end of the cylinder abutting the bottom of the flow channel. PVC round cylinders were machined to form a D-

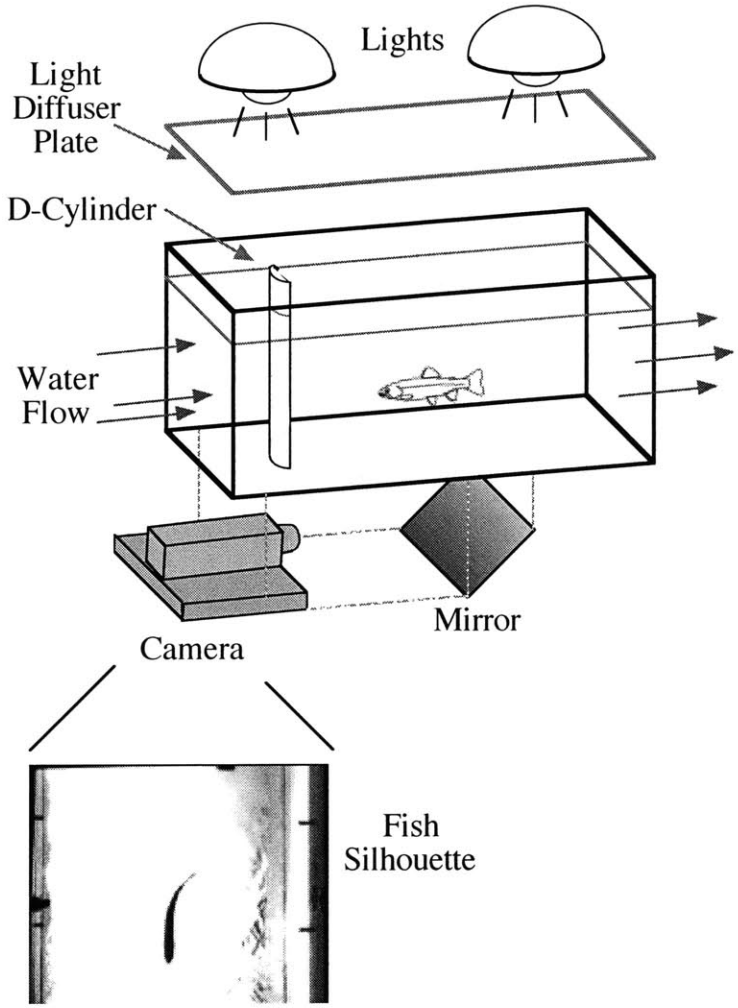

Figure 2-1: The silhouette of the swimming trout was recorded with a high-speed video camera

shaped cross-section, which was found by Anderson to produce a robust 2-S wake despite the presence of other objects in the flow nearby [5].

The video was passed through a digitizing program, written by E. Tytell, which returns the outlines and mid-lines of the fish at each time step, with a discrete number of body-points along the mid-line (30, in this case). This information was then analyzed to give the tail-beat frequency, amplitude, and wavelength, as follows. The analysis software followed the lateral position of each body-point with time. The times of maxima and minima in the lateral motion were recorded for each body-point. The amplitude at each body-point was then calculated using the average of the absolute

value of those extreme positions around the mean, while the frequency was calculated by averaging the measured period between extrema for each body point. Similarly, the phase-speed of the body wave was calculated by following the motion of the extrema down the body, as shown in Figures 2-2 and 2-3, and the wavelength was calculated by simply multiplying the average phase-speed by the average period, as described in [52]. Since amplitudes of lateral motion were very small over the front half of the body for free-stream swimming, only extrema from the back half of the body were used for these calculations.

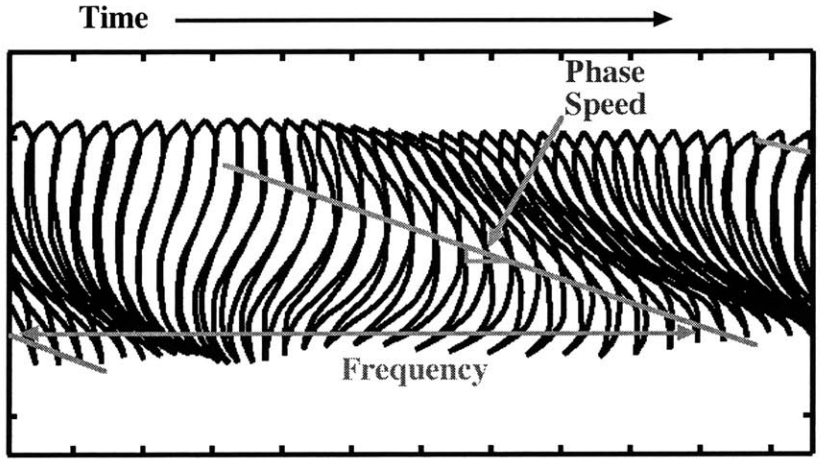

Figure 2-2: The body waves were followed in order to measure phase speed and frequency

The frequency and wavelength of the trout tail-beats were then compared to what was expected for the cylinder wake. However, the constriction effects from the cylinders in the flow channel were non-negligible, at 9% and 18% for the 1" and 2" cylinders, respectively. Hence, the expected shedding frequency was adjusted using

$$U_c = U \cdot \left(\frac{W}{W - D}\right) \tag{2.1}$$

$$St_c = \frac{f_c \cdot D}{U_c} \tag{2.2}$$

where W is the width of the flow channel, D is the cylinder diameter, U_c is the constricted velocity, St_c is the cylinder Strouhal number (0.2 for this Reynolds number

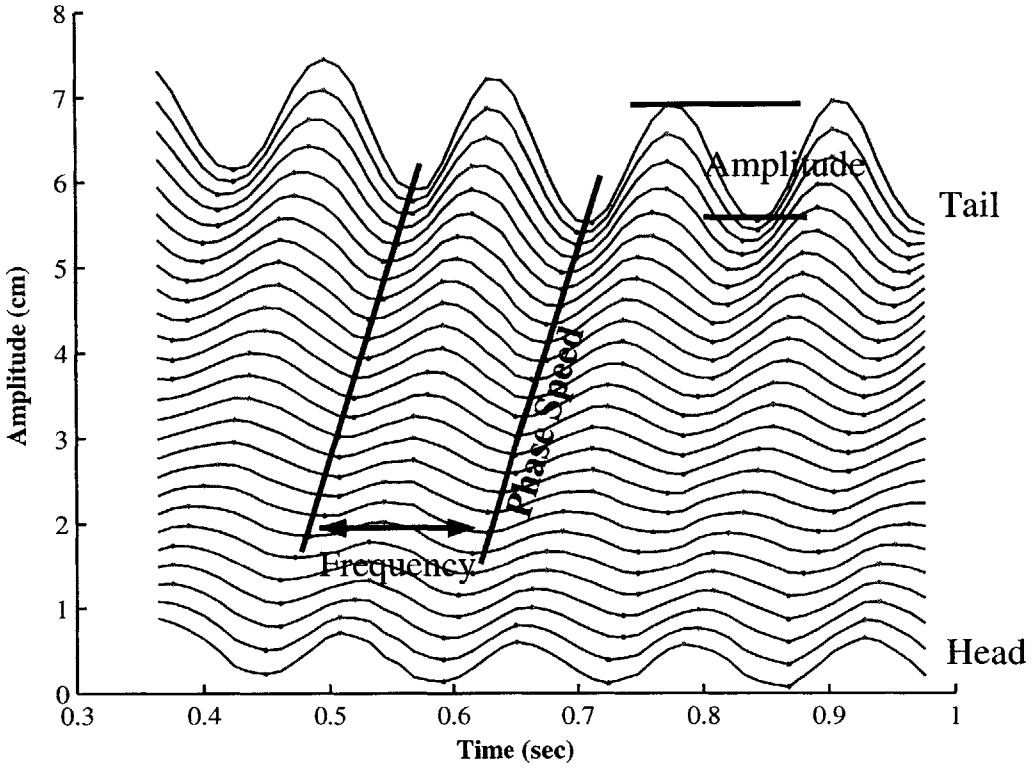

Figure 2-3: The extrema of the body waves, shown from the head (at bottom) to the tail (at top), were used to measure frequency, phase-speed, amplitude, and wavelength. The curves are artificially separated on the y-axis for clarity.

range [9]), and f_c is the shedding frequency.

The wake wavelength was then estimated as $\lambda_w = U/f_c$ because although the cylinder shedding would be determined by the constricted flow, the vortices would then be carried downstream by the unconstricted flow. Using PIV, these estimates were found to be reasonable.

As the control case, fish swam within the flow channel at 4.5 L_f/sec without a cylinder present. Tests were then performed at 4.5 L_f/sec with 1" and 2" cylinders, corresponding to Reynolds numbers (based on diameter) of approximately 12,500 and 25,000, respectively. Additionally, tests were performed using the 1" cylinder at 2.5 L_f/sec, giving the same wake wavelength as the 1" case at higher speed, but also the same frequency as the 2" cylinder at higher speed, after taking into account the constriction effects. This way, it would be possible to see if the fish preferentially

matched frequency and/or wavelength to that of the wake.

Experiments were performed with 8 different trout, and 4 clean tail-beats from each treatment were analyzed for each fish. Every 3 frames of the video was digitized, giving a sample frequency of 83.3 Hz.

The fish were allowed to position themselves voluntarily within the test section of the flow channel. They were given more than 10 minutes to acclimate themselves to the their new surroundings and recover from the stress of being moved from the holding tank before the recirculating pump was turned on. Additionally, the fish were allowed time to 'discover' the cylinder wake, which usually took a minute or two at full speed, and never took more than approximately 5 minutes.

2.2.2 Results and Discussion

These results are also presented in [31], and are shown here with a different emphasis: the 2" cylinder case compared to swimming in a uniform stream. All ranges given are in standard error.

The trout adapted to the presence of the cylinder quickly. Once the flow was turned up to full speed, and the trout could no longer easily swim in the free-stream, they quickly entrained behind the cylinder, usually near the downstream baffles, and then slowly moved upstream until they found a spot approximately 4.0 ± 0.1 D downstream from the cylinder. Once they found the chosen position, they would rarely leave it, only then in the pursuit of a particle of food, and would always return. This implies, although it does not prove, that the fish are positioning themselves in a hydrodynamic 'sweet spot' where conditions are optimal. In addition, some fish also rested in the bow-wake of the cylinder, as discussed in [31] further.

Once entrained behind the cylinder, the fish exhibited large-amplitude whole-body lateral oscillations of 0.32 ± 0.01 D (peak-to-peak), with a frequency within 1% of the cylinder shedding frequency. These oscillations were interspersed with small corrective motions with the tail and pectoral fins. Clearly, the fish were doing something different from the free-stream case, as illustrated in Figure 2-4.

Table 2.2.2 shows the difference in amplitudes between entraining and free-stream

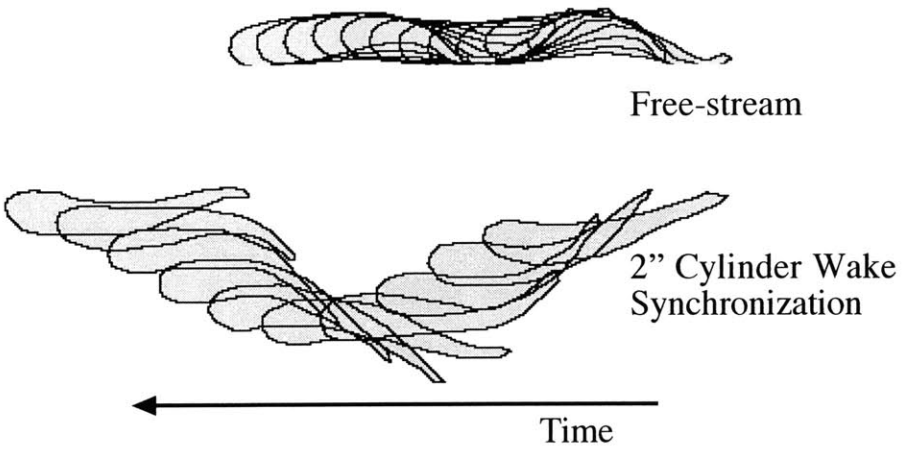

Figure 2-4: Outlines of fish within the free-stream (top) and behind the cylinder (bottom). Steps forward are with time, both for clarity of the diagram and to illustrate the difference in frequency between the two cases.

swimming. Not only is the lateral amplitude for the front half of the body very different between the two cases, but the tail-beat amplitude increases by a factor of 3 over the free-stream case. The frequency not only matches the shedding frequency, but also differs from that of the free-stream by a factor of 3. Although the mean flow speed seen by the fish within the wake is considerably less than that in the free-stream, the frequency of tail-beat changes linearly with velocity [54], which still would not explain a factor of 3 difference between the cases.

	Behind Cylinder	Cylinder Wake	In Free-stream
Head Amplitude (L_f)	0.160 ± 0.008	N/A	0.020 ± 0.001
C.O.M. Amplitude (L_f)	0.153 ± 0.007	N/A	0.018 ± 0.001
Mid-body Amplitude (L_f)	0.165 ± 0.006	N/A	0.024 ± 0.001
Tail Amplitude (L_f)	0.322 ± 0.009	N/A	0.107 ± 0.003
Frequency (Hz)	2.18 ± 0.05	2.22 ± 0.01	6.62 ± 0.11
Wavelength (L_f)	4.05 ± 0.22	2.03 ± 0.01	1.15 ± 0.02

Table 2.1: A comparison between free-swimming and entrained trout, also showing the synchronization between the trout and the expected frequency and wavelength of the wake. The amplitudes of the body points are relative to the mid-line.

The wavelength of the entraining trout was 1.99 times that of the expected values

for the wake, and 3.5 times that of the free-stream case. So although the trout apparently synchronizes in frequency, it does not do so in wavelength. This implies that the trout is interacting with the wake differently with its head than with its tail.

2.3 Flow Visualization of Wake Interaction

Rainbow trout have been found to voluntarily synchronize with the wake of an upstream cylinder. The silhouette of the fish, however, can give only so much information, such as the tail-beat frequency and shape of the body-wave, only leaving as an estimate the characteristics of the flow, and ignoring altogether the phasing of the synchronization between the trout's motion and the oscillating wake.

In order to quantify the interaction strategy of the trout within the wake, we used Digital Particle Image Velocimetry (DPIV) to illustrate the flow around the fish. This would give an accurate and complete assessment of the interaction between the trout and its environment, as well as to proof the estimated wake characteristics used in Section 2.2, above. In addition, if a trout were using the incoming vorticity, as well as drafting within the velocity deficit, it is necessary that it would be synchronizing not just in frequency but in phase as well. So again, although showing synchronicity in phase does not prove that the fish can utilize the vortices in the cylinder wake for energy benefit, if the fish does not synchronize in phase it is unlikely that it can.

2.3.1 PIV Setup

In order to ensure a strong and regular wake, an apparatus was used to sway the 2" diameter D-section cylinder laterally in the flow channel. A Pitmann GM9236S013 5.9:1 geared servo-motor was attached to a Scotch-yoke apparatus, as in [23]. The 500 cpr encoder was read using a Simpson S664 digital counter, enabling an open-loop control of the sway frequency, which was recorded for each test, although the actual shedding value would be later calculated using PIV. For all tests, the cylinder was set to heave at 0.33 D peak-to-peak amplitude and the frequency was set just above the cylinder's natural shedding frequency, so that the wake was seen to be regular and

strong.

The flow channel — the same as in Section 2.2, above — was seeded with 12 μm silver-coated glass spheres. An 8 W argon-ion Coherent laser was used to create a thin horizontal light sheet 15 cm wide across the flow tank, as seen in Figure 2-5. The light sheet was set up at the approximate distance downstream from the cylinder that the fish were seen to position themselves in the previous experiments, 9 cm above the bottom of the channel.

We desired to record both the kinematics of the fish and the flow characteristics around it, simultaneously. Optimally, the flow view would be in the same plane as the centerline of the fish, in the dorsal-to-ventral sense. However, not only were the trout averse to swimming in the light sheet, with a powerful laser in the eye, but having the fish within the particle view makes the PIV considerably more difficult, with shadows from the fish blocking much of the flow, as well as the need to mask the trout from the PIV analysis software. Since the fish appeared to prefer to swim just beneath the light sheet (probably due to a psychological preference for bright light from above, rather than below), we decided to film the flow using a dorsal camera, and, simultaneously, film the fish silhouette (against the light sheet) using a ventral camera, as shown in Figure 2-5. This gave a clean, unbroken view of the flow — which was then analyzed for the entire field around the fish — as well as a clear view of the fish outlines.

Whatever information was lost due to illuminating a plane just above, rather than through, the fish was more than compensated for by the fact that the data taken was considerably cleaner, and consists of the full plane. For instance, the trout used were nearly the length of the light sheet and when they were within the sheet, they would block more than half of the view of the flow. Indeed, when at the laser-side extreme of their lateral motion, the fish blocked the view of most of the particles, which would make analysis difficult and more prone to error.

In a sense, the plane measured is that of the unadulterated flow seen by the fish, without any effect of the fish upon it. The vorticity created by the fish is expected to be considerably smaller in strength and size from the wake vorticity anyway. In

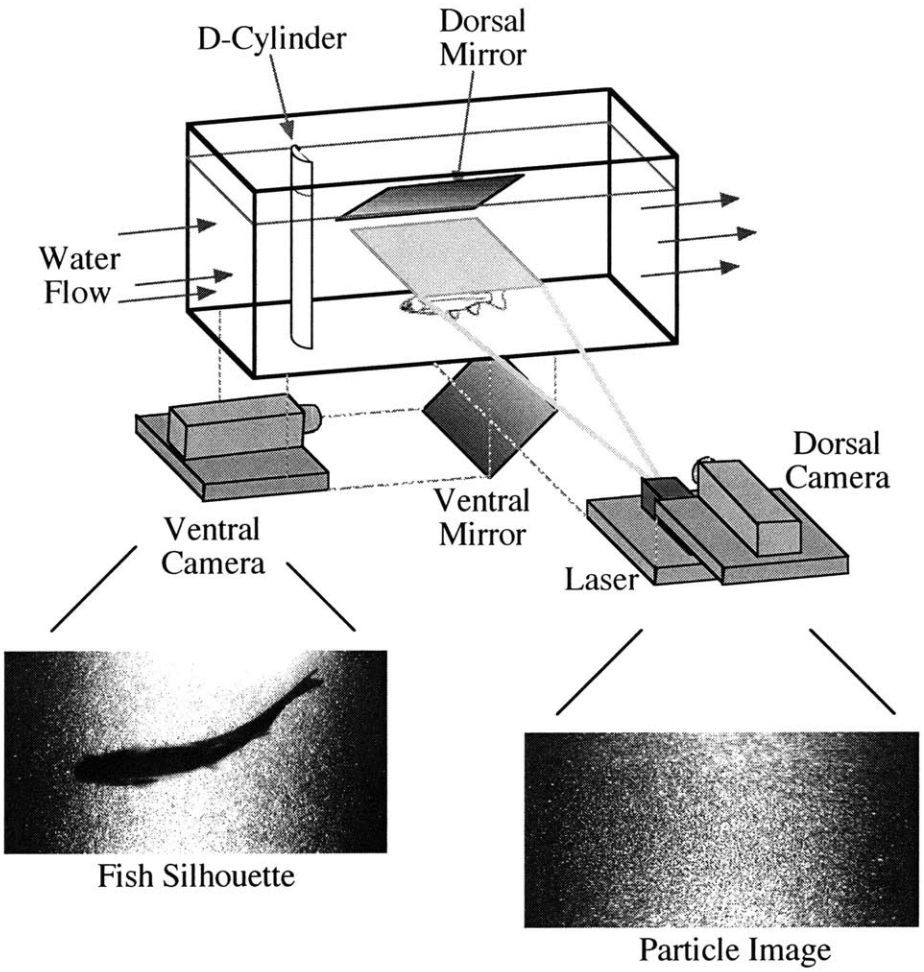

Figure 2-5: The dorsal camera shot an unadulterated view of the particle field, for PIV, while a synchronized ventral camera recorded a silhouette of the fish.

fact, any local effect of the fish on the incoming wake is likely completely washed out a few diameters downstream, due to the size of the large, two-dimensional columnar vortices relative to the span of the fish tail.

We desired to overlay the outlines of the fish, digitized using the video from the ventral camera, upon the vorticity flood-plots obtained from the particle data on the dorsal video. In order to do this, the cameras had to be correlated so that a point on one could be properly placed on the video from the other. A wire probe with 4 discrete points in one plane was placed within the light sheet, and video from both

cameras were recorded. The 4 points could then be translated from one camera to the other, requiring scale, rotation, translation, and mirroring the image so that the 4 points matched up optimally in a least-squares sense. This calibration was recorded so that it could be used to overlay any object in the ventral view onto the field from the dorsal camera.

The particle image from the dorsal camera was analyzed using Insight 3.0 from TSI Inc., which ran a cross-correlation of consecutive frames (at 4 *ms* apart) in a 17x26 matrix of 442 vectors. The velocity vectors were smoothed first by a standard deviation filter, which removed vectors over 1.5 deviations from the mean, second by a mean filter, with a tolerance of 2 and a 5x5 neighborhood, and finally by running a smoothing filter thrice, with a 3x3 neighborhood and a Gaussian radius of 1.1, to give a clear view of the large vortex structures in the wake. Once the ventral view of the trout was digitized to give the mid-lines and outlines at each point in time, the smoothed velocity vectors were read into a MATLAB script, which overlaid the outlines onto a vorticity map produced using the velocity vectors from PIV. This could then be used to compare the positioning of the trout with the instantaneous and unadulterated flow around it.

All of the analysis performed in Section 2.2 was performed again, including the comparison of the tail-beat frequency and body-wave to those of the flow, but using actual values of the flow frequency and wavelength given by the PIV. In addition, we desired to find whether or not the fish were synchronizing with the wake in phase as well as frequency. In order to do this, the phase of the wake needed to be defined. An example of a desirable signal from the wake, as a means for finding its phase, would be periodic with the wake period, reach a maximum when a positive vortex passes the position in question, and reach a minimum when a negative vortex passes. A signal like this, dubbed the wake function W(x,t), was obtained by taking the sum of vorticity passing a given line downstream from the cylinder, as shown in Figure 2-6. The phase of this signal was then compared to the phase of lateral position, with time, for the fish at the same downstream location. Since the fish is not guaranteed to remain in place, although it does not move much in the upstream-downstream

direction, the wake function was calculated for the x-position of each body point with time, and then compared with the y-position of those same body points.

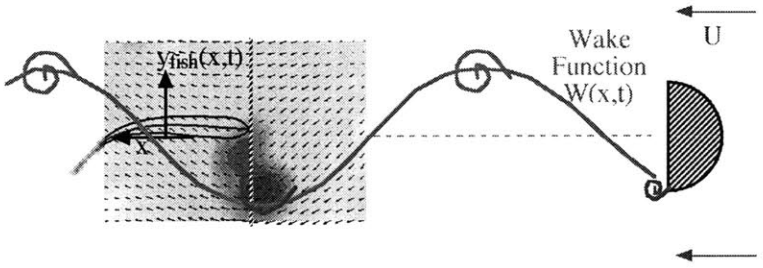

Figure 2-6: The wake function W(x,t) is the sum of vorticity lateral to a given body point on the fish (in this case, the nose). This defines a phase for the oscillating wake.

For a cylinder drag wake, if a trout's lateral position was in-phase with the wake function, its lateral motion would carry it into the vortices as they pass by. Similarly, if it was 180° out-of-phase with the wake function, its lateral motion would carry it through the wake in such a way that it would avoid contact with the vortex centers. In essence, this is a comparison of the trout's side-to-side position with the relative upstream-downstream position of the vortex wake.

Additionally, we wished to know whether or not the trout's lateral motion moves with or in opposition to the instantaneous lateral flow in the wake. Hence, for each body point, the lateral velocity was compared, in both amplitude and phase, with the instantaneous lateral velocity of the flow local to that body point, as shown in Figure 2-7. Although the phase of the lateral velocities in the flow is intrinsically related to the phase of the wake function described above, by 90° (as it is related to the integral of the wake function), we felt that analysis would be easiest to compare similar quantities with each other, position with position, and velocity with velocity, in a way that in-phase and anti-phase are meaningful.

Experiments were performed with 7 different trout, and 4 clean tail-beats were analyzed from each fish. A new batch of fish were purchased for these experiments, averaging 12.9 ± 0.31 cm in length, and 19.5 ± 0.6 g in mass. Every 10 frames of the video was analyzed, giving a sample frequency of 25 Hz.

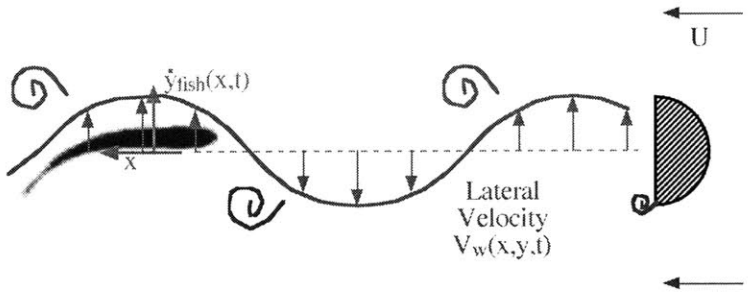

Figure 2-7: The lateral velocities of each body point were compared to the local lateral velocities in the flow.

2.3.2 Results and Discussion

Using PIV to measure the flow, while simultaneously filming the trout swimming just beneath the laser light sheet, proofed the frequency and wavelength synchronization results from Section 2.2. The frequency of the fish motion normalized by the frequency measured in the wake was 1.00 ± 0.01, which clearly shows that the fish tail-beat frequency was locked-in to the wake. The wavelength of the trout body-wave, however, was 1.94 ± 0.05 times the wake wavelength, implying that the trout were not interacting with the individual vortices in the same way for the head as for the tail.

The trout avoided areas of strong vorticity in the wake of the cylinder, as seen in Figure 2-8. It should also be noted that the direction of the trout's lateral motion appeared to generally move with the lateral component of the flow velocity arrows.

A possible strategy for a trout in a cylinder wake would be to always locate itself laterally in the wake so that its location always corresponds to the location with the instantaneous minimum downstream flow. Plotting the fish outlines on a flood plot of U-velocity show that the trout generally remain near regions of low downstream flow, but not in such a way as to suggest that this is the overall strategy, as the body and tail can each be seen to leave low-flow areas during parts of a single tail-beat period in Figure 2-9.

The phase of the wake was represented through a 'wake function', defined as the lateral sum of the vorticity passing by a given body-point. This function results in

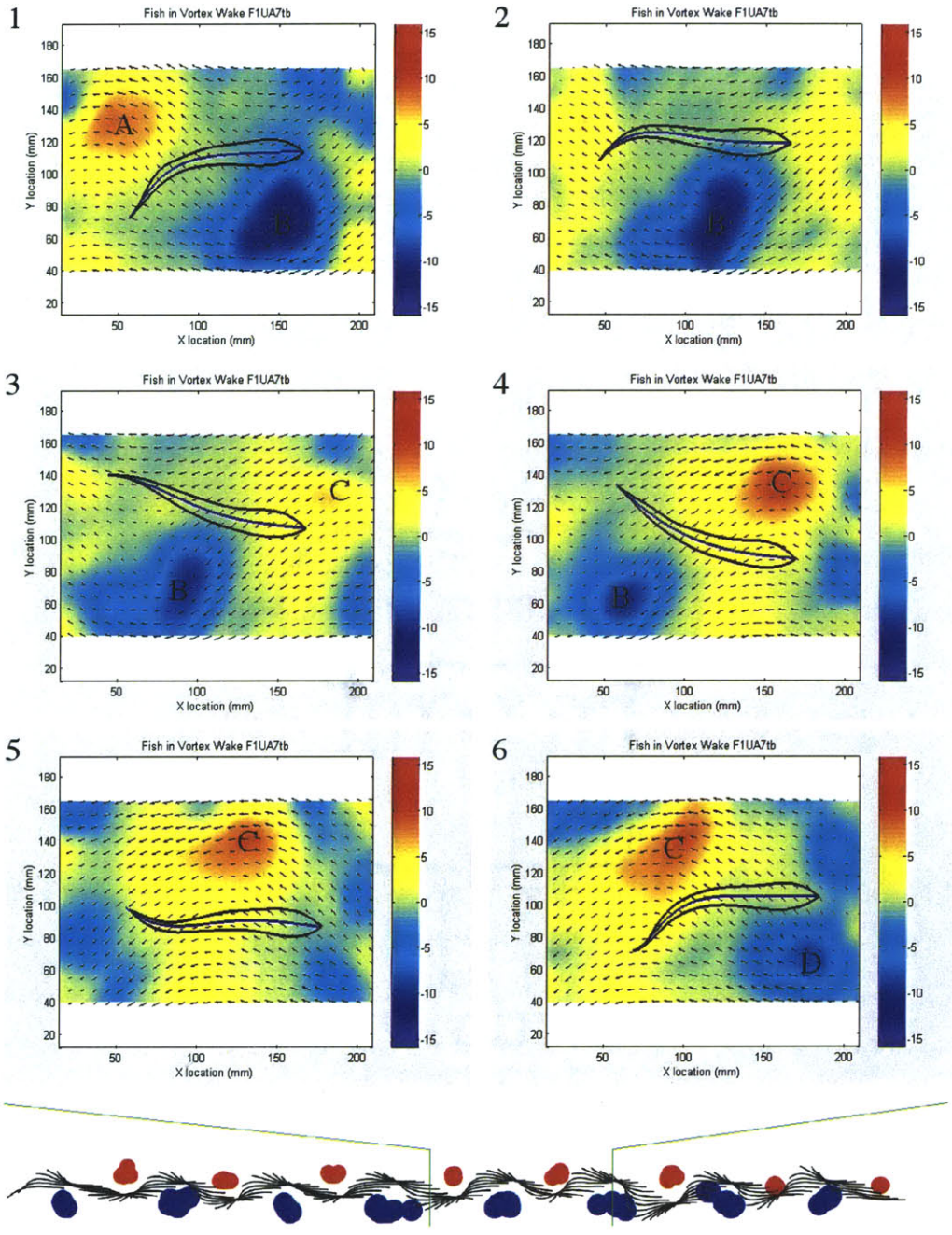

Figure 2-8: Select frames from one cycle of fish motion within the wake. The flood color represents vorticity, in 1/seconds

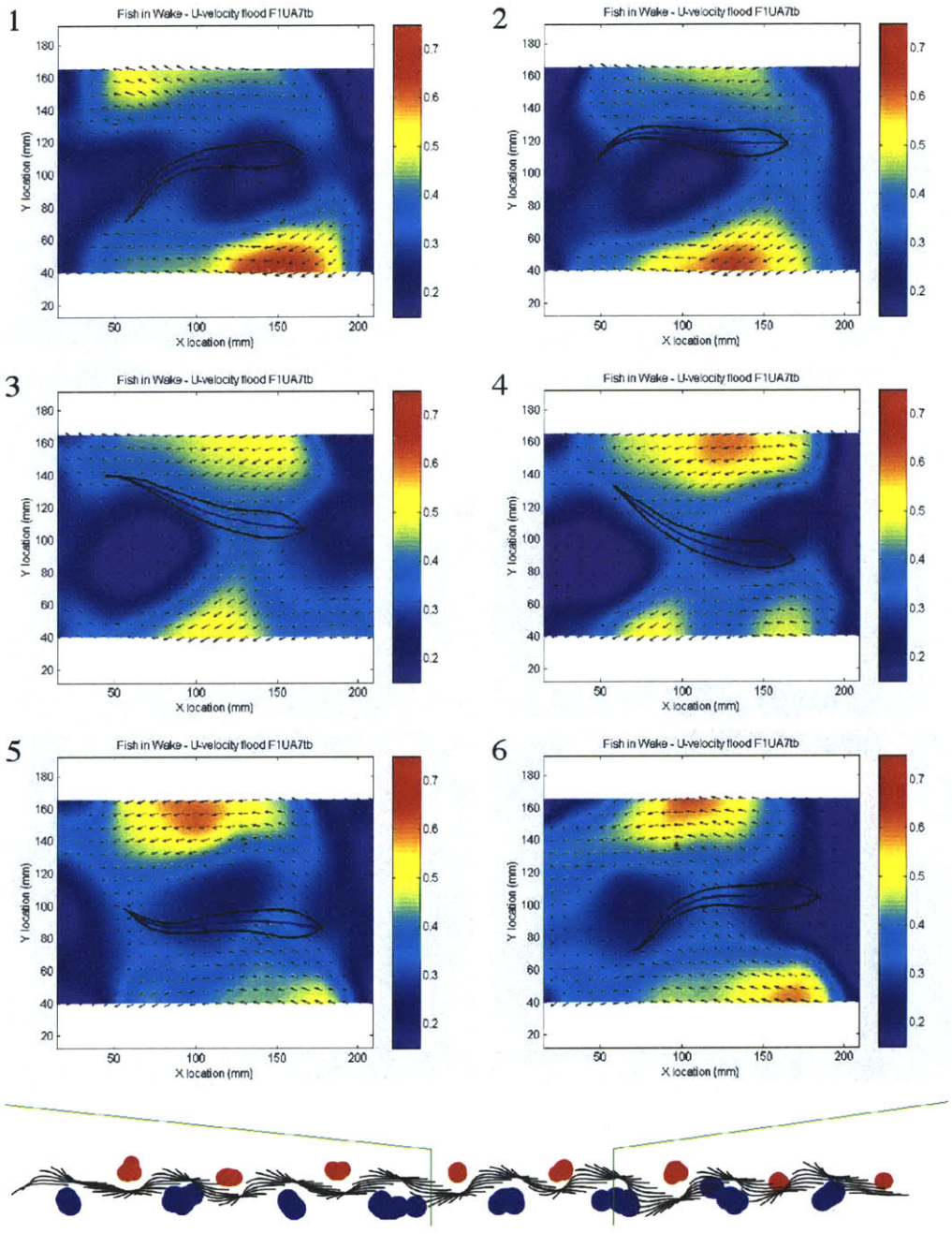

Figure 2-9: Select frames from one cycle of fish motion within the wake, where the color represents instantaneous velocity in the downstream direction, in m/sec

a sinusoidal-looking signal, with the signal high when a positive vortex passes the point, and low when a negative vortex passes the point.

The phase between the body lateral position and the wake function, measured at each body-point, is shown in Figure 2-10. The low scatter (standard error) implies that the phasing relation is fairly strong, and shows that the fish are generally out-of-phase with the wake function, although the head follows a different trajectory through the wake than the tail (100° for the head vs. 160° for the center-of-mass vs. 240° for the tail).

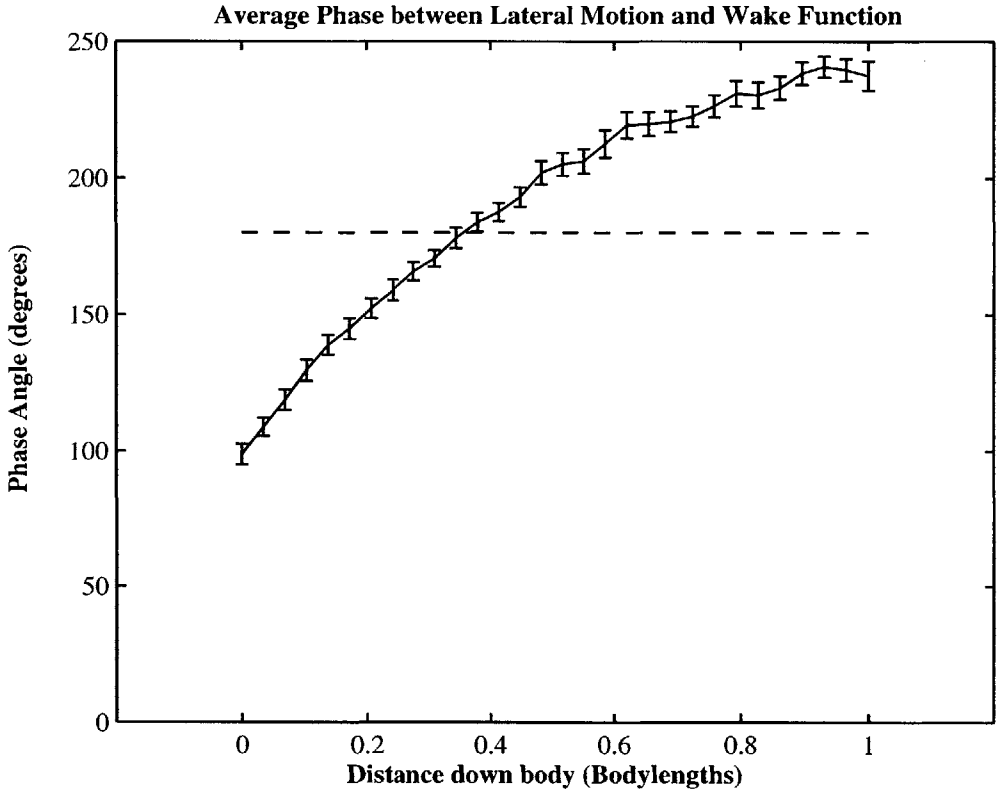

Figure 2-10: The phase difference between the lateral motion of the fish body to the wake function, from head to tail. The dashed line demarks positions 180° out-of-phase with the wake function.

The strong and consistent phase relation between lateral motion and the wake function shows that the fish are indeed synchronizing to the wake in both frequency and phase.

The trout are not opposing the oscillating lateral flow on a large order, as the body points each move laterally back and forth at nearly the same peak velocity as that of the local flow, as shown in Figure 2-11. The exception for this would be the tail, which moves considerably faster than the flow across it. Additionally, the lateral velocity of the trout is very similar in phase to the wake lateral velocity, as seen in Figure 2-12, with deviation from that at the head and tail. This would imply that the oscillating lateral motion seen in the fish is the result of the fish merely allowing itself to be buffeted back and forth by the flow, at the same time that the fish is producing thrust in order to maintain its position behind the cylinder.

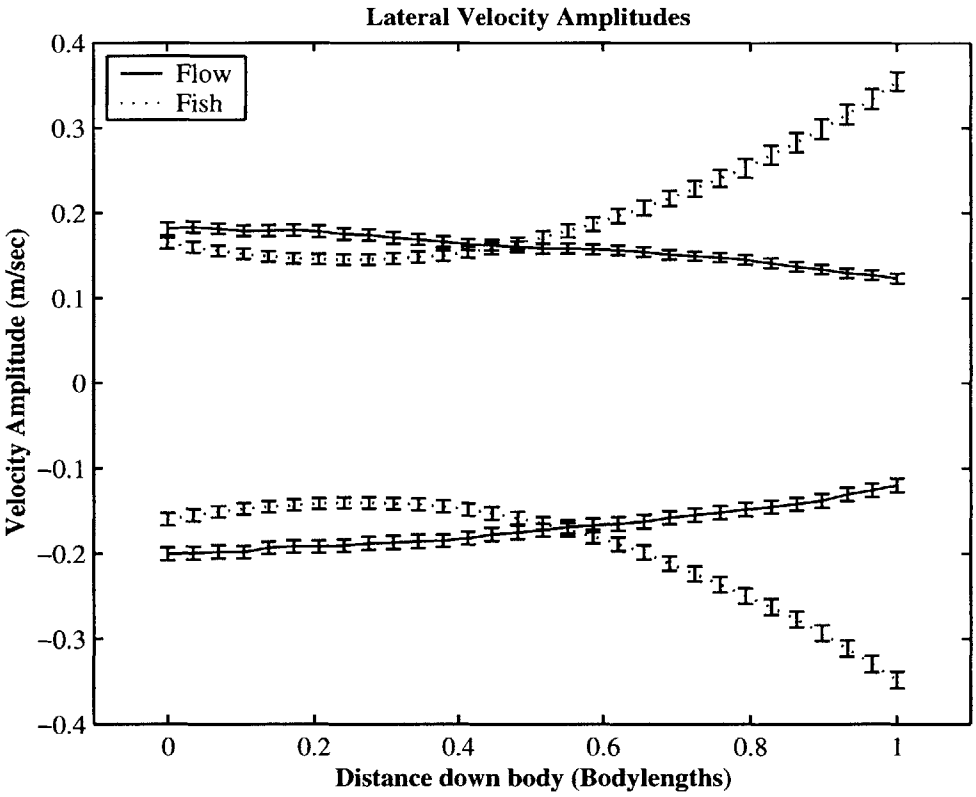

Figure 2-11: Amplitude of the lateral velocity for the trout body points and the instantaneous lateral component of the flow local to those body points, from head to tail.

As the fish voluntarily chose the location behind the cylinder, it should be assumed that there is an advantage to doing so. Indeed, fish entraining behind the cylinder

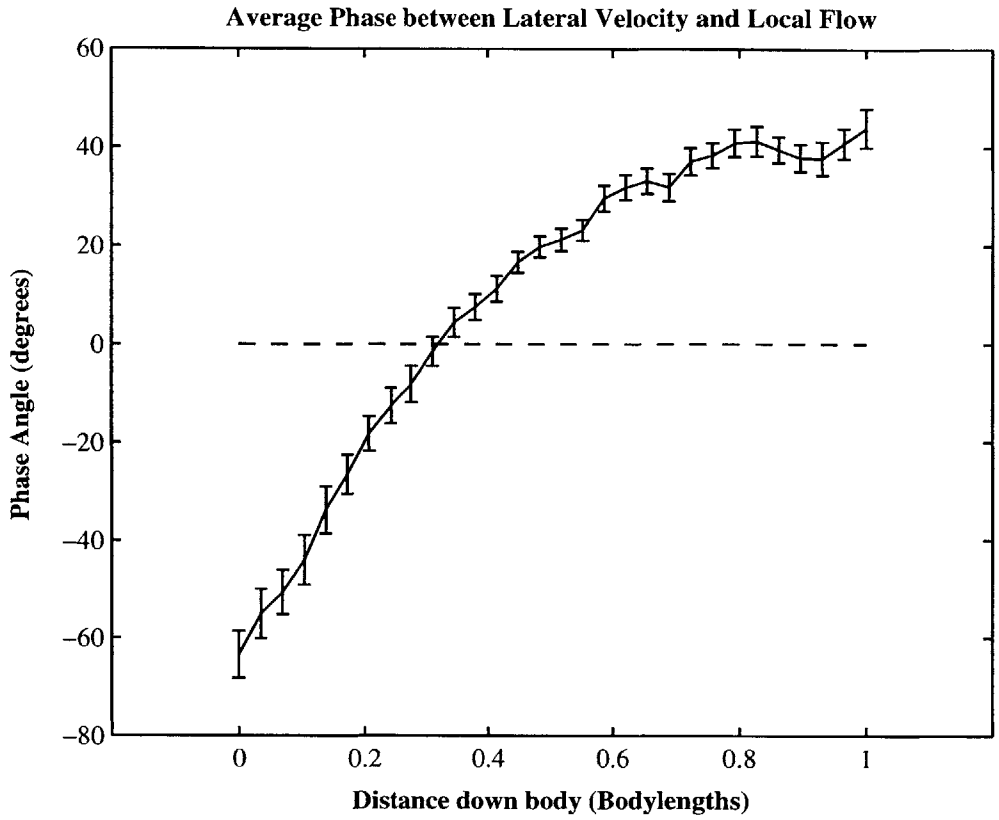

Figure 2-12: The phase between the trout lateral velocity and the oscillating lateral component of the flow local to the trout's body points, from head to tail.

were never to reach a point of exhaustion during the experiments, as was sometimes seen during free-stream swimming. Some benefit is to be expected as the fish take advantage of the lower mean downstream flow speed in the cylinder wake. However, some contrast needs to be made between a fish merely drafting in the velocity defect, and a fish utilizing the vortex street for energy benefit as well.

2.3.3 Summary

As all the fish synchronized with the wake in both frequency and phase, it is clear that the motion is not just a function of the fish swimming normally within a reduced flow. However, it is less easy to distinguish whether or not the trout were synchronizing to a particular phase for thrust or energy benefit, or whether they located themselves in

the wake to take advantage of the velocity deficit, and were compelled to follow the strong lateral flows rather than to fight them.

2.4 Dead Fish within Wakes

The PIV experiments showed that the trout synchronized their motions to the incoming vortex wake in both frequency and phase, but could not prove that the trout were gleaning additional energy benefit from this synchronization, beyond that of drafting alone. The trout generally moved back-and-forth with the lateral flow, as if they were flags in the breeze. Since electromyograms showed little or no muscle activity in the rear two-thirds of the body when the trout were swimming within the wake [30], the motion of the fish within the wake appeared to be passive.

As discussed in the introduction, Wu investigated heaving and pitching foils near a wavy surface. He found that the foil was capable of producing thrust and extracting energy in a fluid-excited motion, meaning that no power input from the foil was required [57, 58]. This was supported experimentally by Isshiki, [26], and applied to whales near the surface by Bose, who found that they could extract more than 25% of their propulsive power through the oscillating wake [10]. These all imply that it may be possible for trout to passively produce thrust through fluid-induced motion in a Kármán wake.

In order to test the hypothesis that the fish were swimming passively in the wake, a euthanized trout was tied to a string attached to the cylinder (all tests were performed prior to rigor mortis). The string, when taut, positioned the dead trout at the downstream location that live fish were seen to choose, approximately 20 cm behind the cylinder. The oscillating flow of the wake was found to excite the trout body in lateral oscillations, which could be expected, but also to entice the trout to move forwards towards the cylinder, against its own drag.

2.4.1 Methods

A fish was euthanized using MS-222, a general anesthetic which shuts down nerve cells, both in the brain and the body [4]. In small doses, this effect is temporary, and it is used to anesthetize fish for surgeries. In large doses, however, its effects are fatal and permanent, and a bath of highly concentrated MS-222 for one hour is the standard method to humanely 'put fish down'. The fish euthanized was of the same batch as the PIV experiments. As some time had passed, it had grown to 17.8 cm.

A line was hooked to the fish and tied to the cylinder, which was held stationary as in Section 2.2. The line was not significantly compliant and, when taut, held the fish 20 cm downstream of the flat backside of the 2" D-cylinder, right in the range in which live fish were seen to hover. The flow speed was set to 57.0 cm/sec, or 3.20 L_f/sec, a happy medium between using similar frequencies as the previous tests and a similar flow-speed relative to body-length. The ventral view was videotaped as in Section 2.2.

The suction region behind the cylinder was conservatively estimated at 2.0 D [22], and the mean and minimum downstream flows at the location of the fish were measured with PIV, which showed that the fish was not in the suction region, and that at no time during the cycle was there even instantaneous upstream flow near the fish, as seen in Figure 2-13.

Six tail-beats of forward motion were digitized, where the line is clearly no longer taut, but the fish has not yet entered the suction region. Every 4 frames of the video was analyzed, giving a sample frequency of 62.5 Hz.

2.4.2 Results and Discussion

When in the Kármán wake, the dead fish buffeted around as one would expect, with the string clearly keeping the fish from tumbling off downstream. However, the fish regularly synchronized with the wake and moved upstream until it entered the suction region behind the cylinder and ran into the cylinder itself, before tumbling back downstream, as seen in Figure 2-14. Since PIV showed that the mean downstream

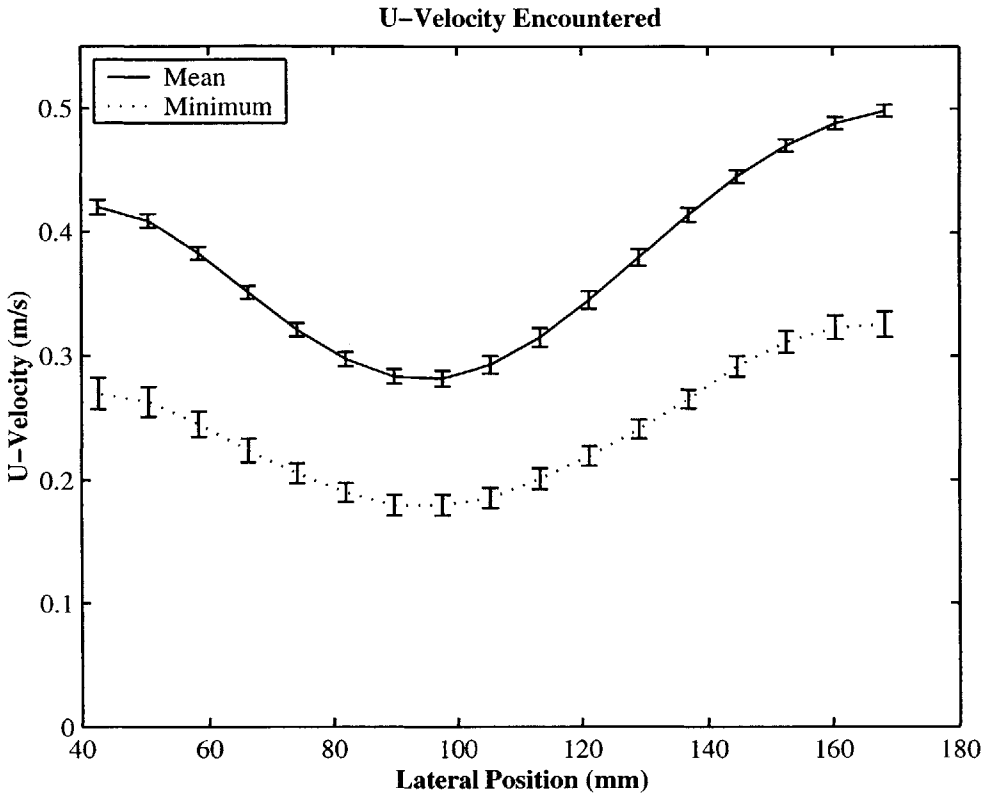

Figure 2-13: The mean and minimum downstream velocities encountered by the fish in its default location 20 *cm* back from the cylinder. The flow at the two sides does not match perfectly due to the dorsal mirror in the flow during the PIV tests of Section 2.3.

flow at the location of the fish, as well as the minimum downstream flow at that location, was not upstream at any time, this motion implies that the dead fish was passively moving forward against its own drag due to the oscillating vortex wake.

In order to test and make certain that it was not 'snap' of the line or some other mechanism pulling the fish forward, the video was digitized and analyzed. Figure 2-15 shows a typical approach. Initially, the fish is being buffeted back and forth by the flow, and its frequency does not even match that of the wake. At around 3.7 seconds, in this run, the fish begins to move forward. At this point the line cannot be taut. However, the fish continues accelerating forward, despite the fact that there are no forces on it other than those from the fluid itself. Once the suction region is reached, the oscillatory motion begins to fall apart as the fish gets pulled into the

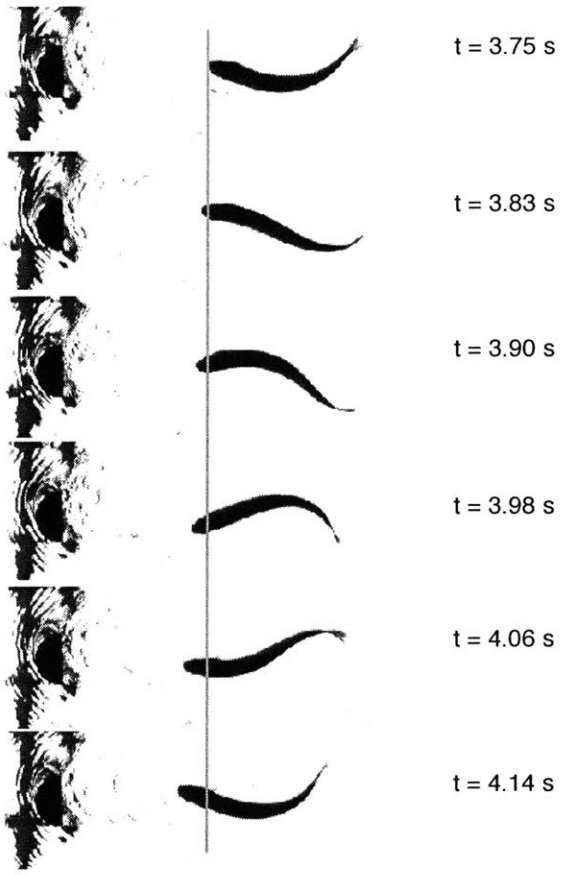

Figure 2-14: The oscillating fluid induces lateral motion on the dead trout's body as well as thrust on the tail, accelerating this dead trout forward against its own drag. The times given correspond to times in Figure 2-15. The vertical line represents a fixed location behind the cylinder.

cylinder. The x-velocity oscillations seen in the figure are perturbations from the lateral motion, at a frequency twice that of the lateral oscillations, as the body points move in a figure-8.

Table 2.2 compares the kinematics of the dead fish with that of the trout used in the PIV experiments, in Section 2.3. The amplitude of the dead fish motion is 58% to 75% of the live fish (center-of-mass and tail, respectively), although it is uncertain as to whether that is a function of life or death, or just a function of the size and mass difference. In both cases, the frequencies were closely matched to that of the wake. However, the dead trout's wavelength was considerably shorter than that of the live trout, only 1.25 times that of the wake, rather than 1.94 times.

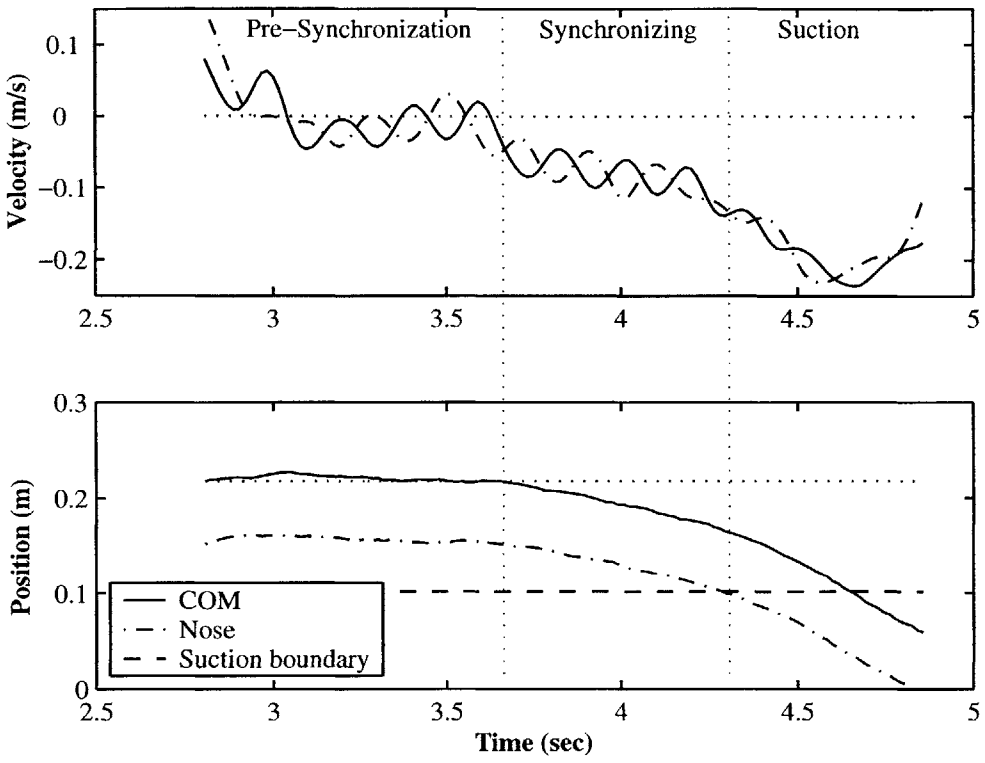

Figure 2-15: Downstream velocity and position of the center-of-mass and nose of the dead trout. The cylinder back is located at position zero, and a negative velocity is upstream.

Also, the average head angle amplitude for the dead fish was 3.4 times that of the live fish. Given that muscle activity has been shown near the head in live fish while synchronizing with the cylinder wake (although not down the rest of the body) [30], it appears that they are stiffening their heads so as to avoid the large angles. This may be for hydrodynamic reasons, but just as likely the fish prefer to minimize their head angles in order to keep their view straight-ahead, instead of continually swinging from side-to-side.

The only mechanism available to the dead fish to allow it to accelerate upstream, against its own drag, is if the wake works to move the fish in such a manner as to set up a beneficial flow across the body and tail. Although seemingly remarkable, there are other comparable and well-known situations that are similar in a basic level. A sailboat can easily 'tack' upwind by taking advantage of the difference in

	Live Trout	Dead Trout
Head Amplitude (D)	0.338 ± 0.015	0.239 ± 0.017
C.O.M. Amplitude (D)	0.317 ± 0.017	0.184 ± 0.015
Mid-body Amplitude (D)	0.340 ± 0.017	0.194 ± 0.018
Tail Amplitude (D)	0.648 ± 0.025	0.484 ± 0.066
ω_f/ω_w	1.00 ± 0.01	1.01 ± 0.01
λ_f/λ_w	1.94 ± 0.05	1.25 ± 0.06
Head Angle Amplitude	$5.4° \pm 0.5°$	$18.5° \pm 1.3°$

Table 2.2: Comparisons between live fish from the PIV tests and the dead fish, where all amplitudes are relative to the mid-line

flow velocities across its sail and hull, where the hull and keel 'anchor' the boat so that it can take advantage of the beneficial lift created by the sail. Similarly, dead whales have been found to move approximately one knot in surface waves. This is due to the surface waves creating an oscillating current across the whale's fluke; far more energy can be extracted if the fluke is allowed to move synchronously with the wave frequency [10].

This last situation appears to be very similar. In both cases, an oscillating flow is induced across a foil — using the body as a flow-anchor — which subsequently moves the entire body through the water. In one case, the flow is set up by surface waves. In the other, it is set up by a vortex street. In fact, this from Bose [10] could very easily apply to either situation:

> In smaller waves, ranging down from wave lengths several times the length of the whale, the whale's body is either steady or oscillates in such a fashion that the flukes are in water oscillating vertically at a different phase and amplitude to the motion of the body. The differential vertical velocity of the flukes can be used to extract energy from the waves.

Consider that each part of the trout body is being acted upon by the local flow as well as the neighboring body sections, which may pull the part in question across the local flow, to some extent, rather than with it. This may explain why the center-of-mass appears to move with the flow, in Figure 2-12, while the rest of the body

moves against it to a certain extent. In the end, each part of the body is being pulled against the local flow, to some degree, because its being pulled by the center-of-mass, which is itself synchronized with its own local flow. Hence, it is expected that, when the wake wavelengths are very long, there will be less differential flow across the body sections, resulting in lesser effects, as seen by Bose [10].

This is not to say that the motion of the live fish is entirely passive. The live fish must not only make certain that it stays within the wake but also cannot let itself drift too far forward or backwards. Essentially, the 'sweet spot' in the wake is a saddle point, where if the fish drifts too far forward it will be sucked into the back of the cylinder, and if it drifts too far back it would likely have to spend some energy producing thrust! This would explain the irregular, small-amplitude, high-frequency correction beats seen fairly often, as well as the considerable amount of action in the pectoral fins. This also explains why the fish appear to improve at synchrony the longer that they are behind the cylinder.

2.4.3 Summary

The experiments with the dead fish prove conclusively that fish are not just positioning themselves behind the cylinder in order to draft within the velocity deficit, they are also extracting energy from the vorticity for additional energy benefit to the point where the trout are essentially resting behind the cylinder. This could help to explain the ability of salmon to sustain long migrations upstream without food, and motivates further research using mechanical foils, where the actual performances can be measured directly.

Chapter 3

Performance of a Flapping Foil within a Vortex Wake

The effects of varying the interaction between a two-dimensional flapping foil and an incoming Kármán wake were quantified. The first case was studied in detail, one in which a foil with constant motion parameters was tested within three different wakes at twelve different interaction phases. The flow incoming towards the foil as well as the combined wake of the foil and cylinder were visualized using both dye and anemometry in order to correlate the peaks of thrust and efficiency with the wake interaction seen.

Additional experiments were performed to study how the wake interaction effects vary with with the foil motion parameters, giving a four-dimensional matrix of foil thrust and efficiency in the wake. Along isosurfaces of constant output thrust for several values of the thrust coefficient, the motion parameters giving the highest efficiency were located, and the wake interaction seen at these locations were compared with each other as well as with the trout studies performed in Chapter 2.

3.1 Review of Literature

When a flapping-foil actuator operates within the Kármán wake of an upstream cylinder, the performance varies considerably depending on the mode of interaction with

the incoming wake. Streitlien [47] numerically evaluated two-dimensional potential flow for a Joukowski foil within a vortex field, and found that, generally, when the foil moved such that it closely encountered the oncoming vortices it would have significantly higher thrust and efficiency then when the foil avoided the oncoming vortices.

Gopalkrishnan [23] used a NACA 0012 hydrofoil ($\frac{span}{chord} = 2.67$) that could pitch and heave in tandem with a heaving D-cylinder upstream ($\frac{chord}{diameter} = 2$). The vortex shedding from a D-section cylinder was relatively insensitive to the presence of the foil downstream, in comparison with a circular cylinder, making it an excellent vortex generator. The entire apparatus was dragged at constant speed through a tank filled with Kalliroscopic fluid, which allows for easy qualitative visualization. All tests were performed at a cylinder Strouhal number of 0.20, and at a cylinder Reynolds number of 540. Independently variable parameters in these tests included the heave amplitude of the foil and cylinder in tandem non-dimensionalized by the cylinder diameter, the pitch amplitude of the foil, the foil Strouhal number, the phase angle between heave and pitch, and the separation length between the cylinder and foil, which was used to alter the mode of interaction between the foil and wake.

Gopalkrishnan employed the upstream, heaving cylinder as a vortex generator, and identified three modes describing the combined wake of the cylinder and foil: vortex pairing, destructive merging, and constructive merging.

Vortex pairing occurs when the trailing edge vortex of the foil pairs with an oppositely signed vortex from the cylinder wake and together move off the flow centerline in a direction transverse to the mean foil motion, resulting in little to no mean wake velocity in the direction of motion.

Destructive vortex merging occurs when oppositely signed vortices of differing strength pair and twist into one another, eventually obliterating the weaker. This results in a wake with less total energy and, depending on the foil motion, the resulting vortices could be positioned in such a manner as to reduce or eliminate the average wake velocity in the direction of mean foil motion.

Gopalkrishnan identified a third interaction mode, constructive vortex merging, in which foil trailing edge vortices merge with drag vortices of the same sign, resulting

in a wake with greater total vorticity. He correlated his high foil efficiency tests, in a different set of experiments at much higher Reynolds number, with destructive merging, and those of low efficiency with constructive merging.

Using the same apparatus as Gopalkrishnan, but employing Digital Particle Image Velocimetry (DPIV) for quantitative flow visualization, Anderson [7] defined two extrema for the interaction between the foil and cylinder. Interception was defined as the mode where the foil motion brings it close to the oncoming vortices, while slaloming was defined as the opposite situation, where the foil would avoid the vortices in the Kármán wake. She found that, at higher pitch amplitudes (resulting in a lower angles-of-attack to uniform incoming flow), interception resulted in the cylinder vortices being annihilated by stretching, with a 32% higher thrust than while slaloming, which resulted in constructive merging.

The experimental work of Gopalkrishnan and Anderson varied the interaction mode by varying the distance between the foil and cylinder. Hence, the results do not separate the effects of distance from the effects of interaction. Additionally, efficiency data was not found for any experimental apparatus for which the interaction was identified through visualization. Hence, further experiments were necessary, using independently heaving cylinders and foils.

3.2 Motion Trajectories

Using a 3" D-section cylinder as a vortex generator, a heaving and pitching foil located downstream was swum within a variety of wakes using a variety of foil motion parameters. The effects of the cylinder wake on the foil performance was quantified as a function of wake interaction and foil motion.

For all of the foil experiments, the heave and pitch motions are sinusoids of a desired frequency, amplitude, and phase relation between each other. The foil's interaction with the wake was varied by changing the phase between the cylinder and

foil heave motions. The motions are described as

$$h_f(t) = H_f \sin(\omega t) \tag{3.1}$$

$$h_c(t) = H_c \sin(\omega t + \phi) \tag{3.2}$$

$$\theta(t) = \theta_o \sin(\omega t + \psi) \tag{3.3}$$

where $h_f(t)$, $h_c(t)$, H_f, H_c, $\theta(t)$, θ_o, are the positions and amplitudes of the foil heave, cylinder heave, and the pitch, respectively, ω is the motion frequency, ϕ is the phase between the cylinder and foil heave motions, and ψ is the phase between foil heave and pitch motions.

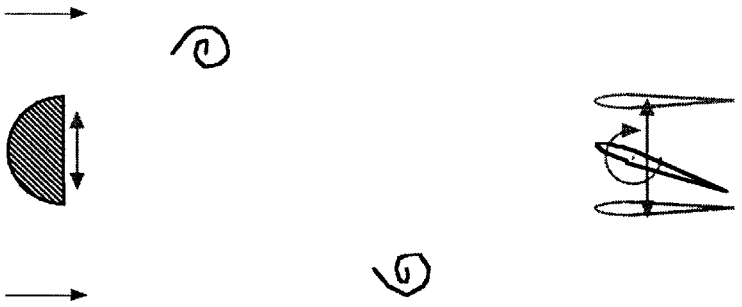

Figure 3-1: Foil heaving and pitching within a cylinder wake

For a foil within a uniform incoming stream with velocity U, Read *et al* [43] identified amplitude ratio $\frac{H_f}{c}$, Strouhal number St_f, maximum angle-of-attack to the incoming flow α_{max}, and ψ as useful independent parameters to determine the foil motion and resultant thrust and efficiency, where c is the foil chord, and St_f and α_{max} are defined as

$$St_f = \frac{H_f \omega}{\pi U} \tag{3.4}$$

$$\alpha(t) = \arctan\left(\frac{\dot{h_f}(t)}{U}\right) - \theta(t) \tag{3.5}$$

The foil's performance was calculated through measurements of lift L, thrust T, and pitch torque τ, in the form of the thrust coefficient C_T, efficiency η, and lift

coefficient C_P, as defined below.

$$C_T = \frac{\overline{T}}{\frac{1}{2}\rho U^2 cs} \tag{3.6}$$

$$\eta = \frac{\overline{T}U}{\overline{P_{in}}} \tag{3.7}$$

$$C_P = \frac{\overline{P_{in}}}{\frac{1}{2}\rho U^3 cs} \tag{3.8}$$

where s is the foil span and $P_{in}(t) = L(t)\dot{h_f}(t) + \tau(t)\dot{\theta}(t)$.

If, in a purely theoretical case, the foil was drafting behind an upstream obstacle whose wake contains no large-scale discrete vortices, then one can easily see that as the incoming velocity decreases St_f and α_{max} will increase for most of the situations studied by Read, where the arctan term in Equation 3.5 dominates over $\theta(t)$. Increases in St_f and α_{max} are generally correlated with increasing thrust [43]. Hence, we hypothesized that swimming a foil within a velocity defect will generally act to increase the foil's thrust.

When the foil is moving such that it is in-phase with the oncoming vortex wake function, as defined in Section 2.3, its lateral motion will oppose the lateral velocity of the flow, as seen in Figure 3-2, resulting in a further increase in α_{max}, as

$$\alpha_{In-Phase}(t) = \arctan\left(\frac{\dot{h_f}(t) + V_w(t)}{U_w}\right) - \theta(t) \tag{3.9}$$

where $V_w(t)$ and $U_w(t)$ are the lateral and downstream velocities seen by the foil in the wake, respectively. When within a cylinder drag wake, moving in-phase with the wake function would lead to interception of the vortices in the wake, as defined by Anderson [7]. Thus, it should be expected that, when intercepting a cylinder wake, the foil should produce higher thrust than drafting alone, at the cost of higher power expenditure.

Alternatively, if the foil is moving out-of-phase with the wake function, its lateral motion will move with the lateral flow, as seen in Figure 3-3, resulting in a decrease

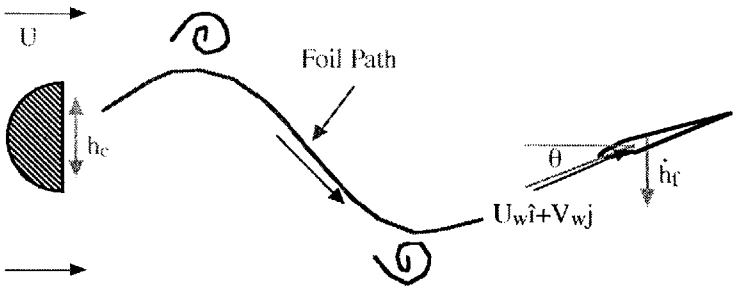

Figure 3-2: When $h_f(t)$ is in-phase with the vortex wake, its motion opposes the lateral flow

in α_{max} relative to drafting alone, as

$$\alpha_{Anti-Phase}(t) = \arctan\left(\frac{\dot{h_f}(t) - V_w(t)}{U_w}\right) - \theta(t) \tag{3.10}$$

When within a cylinder drag wake, moving out-of-phase with the wake function will result in the avoidance of the centers of vorticity, defined by Anderson as slaloming [7]. Thus, it should be expected that, when slaloming through a cylinder wake, the foil should produce lower thrust than drafting alone, while using less power.

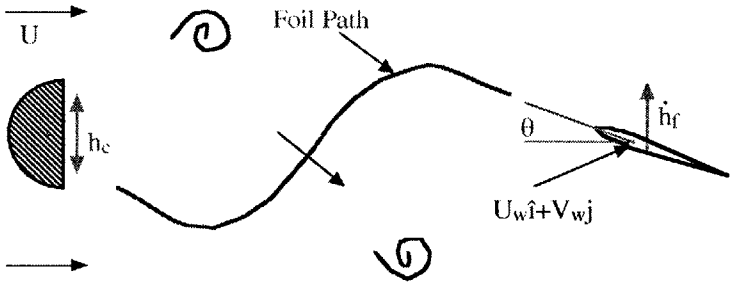

Figure 3-3: When $h_f(t)$ is anti-phase with the wake, the lateral flow aids its lateral motion

Hence, the foil interaction with the wake should be expected to change both C_T and C_P. However, it is less clear from hand-waving arguments as to how interaction will effect efficiency.

3.3 Apparatus

The experiments make use of the foil and carriage apparatus described by Read [42], with only a few minor changes.

All of the mechanical hydrofoil experiments were performed at the MIT Towing Tank. The tank is 30 m long and 2.6 m wide, with a water depth of 1.14 m. A velocity-controlled testing carriage rests on a pair of rails which run down the length of the tank. The carriage has a cable-carrier running to the end of the tank, which carries power and data. A control room is stationed at the end of the tank, dubbed the 'bridge', where a user can control the carriage and foil motions, and where the data collection and analysis computers are located.

A pair of 1-pitch lead-screws and linear tables are mounted to the carriage, in an upstream and downstream position, in order to give motion in the vertical (heave) direction, using Parker ML3475B direct-drive motors powered by Parker BLH150 220V amplifiers. Each slide was fitted with an aluminum mounting bracket capable of clamping onto a 2.75" diameter cylinder, as shown in Figure 3-4.

The cylinder and foil were each mounted from the ends using vertical foil-shaped cross-section aluminum struts, which were themselves welded to a 2.75" aluminum cylinder capable of mounting to the linear slide mounting brackets. Circular end-plates were mounted to the aluminum struts at the ends of the foil and cylinder, in order reduce 3-D effects.

The 3" diameter, 60 cm span, polyethylene, D-section cylinder was mounted onto the forward linear drive, and used as a vortex generator for the foil. The cylinder was set with a vertical flat face using a level.

The foil used for all tests was a laminated wood, 60 cm span, 10 cm chord NACA 0012 foil, attached to the rear linear slide. The foil pitches around its quarter-chord point. One end of the foil was set into a Kistler 9601 load cell in order to measure the lift and thrust forces on the foil. The other end was mounted to a chain and sprocket leading to a Pittman GM14900 5.9:1 geared servomotor, which controlled the foil in pitch through a Kistler 9069 torque cell. A potentiometer returned the absolute pitch

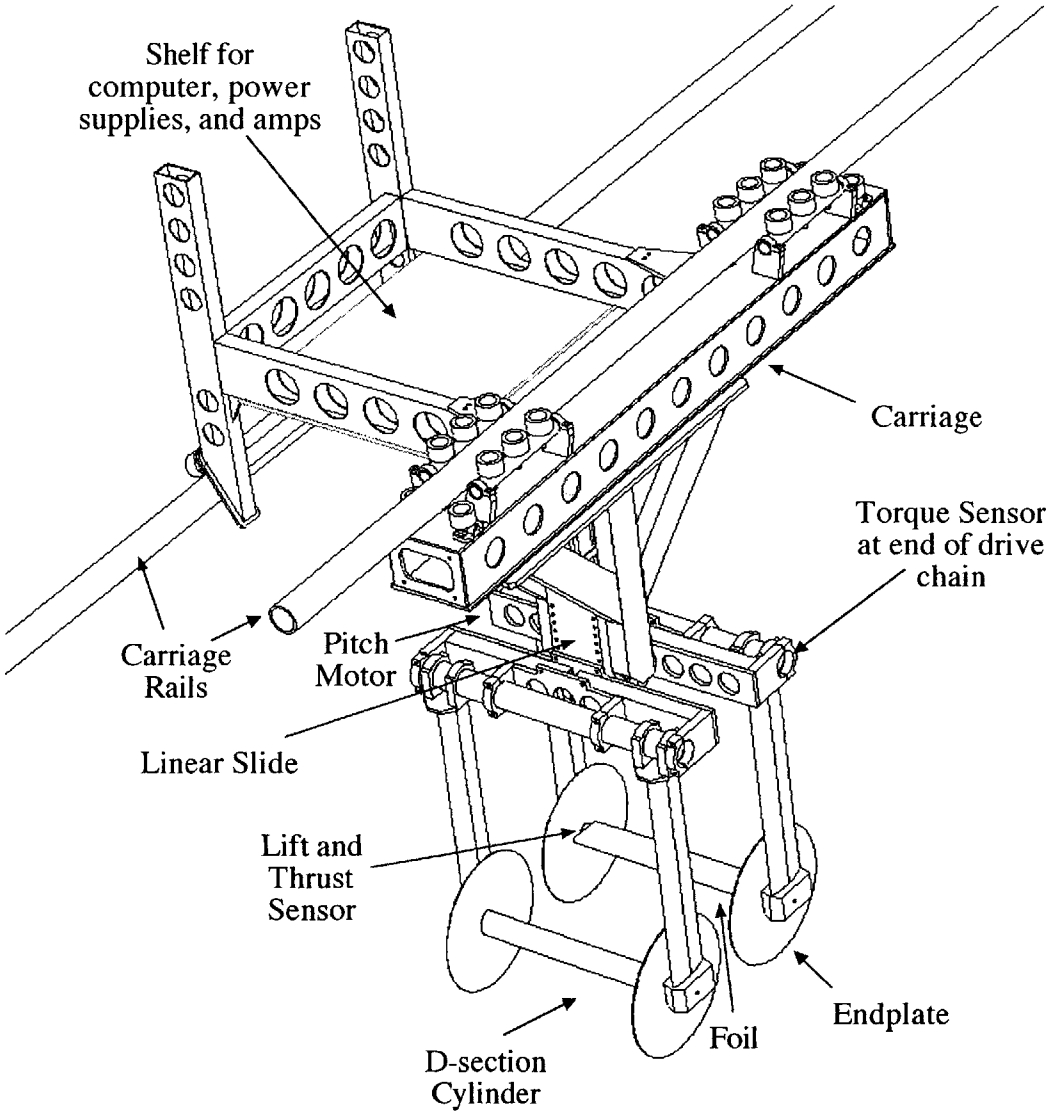

Figure 3-4: Diagram showing the foil and cylinder relative to the towtank carriage. Drawing modified from [13]

position.

The distance from the connection point of the cylinder to the pivot of the foil was set at 5 D, or 4.44 D from the back edge of the cylinder to the leading edge of the foil, as can be seen in Figure 3-5. Moving the foil even closer to the cylinder was found to yield more dramatic effects, but it was more likely that the foil was altering the cylinder shedding. Although the data was legitimate, this upstream effect was likely to complicate analysis. The distance between the foil and cylinder could be adjusted by angling the cylinder struts. The cylinder and foil were zeroed to the same heave position using a level.

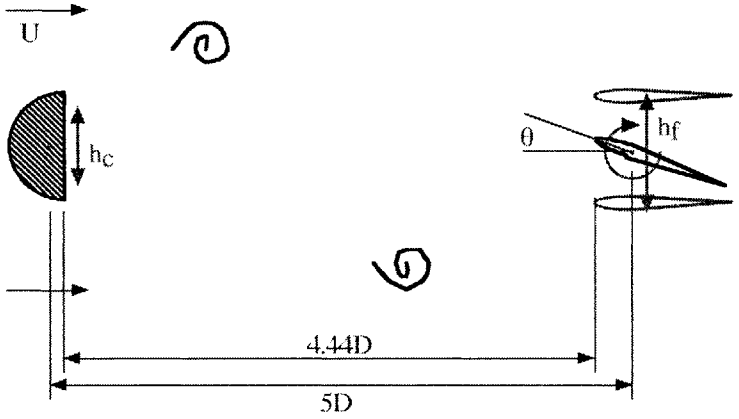

Figure 3-5: The foil is located a fixed distance downstream from the cylinder

The motion-control computer for the foil apparatus is located on the carriage, with an extension for the monitor, keyboard, and mouse so that the computer could be seamlessly accessed by a user on the bridge. Using an MEI 3-axis motion-control card, the controller commands position through a 1.25 MHz PID control loop using higher-level C++ commands from the control program.

The control program ran the control loop at 7.5 ms, during which time it checked all axes for error, calculated the next position, and commanded the velocity to reach that position for the duration of the next period. This control loop was fast enough to give smooth motions, while leaving plenty of time available for additional calculations, like those used in the synchronization routine discussed in Chapter 4.

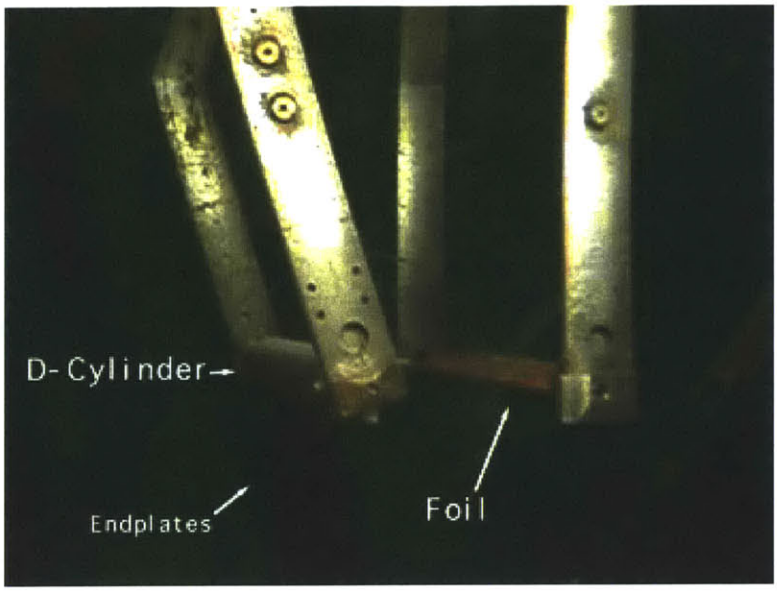

Figure 3-6: Photograph of foil and cylinder, viewed through a window in the side of the towtank

The foil and cylinder heave encoder values were outputted as a voltage using a D/A converter card in the motion-control computer located on the carriage. These positions, as well as the lift, thrust, torque, and pitch position signals, were then sent through a bus to a data acquisition computer on the bridge, as shown in Figure 3-7. Separating the data collection and motion control computers dramatically eased the programming chores.

The load cells were calibrated using hanging weights. For calibration in the thrust direction, the foil struts were swung up 90°, and a 0.5 kg weight was hung from the shaft nearest the force sensor. Lift and torque were calibrated with the struts in the default (vertical) position, by hanging the weight from the center of the foil span, being careful to subtract the buoyancy of the weight when hanging underwater. In order to apply a torque, the weight was hung by a string hooked over the foil leading edge, while the weight dangled off of the trailing edge. Kistler load cells have slight cross-talk between thrust and lift axes, so the cross-correlation terms were also calibrated. Calibration linearity, and the effects of measuring forces from only one side of the foil, are not significant issues, as discussed thoroughly in Read [42].

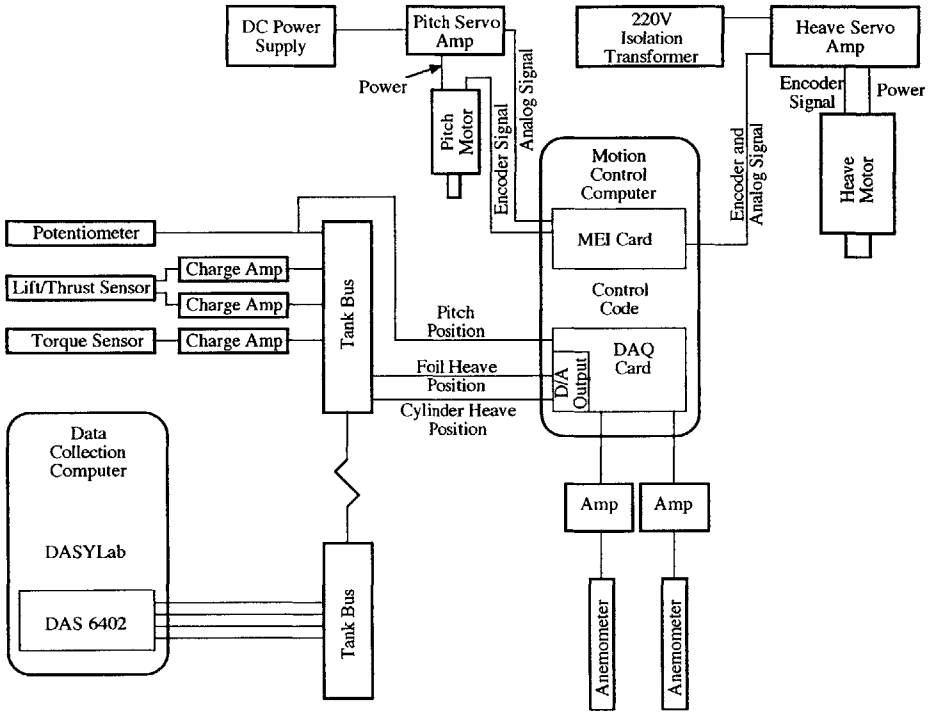

Figure 3-7: Diagram showing the power and data signal paths

3.4 Foil Performance within Varying Wakes

When a foil is heaving and pitching within a vortex wake, it is expected that the foil thrust and power input should change with the wake interaction, as discussed in Section 3.2. Using the foil and cylinder apparatus discussed above, we performed a systematic set of experiments in order to quantify how thrust and efficiency are dependent on the foil's interaction with the wake, using the phase between foil and cylinder motion ϕ to control that wake interaction.

Tests were performed within three different wakes: one with $H_c = 0.75D$, $St_c = 0.30$, another at a lower heave amplitude but the same frequency ($H_c = 0.5D$, $St_c = 0.20$), as well as another at a higher frequency ($H_c = 0.75D$, $St_c = 0.33$). The foil was swum similarly for all tests, with heave amplitude $H_f = 1.0D$, pitch amplitude $\theta_0 = 52.2°$, phase between heave and pitch motions $\psi = 90°$, and at the same frequency as

cylinder motion. The phase between foil and cylinder heave motions, ϕ, was varied at 12 settings between 0 and 330 degrees. For all runs, the carriage velocity was set to 0.4 m/s, corresponding to Reynolds numbers for the cylinder and foil of 30,480 and 40,000, respectively. Each trial was run at least 10 times, over several days.

The cylinder frequencies and amplitudes were chosen to ensure lock-in between shedding and the cylinder heave motion. The variety of amplitudes and frequencies were used to show whether or not variation in these parameters produced any significant effects in the results. The foil motion parameters chosen were relatively arbitrary, but were found to give significant variation with interaction phase. Section 3.6 studies the effects of changing the foil motion parameters in the wake in detail.

The wake interaction phase is not the only instrument for performance change within the wake. The foil is also drafting within the velocity deficit behind the cylinder. In order to estimate a 'drafting baseline' performance within the wake, the foil was swum in a uniform incoming flow at a lower carriage speed, corresponding to the lower velocity in the cylinder wake, while continuing to calculate thrust and efficiency using the higher velocity used in the interaction experiments. This represents doing the foil/cylinder tests behind a cylinder which somehow creates a velocity deficit without creating a vortex wake. The mean velocity deficit behind the cylinder was found using anemometers in the cylinder wake, as discussed further in Section 3.5.

For the baseline tests, the carriage was run at a velocity of 0.1481 m/s for the $St_c = 0.20$ tests, 0.0936 m/s for $St_c = 0.30$, and 0.1028 m/s for $St_c = 0.33$.

Clearly, even the mean velocity deficit behind the cylinder is not uniform as the foil moves laterally from the wake centerline. So, this baseline should be seen as an estimate as to how wake interaction varies from drafting alone, rather than a hard figure.

3.4.1 Results

Traces of the forces and positions with time are shown in Figure 3-8. Note that the thrust trace has twice the motion frequency, as thrust production is symmetric across the motion centerline.

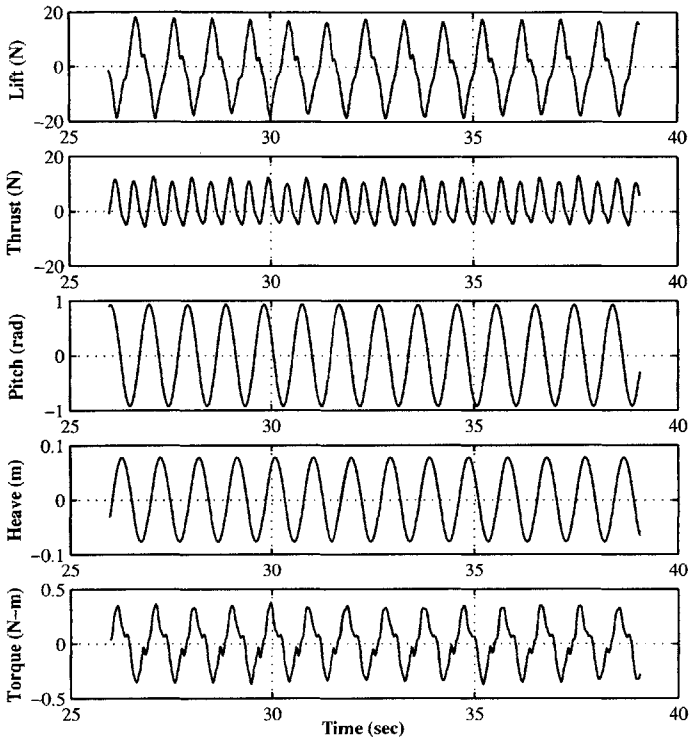

Figure 3-8: Traces of foil forces and positions with time. $H_c = 0.5D$, $St_c = .20$, $H_f = 1.0D$, $\theta_0 = 52.2°$, $\psi = 90°$, $\phi = 0°$.

All three wakes gave similar results, so, for brevity, only one is presented here. Results for the other two scenarios can be found in the Appendix. In each case the thrust was highly dependent on ϕ, varying by 0.4 from maximum to minimum, while the efficiency was much less so, varying only by 0.1 from maximum to minimum, as shown in Figure 3-9. Also, within a given wake, the peaks of thrust and efficiency were at nearly the same phase, with the thrust maximum at 120°, the efficiency maximum at 90°, and with the minimum thrust and efficiency seen at $\phi = 300°$.

Thrust and efficiency variation between runs was relatively large, at 0.1 standard deviation for C_T, and 0.05 to 0.1 deviation for efficiency, depending on ϕ. This variation is significantly higher than that seen for tests of the foil alone, in a uniform wake. This is likely due to some run-to-run variation in cylinder shedding, possibly caused by the foil motion itself. Indeed, a couple of outliers were removed in which the foil produced extremely low thrust (near-zero or negative), where it is likely that

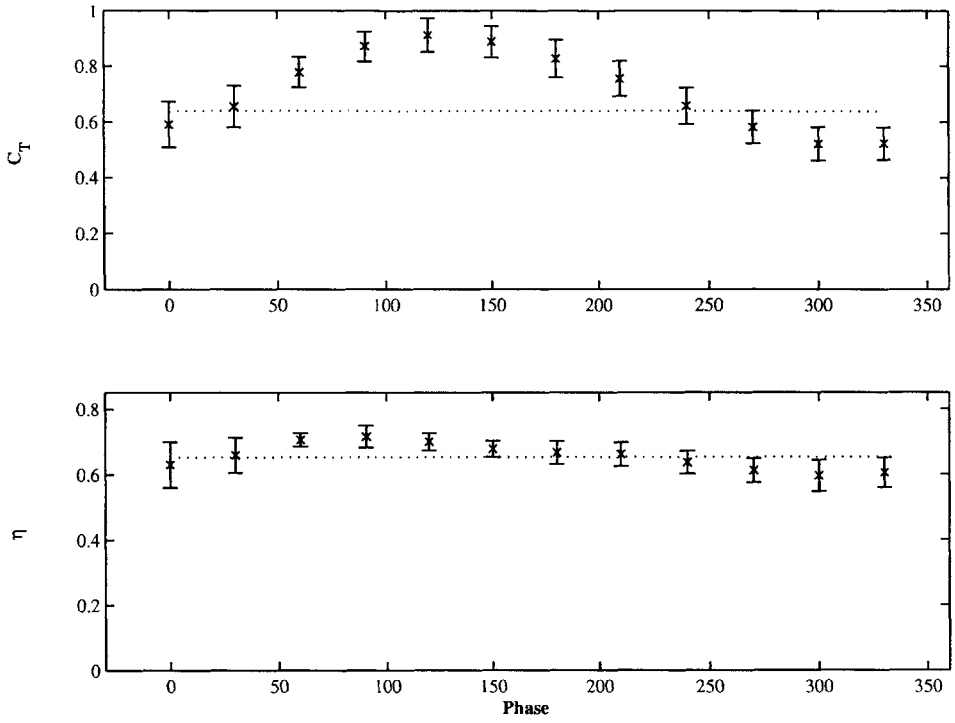

Figure 3-9: Foil swimming within a cylinder wake, using the foil/cylinder phase to determine the interaction mode. $H_c = 0.5D$, $St_c = .20$, $H_f = 1.0D$, $\theta_0 = 52.2°$, $\psi = 90°$. The dashed line represents the baseline drafting performance, and the error bars represent the standard deviation.

the foil was significantly altering the cylinder shedding. These cases occurred no more than one time in a hundred, so it was impossible to do further study on them with a flow visualization technique in order to better tell what was happening.

In order to show how the foil would perform within a velocity deficit with no vorticity, we performed a series of baseline drafting tests using a slower carriage velocity. These results, shown in Table 3.1, exhibit thrust within the bounds of the wake interaction tests within all three wakes, but efficiency on the low side for both $St_c = 0.30$ and 0.33.

3.4.2 Discussion

For all three wakes, the baseline drafting performance lay within or just below the range of thrust and efficiencies seen in the wake interaction tests. This implies that

St_c	U	C_T	η
0.20	0.1481 m/s	0.709 ± 0.015	0.682 ± 0.017
0.30	0.0936 m/s	0.830 ± 0.018	0.731 ± 0.015
0.33	0.1028 m/s	0.829 ± 0.006	0.589 ± 0.002

Table 3.1: Baseline data to estimate the effects of drafting within the velocity deficit, using a slower carriage velocity, was run for all three wakes

the estimate is not unreasonable, and that the drafting and wake interaction effects can be additive improvements to the foil performance if the foil is set to interact with the wake with the right phase of motion.

In a uniform flow at full speed ($U = 0.4\ m/s$), a foil swimming with the foil motion studied here — $St_f = 0.40$, $\alpha_{max} = 6°$ — would not be producing thrust at all, due to the extremely low angle-of-attack. The drafting alone produces an extremely beneficial effect for this foil motion, as seen in Table 3.1. The relative change, however, is not universal, as tests with higher α_{max} were not seen to have nearly the increase in baseline performance (which was part of the reason why these parameters were used as the example).

These results show that the wake interaction mode has a significant effect on the foil's ability to produce thrust, and a lesser effect on the foil's efficiency. However, although the foil/cylinder heave phase ϕ is directly related to the wake interaction phase, and was a useful deterministic way to change that interaction, flow measurement techniques were needed in order to quantify that correlation, as will be shown in the next section.

3.5 Wake Interaction and Combined Wake Modes

As it is clear that the variation of foil/cylinder heave phase ϕ can significantly effect the foil thrust, it is necessary to correlate ϕ with the wake interaction. This was done qualitatively, with dye visualization, and quantitatively, with anemometers in the wake. In addition to the wake interaction mode, we also studied the combined wake of the foil and cylinder.

3.5.1 Dye Visualization

Dye was used to visualize the wake interaction mode at the phase angles showing the extrema of performance, as well as a few other locations. The combined wake of the foil and cylinder can also be seen. Presented below is the visualization results for $St_c = 0.20$, $H_c = 0.50D$. Results for the other two cases are similar, and photographs of the dye visualization can be seen in the Appendix.

A fluorescent green dye was mixed with paint thickener until is was no longer runny, and then painted on the cylinder and allowed to dry. A section of the mid-span, 4" wide, was painted. Similarly, a section of the foil was also painted using a red fluorescent dye. When placed in the water, the dye slowly seeped off of the surface of the cylinder and foil, being left behind as the carriage moved up the tank. Through a window in the side of the towing tank, a Canon Elura2MC digital video camera filmed the carriage and dye as it passed by.

At $\phi = 100°$, near the peak for both thrust and efficiency, the foil leading-edge pierced each vortex as it moved past. The pierced vortices were torn apart due to stretching, but the wake reformed downstream slightly nearer to the wake center-line, as seen in Figure 3-10. This agrees well with the work of Gopalkrishnan [23], whose photographs show that when a foil is intercepting the incoming wake, the combined wake vortices, formed from the cylinder vorticity combined destructively with oppositely-signed foil vortices, tend to be weaker and nearer the centerline.

At $\phi = 300°$, where both thrust and efficiency are at their lowest, the system was clearly slaloming, as in Figure 3-11, with the combined wake vortices far from the centerline. This also agrees well with Gopalkrishan, who found that a foil slaloming through a wake will generally produce a stronger, wider, drag wake consisting of vortices created from the combination of the cylinder vortices with like-signed vortices shed by the foil.

At $\phi = 180°$, where the thrust has begun to fall off from its peak, and the efficiency is average, the combined wake vortices are very near the centerline, and the foil intercepts the vortices near the mid-chord, as seen in Figure 3-12.

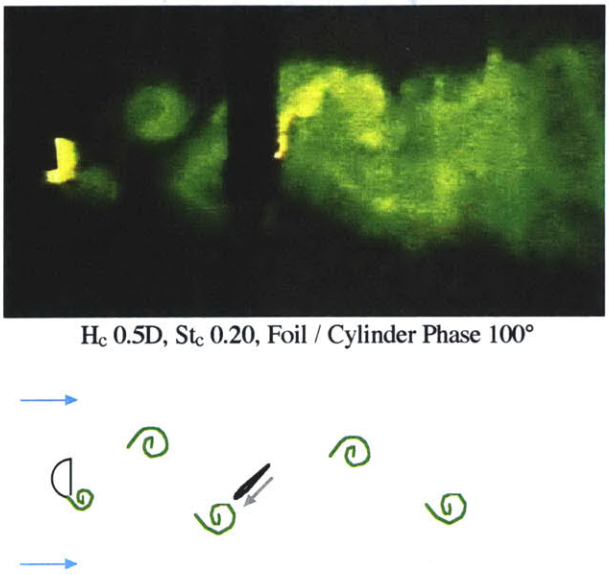

Figure 3-10: Dye visualization showing leading-edge interception, at a foil/cylinder phase resulting in high thrust and efficiency

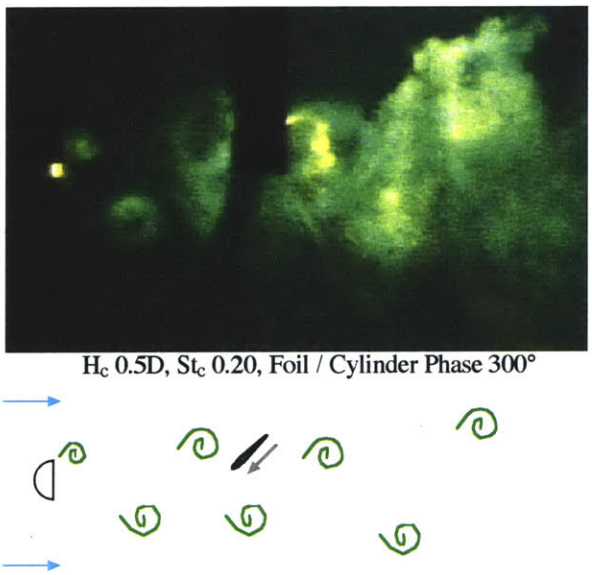

Figure 3-11: Dye visualization showing slaloming, at a foil/cylinder phase resulting in relatively low thrusts and efficiency

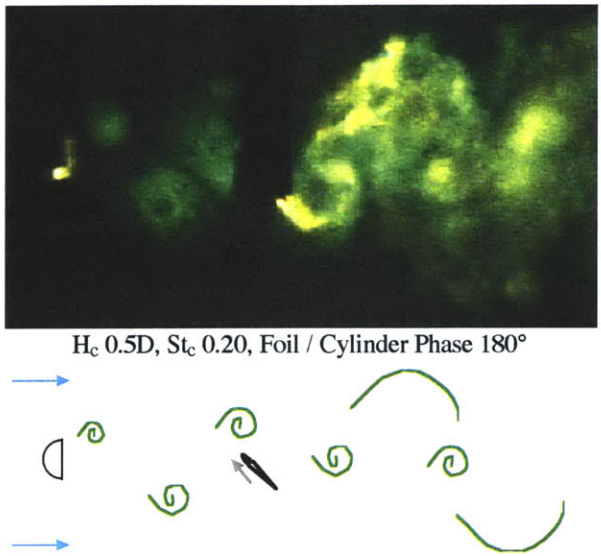

Figure 3-12: Dye visualization showing interception near the mid-chord, at a foil/cylinder phase resulting combined wake vortices near the centerline.

The dye visualization illustrated the general interaction between the foil and vortices. Although useful in a qualitative sense, it was necessary to use a more quantitative method to support these results, as discussed below.

3.5.2 Anemometry

In order to better describe the interaction mode and combined wake, we used hot-wire anemometers to measure the flow in the wake. The wake interaction phase was found using two anemometer probes attached to the second (downstream) linear slide mount, replacing the foil. The anemometers were single-axis TSI 1210-20W types, which do not separate U- from V-velocity. Hence, all of the following data measure velocity magnitude seen by the sensor, rather than downstream velocity alone.

The pair of anemometers were arranged 3 diameters apart, centered on the centerline of the cylinder, as shown in Figure 3-13. The distance between the anemometers and the cylinder was adjustable.

The wake interaction was defined by the relation between the phase of the wake with the phase of foil heave position. The phase of the wake was defined as the

instantaneous phase of the signal $S(x,t)$ created by the difference in measured speed seen by the two probes at the downstream location x, as shown in Equation 3.11. The phase between the cylinder position and the wake can then be found, as in Equation 3.12 (which is related to the foil pivot-point heave position through ϕ). This was then compared with the instantaneous heave position of the corresponding part of the foil, including the effects of foil pitching, creating a wake interaction phase $\phi_{foil,wake}$ for every point along the chord, as follows for the foil leading-edge

$$S(x_{LE},t) = P_{upper}(x_{LE},t) - P_{lower}(x_{LE},t) \tag{3.11}$$

$$\phi_{cyl,wake} = \angle h_c(t) - \angle S(x_{LE},t) \tag{3.12}$$

$$\phi_{pivot,LE} = \angle h_f(t) - \angle(h_f(t) + \theta(t) \cdot r_{pivot,LE}) \tag{3.13}$$

$$\phi_{LE,wake} = \phi_{cyl,wake} - \phi + \phi_{pivot,LE} \tag{3.14}$$

where $S(x_{LE},t)$ is the Wake Signal measured at the leading-edge position x_{LE} through P_{upper} and P_{lower}, the instantaneous flow speeds measured by the upper and lower probes, $\phi_{cyl,wake}$ is the phase between the cylinder position and $S(x_{LE},t)$, $\phi_{pivot,LE}$ is the phase between the foil pivot heave position and the leading-edge heave position, $r_{pivot,LE}$ is the distance from the pivot point to the leading-edge, and $\phi_{LE,wake}$ is the wake interaction phase between the leading-edge and the wake. Other points along the foil chord are calculated similarly.

The wake signal $S(x,t)$ is thus defined to be high when a vortex passes the upper probe, and low when a vortex passes the lower probe, as seen in Figure 3-13. When within a cylinder wake, a wake interaction phase $\phi_{foil,wake}$ of 0° would result in the interception of the vortices, and a phase of 180° would result in slaloming.

This measure of wake interaction is not ideal. Since the foil was producing significant thrust, and can significantly effect the cylinder wake through the repositioning of vortices, as was seen with dye visualization, it should be expected that the phase of the incoming wake with no foil present may not be the same when the foil is producing high thrust. In order to quantify this effect, additional anemometry tests were performed with a pair of TSI 1231W anemometers mounted in between the foil and

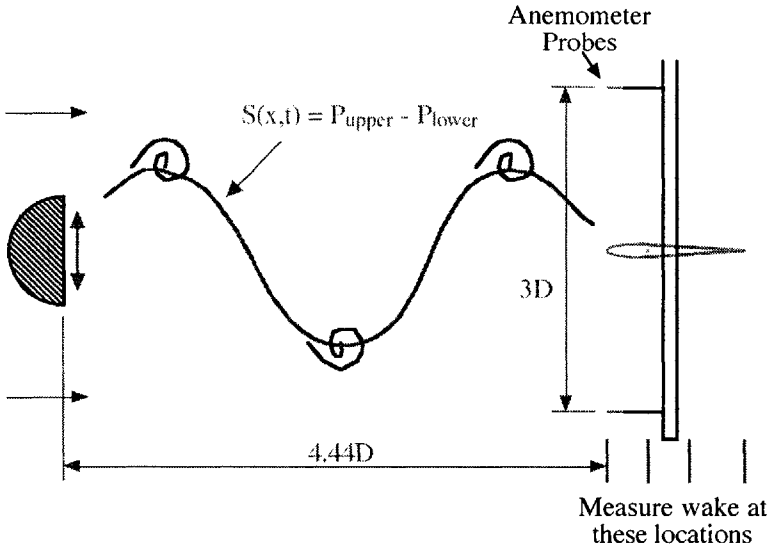

Figure 3-13: Probes were placed in 4 locations downstream from the cylinder in order to measure when the vortices passed by relative to the cylinder motion. The foil was not present during these tests.

cylinder (as described for the synchronization experiments in Chapter 4), with and without the foil, and the phase of the wake signals found were then compared.

The wake signal with the foil present led that for no foil by 36.9° for the $St_c = 0.20$ runs, 31.3° for $St_c = 0.30$, and 34.7° for the $St_c = 0.33$ experiments. While these values are small relative to half a cycle (180°), they do add an important footnote to the results of this method. This is a measure of how much the foil accelerates the vortices downstream towards it. However, this measure does not include effects for continuing acceleration of the vortices, nor does it take into account how the wake signal would change with changing foil thrust, foil amplitude, or wake width. Hence, it is not intended to be used as a calibration for the interaction phase, rather it should be considered an estimate as to the error in this wake interaction measure.

Twelve tests were run within each of the three wakes studied above, with 3 runs each at the leading-edge, $0.3c$ and $0.6c$ from the leading-edge, and the trailing edge. The results were then phase-averaged and compared.

Figure 3-14 shows the wake interaction phase $\phi_{foil,wake}$ for foil/cylinder phase $\phi = 0$, along the chord of the foil. The interaction phase for a non-zero ϕ can be

found simply by subtracting ϕ from the value on the plot for $\phi_{foil,wake}$.

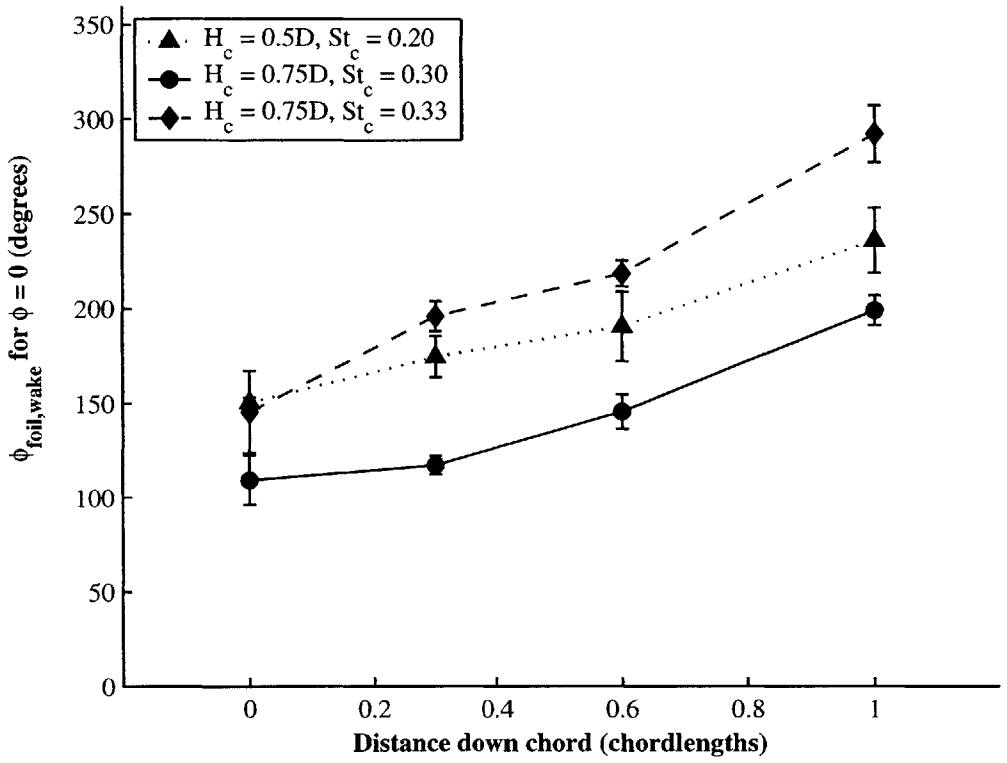

Figure 3-14: The wake interaction phase $\phi_{foil,wake}$ for foil/cylinder phase $\phi = 0$, and no foil

Plotting the interaction phase for the tests that were visualized above ($\phi = 100°$ and 300°), places the leading-edge interaction phase for $\phi = 100°$ as $\phi_{LE,wake} = 50°$, and that for $\phi = 300°$ as $\phi_{LE,wake} = 210°$, as shown in Figure 3-15. Considering that the foil speeds up the wake signal, decreasing the interaction phase for each of these scenarios, these values lie reasonably close to leading-edge interception and slaloming, corresponding to 0° and 180° respectively, seen with the qualitative dye visualization data.

As discussed in Section 3.2, the foil opposes the lateral flows in the wake when it intercepts the oncoming vortices (for a drag wake). These tests confirm that higher coefficients of thrust are attainable when the foil opposes the flows in the wake.

The wake signal S(x,t) is compared, in detail, with the wake function W(x,t) from Section 2.3 in Section 3.7, below.

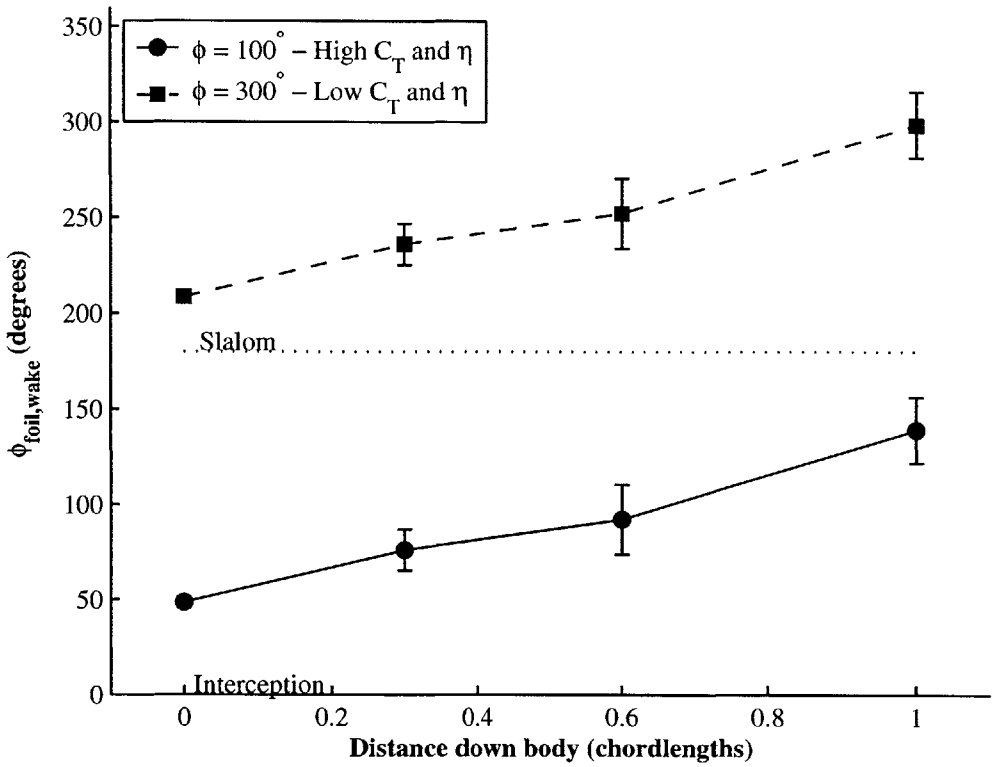

Figure 3-15: The interaction phase ($\phi_{foil,wake}$) down the foil chord, for high performance ($\phi = 100°$), and low performance ($\phi = 300°$), inferred from Figure 3-14

Combined Wake Profiles

The dye visualization of the combined wake from the foil and cylinder shows that the foil is capable of repositioning the cylinder vortices nearer or further from the wake centerline. Using anemometers, we desired to quantify this effect more clearly. A rake of 4 anemometers was attached to the carriage downstream from the foil and cylinder linear drives. The lowest anemometer was positioned at the wake centerline, and the other three were positioned a diameter apart from each other up from the centerline, as shown in Figure 3-16. The wake was then measured behind the foil and cylinder for each of the conditions described in Section 3.4. In order to increase resolution, the rake was moved one-half a diameter up, and the tests were re-done. Hence, these tests illuminate only one side of the wake, in detail.

For brevity, only the results for the $H_c = 0.5D$, $St_c = 0.20$ wake are presented.

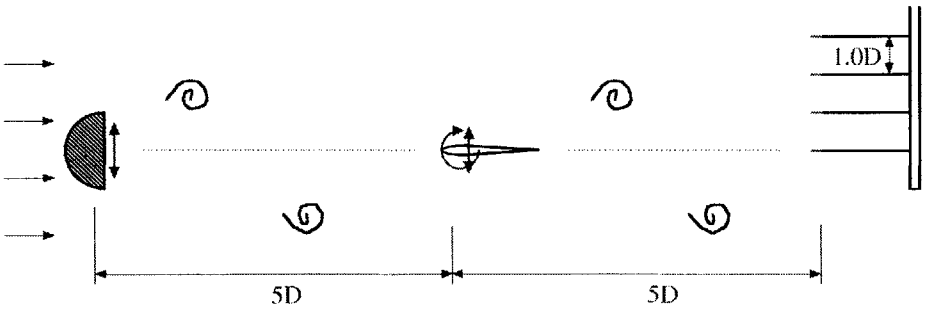

Figure 3-16: Diagram showing the placement of the anemometer rake downstream from the foil and cylinder

Results for the other two scenarios can be found in the appendix.

As seen in Figure 3-17, when ϕ is near 0 or 360°, the combined wake shows a low velocity of $0.4U$, while near $\phi = 180°$, the velocity is $0.9U$. It needs to be stressed that the anemometers measure velocity magnitude, not velocity in the U-direction only. Hence, care must be taken to avoid making conclusions regarding the velocity deficit in the combined wake. However, it should be pointed out that the wake velocity profile for $\phi = 0°$ looks very similar in form to the wake of a cylinder alone.

More interesting in terms of vortex repositioning, Figure 3-18 shows a graph providing the range of velocities seen by the probes over a period in the combined wake. The probes near the y-positions of the vortices will see a high range of velocities over a cycle. The profile range is highest at $0.5D$ for $\phi = 180°$, where dye visualization shows that the vortices have been repositioned near the centerline, whereas the range is highest at $1.5D$ for $\phi = 300°$, where dye visualization shows that the vortices are far from the centerline.

These two particular cases are also shown in Figure 3-19, in detail.

This data agrees with Anderson's conclusions regarding the interception mode generally resulting in a higher thrust coefficient [7], and resulting in higher mean centerline velocities due to the combined wake vortices having been reformed near the centerline. However, it appears that the centerline velocity magnitude is only a mild indicator of thrust production, as the thrust peak in this case is at $\phi = 120°$

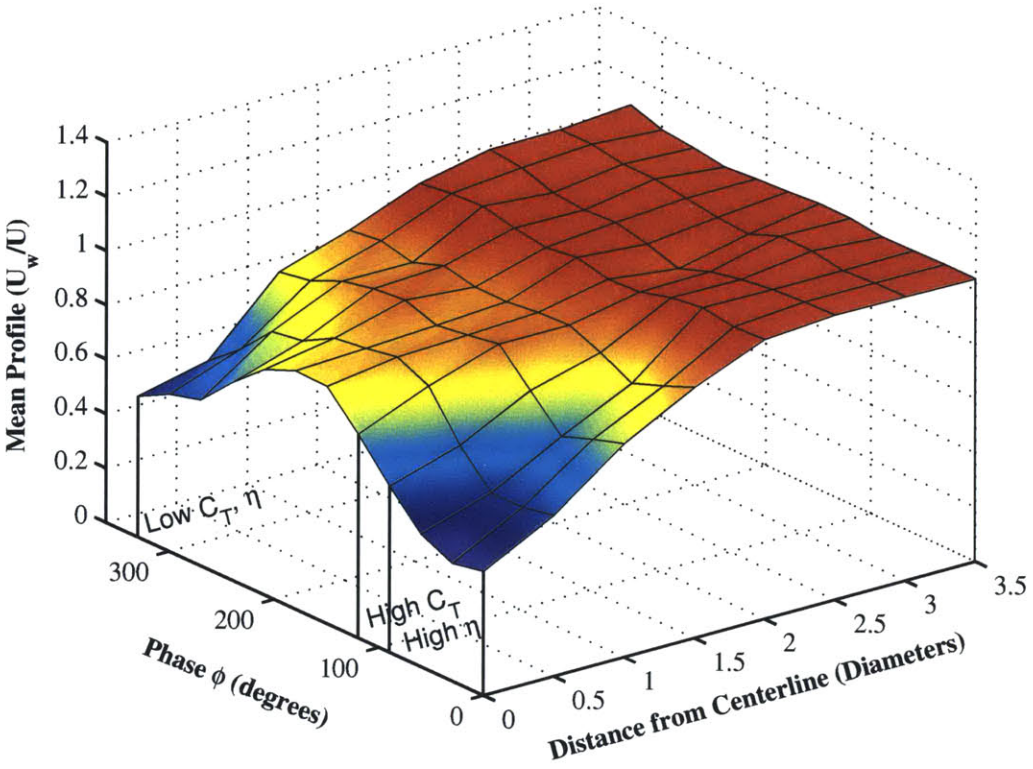

Figure 3-17: The mean velocity profile seen within the combined wake, as a function of foil / cylinder heave phase ϕ

while the peak of centerline velocity is at $\phi = 180°$. It should be noted that the anemometers measure velocity magnitude, and it is undetermined how this relation would change if the probes were measuring x-velocity only.

3.6 Variation of Foil Motion Parameters

The previous runs all showed better performance while moving with the leading-edge nearly in-phase the wake, in three different wakes. However, all tests were performed using the same foil motion parameters, and it was necessary to see if this interception mode is reasonable as a general rule, or if its dominance is only really a function of the particular foil motion used in those tests. A systematic set of tests was thus performed, varying all foil parameters within an identical wake.

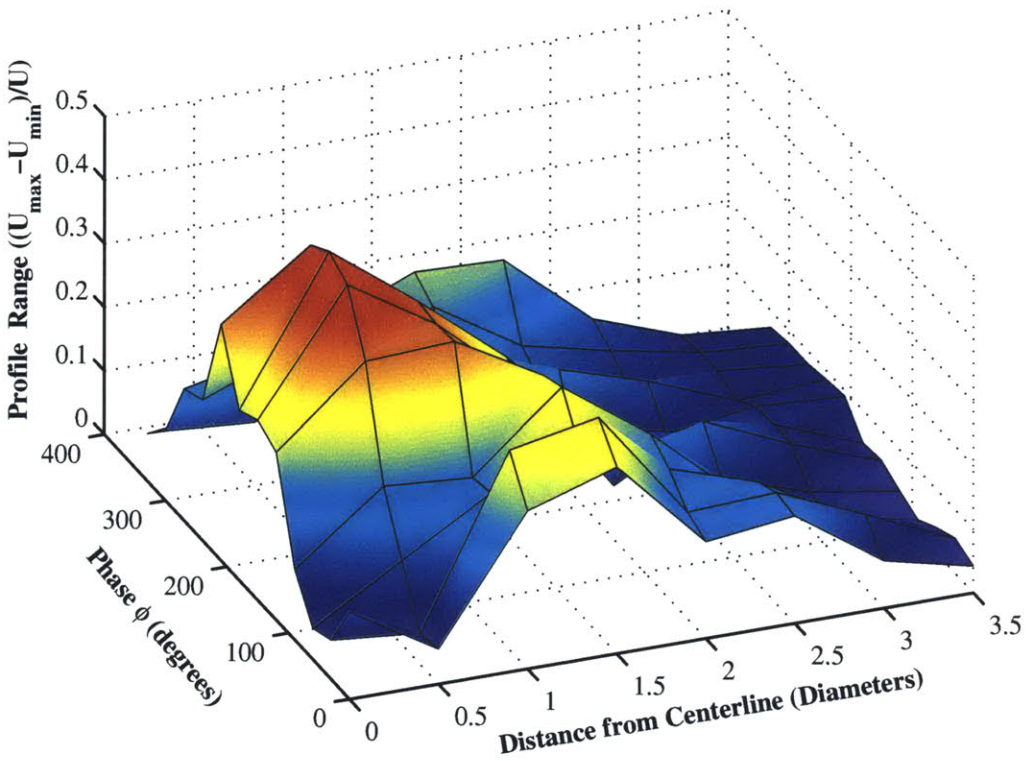

Figure 3-18: The range of velocities seen within a period of the combined wake. Note that the range is highest nearer to the centerline for $\phi = 180°$, which was shown by dye visualization to have vortices repositioned near the wake centerline.

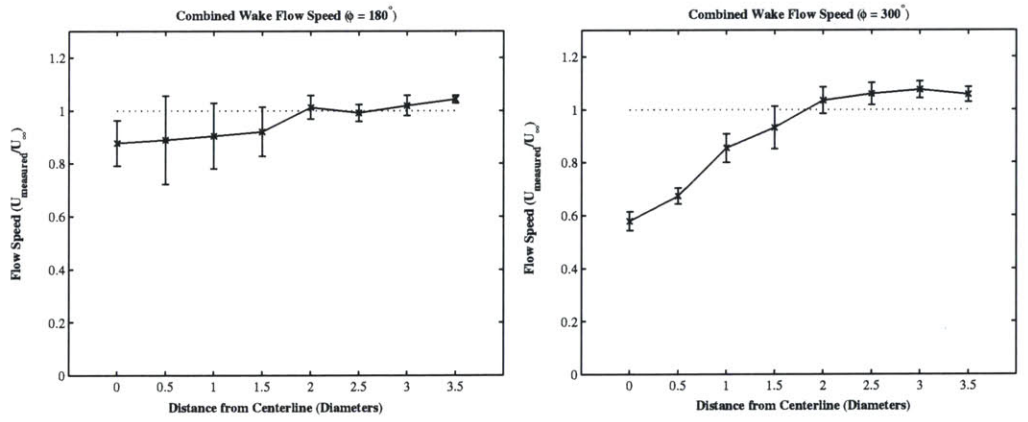

Figure 3-19: High centerline velocities are seen for $\phi = 180°$, left, while the profile for $\phi = 300°$ looks very similar to that of a cylinder alone.

$Metric$	ψ	θ_0	ϕ	H_f	α_{max}
C_T	$0.47/rad$	$-0.39/rad$	$\pm 0.15/rad$	$1.25/D$	NA
η	$-0.18/rad$	NA	$\pm 0.03/rad$	NA	$-0.68/rad$

Table 3.2: Average Sensitivities to Foil Motion Parameters

The following parameter space was searched, all within a $H_c = 0.50D$, $St_c = 0.20$ wake, with a foil and cylinder separation of $5D$: $H_f = 0.5, 0.75, 1.0D$, $\psi = 80, 90, 100°$, $\phi = 0, 60, 120, 180, 240, 300°$, and $\theta_o = 26.13, 39.19, 52.25°$. The values of θ_o were chosen so that, for each value of H_f, one of the θ_o's would correspond to a maximum angle of attack to a uniform incoming flow (α_{max}) of 6°.

The foil thrust and efficiency for $\psi = 90°$ is shown in Figures 3-20 and 3-21, respectively. As can be seen, thrust universally increases with increasing H_f, and generally increases with decreasing θ_0 from $\theta_0 = 52.25$ to 39.19°. Efficiency is highest along the plane correlating to $\alpha_{max} = 6°$, with the low H_f, low θ_0 end of that plane showing the highest efficiencies. Thrust is universally highest along the interaction phase previously associated with the foil leading-edge position moving in-phase with the wake. Efficiency, however, shows no real strong dependence on interaction. Also, thrust increases and efficiency decreases with increasing ψ (not shown).

The average sensitivities to each input parameter is given in Table 3.2. Note that the numbers for the variation of different parameters can not be directly compared, due to the different units. What Table 3.2 does illustrate, however, is whether or not one could expect to be able to follow a gradient in any given direction. As can be seen, efficiency is not very sensitive to ϕ, and thus is not very sensitive to the interaction mode.

The data in Figures 3-20 and 3-21 show how the thrust and efficiency vary with the interaction mode over a wide range of reasonable foil motions. In application, however, one would not want to limit oneself to varying the interaction phase alone in order to vary the performance of the propellor. One would usually aim at a needed thrust, and vary any available parameter to meet that thrust at the highest efficiency. Through interpolation of this data, it is possible to pick out a location of highest possible efficiency for a given needed thrust, through searching along a

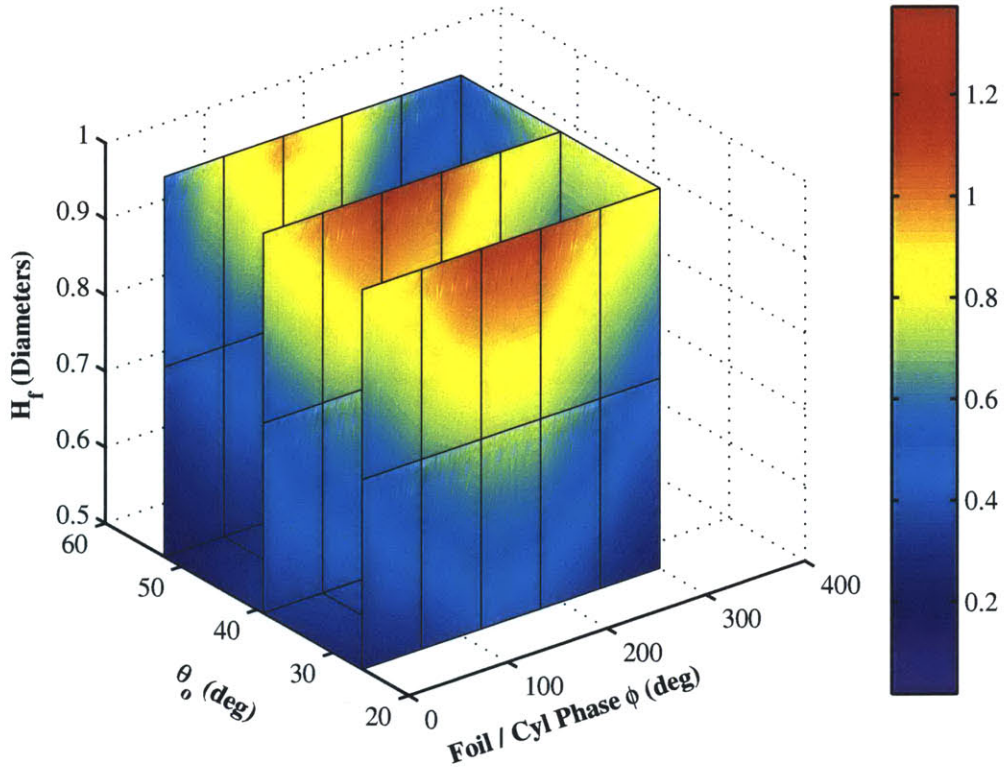

Figure 3-20: Thrust coefficient as a function of ϕ, H_f, θ_o for $\psi = 90°$

particular thrust isosurface.

As can be seen in Table 3.3, for higher thrust coefficients, the optimum foil/cylinder phase ϕ corresponds well with the phase found earlier corresponding to in-phase motion and the interception mode. At lower thrusts, however, the phase clearly moves away from in-phase ϕ's.

Certainly one cannot expect that an arbitrary incoming wake will happen to correspond with that used in these tests. However, the results of this test matrix provide at least a qualitative outline as to the effects of changing various foil motion parameters within a wake, which likely remain generally similar for a wider variety of incoming wake frequencies, amplitudes, and strengths.

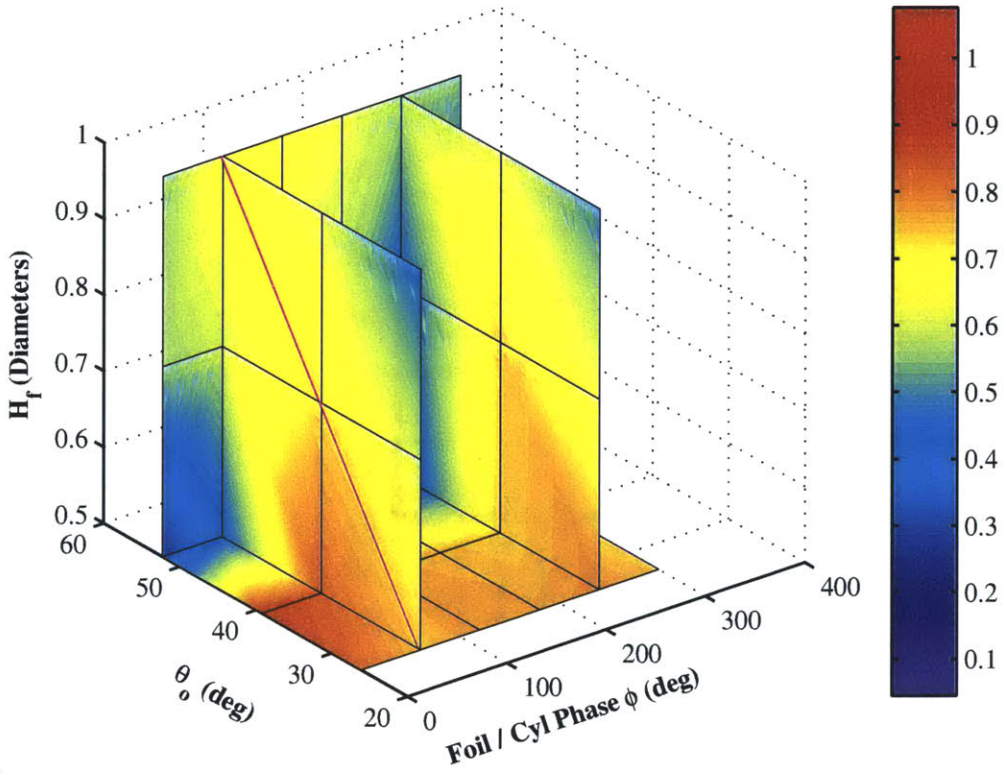

Figure 3-21: Efficiency as a function of ϕ, H_f, θ_0 for $\psi = 90°$. The magenta line demarks $\alpha_{max} = 6°$.

3.7 Comparison of Trout and Foil Motion

We have now shown that there are advantages to synchronizing with an incoming vortex wake beyond that of drafting within a velocity deficit alone. This has been seen with mechanical hydrofoils as well as with rainbow trout. The question we pose next is whether the trout and the foil are making use of the same techniques.

Before comparing the interaction strategies seen with the foil and the trout, the differences between these systems should be identified. Firstly, the trout has a very small 'span' relative to the length of the columnar vortices in the flow channel, whereas the foil has the same span as the cylinder used in the towing tank tests. Therefore, the foil can actually affect the global flow, as we have seen by its capability to reposition the wake vortices. The trout likely has little effect on the global flow; in fact, a few

C_T	η	ψ	θ_0	ϕ	H_f
.3	.894	80°	26.13°	22.5°	.531D
.4	.830	90	39.19	30	.563
.5	.786	90	39.19	52.5	.625
.6	.749	90	39.19	75	.688
.7	.735	90	39.19	187.5	.750
.8	.704	90	39.19	187.5	.813
.9	.673	90	39.19	180	.875
1.0	.673	90	52.25	120	1.000
1.1	.635	90	44.09	120	1.000
1.2	.601	92.5	39.19	120	1.000
1.3	.575	98.75	39.19	120	1.000

Table 3.3: Foil motion parameters showing the highest performance for a given needed thrust, for a $H_c = 0.5D$, $St_c = 0.20$ wake

diameters downstream, the columnar vortex would likely fill in any effect that it had.

Secondly, the flow around the fish was visualized in a plane near to but above the fish. However, in the dye experiments, the flow around the foil was visualized in a region that is likely significantly altered by the foil's presence. In order to compare the phases seen, the phase of vortex approach must be measured without the foil present. Hence, a better comparison between the foil and trout work would be the results presented Section 3.5.2, where anemometers were placed in the flow at various points downstream from the cylinder, without the oscillating foil present. It was found that the foil would speed up the interaction with the vortices by 30-40°, altering the wake interaction phase towards in-phase motion from that seen with the anemometers without the foil present.

The flow around the foil, with its long span and end-plates, can be seen as two-dimensional, whereas the flow around the trout is three-dimensional. The foil chord is rigid, whereas the trout's stiffness is variable along the body, as well as controllable by the fish itself, within some range. Also, it is uncertain whether to treat the trout as a whole as the 'foil' in the wake, or just its tail. Clearly, in a uniform flow the tail will create most of the thrust. But in the wavy stream, the lifting ability of a surface will be a key characteristic as to how it interacts with the wake. To compare, the body had an approximate 'span' of 1", with a 'chord' of 4", while the tail had a

'span' of 1", and a 'chord' of 0.5". As the lifting ability of low-aspect ratio wings is proportional to its aspect ratio as well as the area [1], the approximate lift ratio of the body to the tail would be $\frac{AR_{body}A_{body}}{AR_{tail}A_{tail}} = 1$, implying that the entire body makes as good a lifting surface as the tail alone, and that neither can be ignored.

With both the fish and the foil, the phase difference between lateral motion and the wake was identified. However, in the trout experiments, the wake phase was defined using the wake function W(x,t), calculated using the lateral-sum of vorticity passing a point downstream from the cylinder, while in the foil experiments, the wake phase was defined using the wake signal S(x,t), defined as the difference in flow velocities seen by two probes equidistant from the wake centerline, at the same downstream location. In order to ensure that these two methods return similar results, two virtual 'probes' were placed in the PIV flow field, each returning the velocity magnitude seen at that location, as illustrated in Figure 3-22. As the flow field was not wide enough to split these probes $3D$ apart, as was done in the anemometry experiments, they were positioned $2D$ apart instead.

The two signals returned similar results, as seen in Figure 3-22, although the wake signal led the wake function by $30.35 \pm 12.24°$, which was nearly the same as the resolution, in time, of the PIV data, at 30°. This value should be seen as a magnitude of error between comparing these two methods. It should be noted that this error tends to the opposite direction as the error introduced by the foil thrust accelerating the vortex wake, as discussed in Section 3.5.2.

The reason why the wake signal was not used in both situations is that the wake function, measured using the vorticity crossing a plane lateral to the downstream flow, is intrinsically related to the phase of the lateral flow in the wake, and is a considerably more powerful concept than that of the wake signal. The wake signal has no intrinsic relation with the local flow in the wake — which, to the foil or fish, matters far more than the proximity to a vortex — and should only be seen as an estimate of the wake function, and then only for cylinder drag wakes. For instance, if the wake being followed were an inline wake, rather than a drag wake, the wake function would still reveal the phasing and sign of the lateral flows in the wake, whereas the wake signal

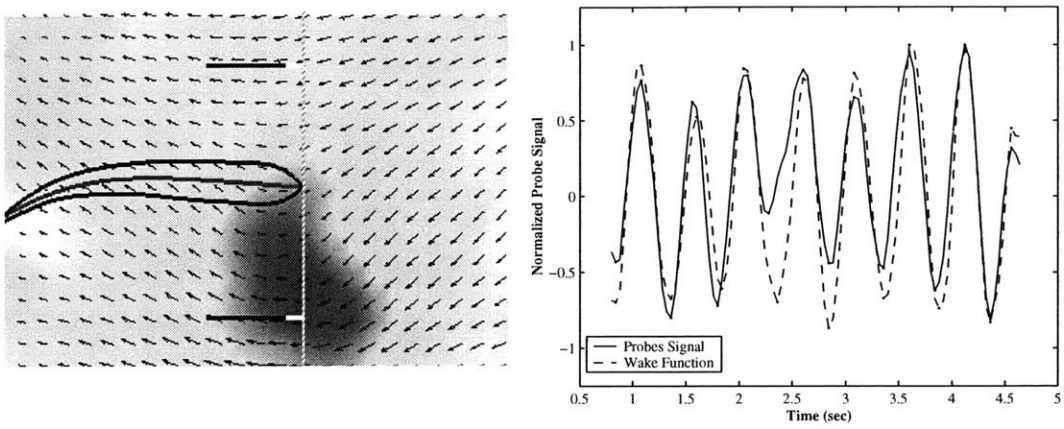

Figure 3-22: Two virtual 'probes' were placed into the PIV data, left, in order to compare S(x,t) with W(x,t), right

would be useless. Indeed, the wake signal was only used because the information required to calculate W(x,t) was not available using the sensors on-hand. A sensor which measured the lateral flow at the centerline could also have been used in these experiments, and would have returned information similar to W(x,t), but at a 90° phase-shift. The use of such a sensor for future experiments is highly recommended.

The work with the live fish found that they generally move out-of-phase with the wake, as discussed in Section 2.3, meaning that the trout's lateral velocity is in-phase with the local lateral flow, with the head leading the wake function by 100°, the center-of-mass by 160°, and the caudal fin by 240°. Whereas the dye visualization with the foil, from Section 3.5, correlated high thrust with leading-edge interception, the anemometry revealed that the foil was moving with the leading-edge leading the wake by 50°, and the trailing-edge by 140°, resulting in only a 50° difference if one were to compare the foil leading-edge to the fish nose.

Whereas the dye visualization was performed at a foil/cylinder phase of 100°, many of the optimum parameter sets for a given thrust, found in Section 3.6, were at a ϕ lower than that. In fact, for lower thrusts, the motion approximates the interaction phase seen for the trout, as seen in Figure 3-23. Considering the differences between the systems, these numbers should not be taken as a hard comparison, and one should

focus rather on the general similarities between the strategies seen for the fish and foil.

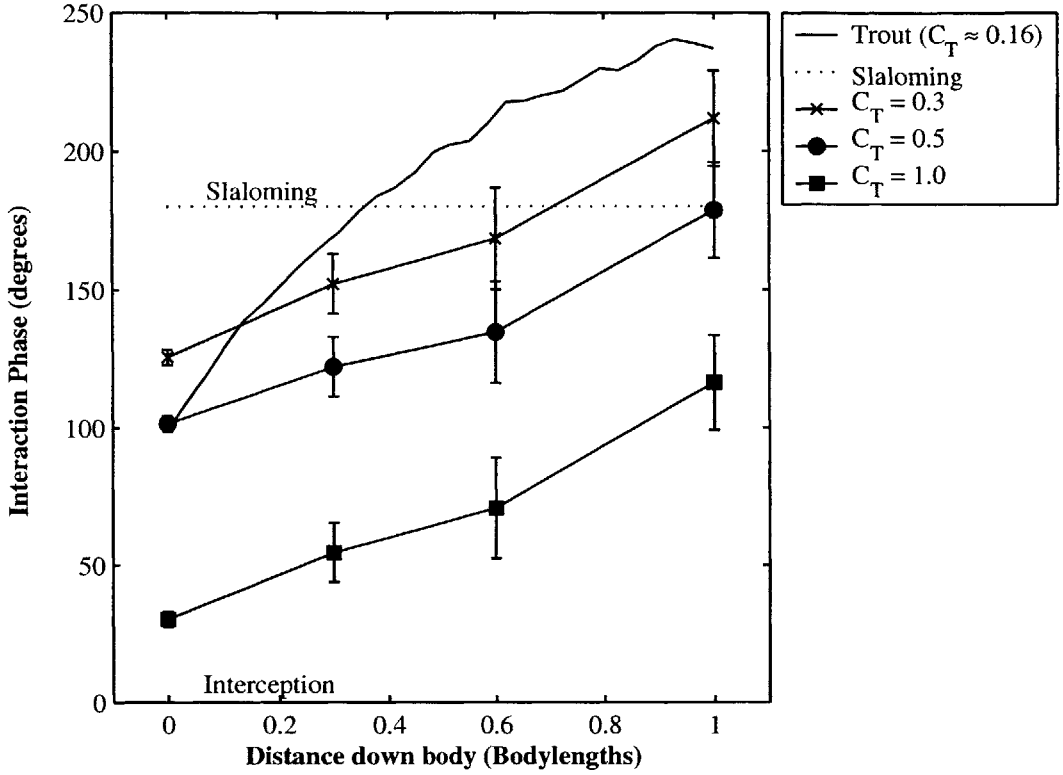

Figure 3-23: The phase between lateral motion and the untouched wake for the fish and for three of the 'optimal' foil thrusts. The distance down the body is measured from the nose to tail for the fish, and from the leading to trailing-edge for the foil.

The thrust coefficient necessary for the trout tail to move the body through the water could be approximated using $A_{wetted} = 8in^2$, $A_{tail} = 0.5in^2$ and $C_D = 0.01$ giving $C_T = C_D \frac{A_{wetted}}{A_{tail}} = 0.16$, where the value for C_D is a reasonable approximation from Videler [52]. Considering the information in Figure 3-23, it does not seem surprising that the fish swims at the phase that it does. Indeed, despite all of the differences between the systems, it appears that the foil and fish are taking advantage of the same mechanism in the wake. In both cases, the wake creates an alternating flow across the foil and tail. When combined with the foil apparatus yoke or fish body acting as an anchor in the flow, it can increase the thrust produced by the foil to the point where a passive tail can propel a dead fish upstream.

3.8 Summary

The tests with the foils and fish encompass 2 out of 3 parts of the spectrum of cases regarding foils in Kármán wakes. Most of the tests performed with the 2-D foil represent the use of a propellor which is required to produce high thrust, whether for maneuvering, or because it needs to overcome a significant drag on a large body. For these tests, the results have shown that a strategy where the foil heave motion opposes the lateral flows in the wake can be optimal. The fish, however, and tests performed with the foil at low amplitude, represent the middle of the spectrum, where little thrust is necessary, and a premium is placed on using minimal power. It should not be surprising, then, that swimming out-of-phase with the wake would be the path of least resistance, as the foil or fish moves with the lateral flow instead of against it.

Chapter 4

Active Wake Synchronization

In order to best make use of the performance gains from an incoming wake it is necessary to lock-in to the wake frequency at the proper phase. In application, however, it would be a rarity when an incoming wake was fully known in both frequency and phase. A method was developed that would enable the foil motion control system to detect and properly synchronize with a wake of unknown frequency, amplitude, and phase, within a frequency range realistic for the foil apparatus.

Additionally, it is necessary to be able to position the foil propellor to the centerline of the wake, the location of which will also not be typically known, in order to maximize the reduction in drag due to the velocity deficit and avoid non-zero mean lift on the foil propellor. Since this would probably involve moving the entire vehicle into the wake center, this was considered a different sub-problem from the frequency and phase synchronization problem, and is discussed further in Section 4.2.

The synchronization and wake centering systems were designed to use simple sensors and calculations, so that the methods presented here may remain relevant when applied in practice.

4.1 Wake Synchronization

In order to utilize a vortex wake in front of a flapping-foil apparatus, it is necessary to be able to synchronize to the frequency of that wake at an interaction phase found to

be desirable for performance (i.e. in- or out-of-phase with the wake). Two methods for doing this are presented below, and are compared to the default case where the foil motion is controlled with *a priori* knowledge about the incoming wake.

To be considered satisfactory, the methods should be able to synchronize to wake frequencies in a range from 0.5 to 2 Hz, converge to within 10 degrees of the desired phase within 10 seconds, and be able to withstand a sudden loss of or change to the wake frequency without sudden or unreasonable reactions and while retaining a sinusoidal oscillatory behavior.

Additionally, the synchronization system should be both relatively simple computationally as well as at least indirectly applicable to real-world situations (ruling out, for instance, using PIV to illustrate the flow field). We chose to use a pair of anemometers to measure the flow, located at the same distance upstream from the foil and located above and below the foil centerline. When passing through a vortex wake, the difference in the velocities measured by the probes yields a sinusoidal-like signal with a frequency equivalent to the wake frequency, and a phase defined by the times at which vortices pass the upper and lower probes.

In conclusion, the system should use a minimal amount of incoming information in order to synchronize in frequency and phase to the incoming wake.

4.1.1 Experimental Setup

All tests were performed at the MIT Towing Tank, using the apparatus described in Chapter 3. The wake was created by oscillating the cylinder in heave at a given frequency and amplitude. All tests hereafter were performed with $St_c = 0.20$ and $H_c = 0.5D$ unless otherwise specified.

The wake was measured using a pair of TSI 1231W conical anemometers located a fixed distance upstream from the foil, as shown in Figure 4-1. Subtracting the lower probe's signal from that of the upper probe results in a sinusoidal-like signal of the same frequency as the wake, with a phase corresponding to a peak in signal when an upper vortex passes, and a trough in the signal when a lower vortex passes. Locating the probes upstream from the foil gives the control system time to work as

the vortices translate downstream towards the foil, as well as reduces the effect of the foil motion on the wake signal.

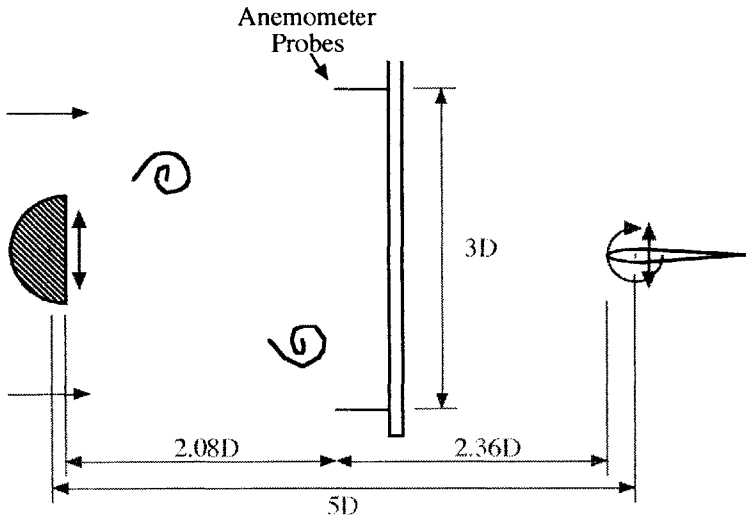

Figure 4-1: Diagram of the foil/cylinder synchronization setup

We chose to use the anemometers due to experience with the sensors and the existence of probes, amplifiers, and multiple mounting arrangements already present on the carriage. Additionally, the signal produced by these sensors ties in nicely with the Wake Signal defined in Chapter 3 and the Wake Function defined in Chapter 2, which should all ideally return signals with the same frequency and phase.

The anemometer pair is by no means the only flow sensor setup that could be used for synchronization. A single y-velocity sensor, measuring the lateral flow behind the cylinder and mounted at the centerline of the wake, would also give the information necessary to synchronize in both frequency and phase. In application, one would not wish to use fragile anemometer probes sticking out into the flow. The probes represent the flow sensors on a foil-propelled vehicle, such as pressure sensors on the hull located upstream of the foil propellor, or a Doppler-Velocimeter looking at the flow incoming towards the foil. Either of those systems would give the information necessary to use the methods in this chapter, with little modification.

The anemometers were placed $3D$ apart, centered on the wake centerline, mounted

to an aluminum foil-shaped strut attached to the carriage. This distance was seen to give a strong sinusoidal-like signal, as implied by the high range of velocities seen at $1.5D$ from the centerline in the anemometer wake plots in Chapter 3. Although the system was seen to work even when the signal produced by the anemometer pair was less sinusoidal, it was clearly desirable to get the clearest signal possible, at least for the first look. Different wake widths would likely have different 'optimal' anemometer locations. However, an array of flow sensors could be used with little change in the principles put forth in this chapter.

The foil heave and pitch motion was then set to follow the phase of Wake Signal produced by the anemometer pair. This was attempted experimentally and resulted in essentially instantaneous phase-locking at the proper frequency. However, the system would also follow every inconsistency and low-frequency noise in the input signal, resulting in erratic motions when the incoming wake collapsed if the cylinder frequency was suddenly changed during the run. Additionally, the motion would be non-symmetric about the motion centerline if the anemometers were not exactly centered in the wake. Since it is assumed that wake inconsistency would be more common than not in application, the addition of a phase-smoothing method was required to ensure that the system worked smoothly and robustly when the incoming signal was imperfect.

4.1.2 The Synchronization Algorithm

Within a strong and steady wake, the signal from the anemometer probes approximates a sinusoid. In the laboratory, it is a sinusoid with high frequency noise, uneven amplitude, and slightly non-steady frequency. In the wild, the signal would be even worse, with an unsteady flow speed, unsteady frequency, significant levels of turbulence, and imperfect shedding from some not-quite cylindrical object, such as a branch or rock. And when the sensors are not centered within the wake, the signal favors one side over the other. For a synchronization method to be useful, it would need to be robust to many of these conditions, or some laboratory approximation to these problems.

In order to deal with these issues, the signal was manipulated with digital filters, as seen in Figure 4-2. Firstly, the signal from the anemometer probes is passed through a 2 Hz 4th-order low-pass Chebyshev filter to get rid of any high frequency noise or signal harmonics. The foil actuator is limited to less than 2 Hz motions, so there is no penalty for setting the break frequency this low.

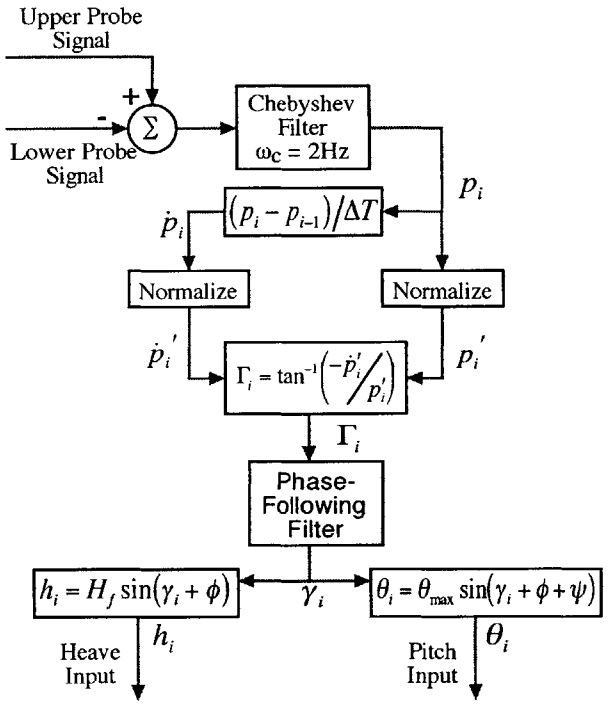

Figure 4-2: The input signal from the anemometer pair is filtered, then its phase is calculated and passed through an additional filtering method before being passed on as the input for heave and pitch motions.

It was desired to estimate the arrival time of the vortices at the foil downstream position. The 2 Hz filter can be modeled as a constant time lag for frequencies within the pass band (see Figure 4-3). Given that the probes are located upstream from the foil, this time lag can be accounted for later.

The vortices were assumed to translate downstream at $0.71U$ [9], which, from experiments performed previously using anemometry, appears to be a reasonable rate. Using the distance between the probes and the foil, we could estimate the time required for a vortex to pass between the probes and the foil. Subtracting the time lag

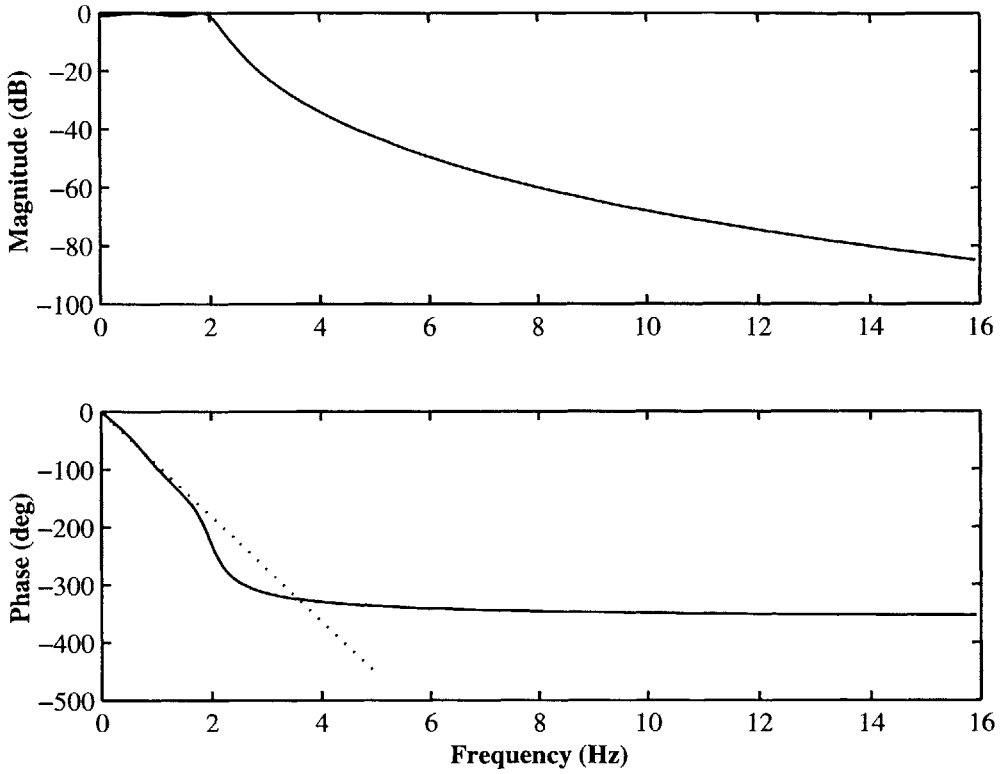

Figure 4-3: Bode plot for the 2 Hz 4th-order Chebyshev filter. In the phase plot, the dotted line represents a linear fit to the system phase in the pass-band. This can be used to estimate a constant delay for the filter.

from the low-pass filter, we could then estimate the total delay between the filtered probe signal and the foil, allowing the foil to phase-lock with the expected wake at the leading edge.

However, as seen in Section 3.5.2, the foil produces significant thrust, and significantly effects the upstream wake. In particular, the rate of vortex translation is increased, making the estimate above rather useless. To add to the difficulty, this change in rate would likely vary with changing foil thrust, amplitude, and wake width, requiring a complicated calibration in order to estimate the effects *a priori*. In the experiments that follow, we simply synchronize the foil to the wake signal at an interaction phase found by previously doing forced-motion tests with the desired motion parameters, at the desired foil/cylinder heave phase ϕ. Presumably in application a

second set of flow sensors could be placed upstream from the existing set, allowing the algorithm to better estimate the vortex translation speed, which is even more important if one considers that the estimate as calculated previously requires reasonable knowledge of the uniform flow speed, which may not be available to a vehicle in a wake.

The phase of the filtered signal can be found using a Hilbert transform. Due to the complexity and time required to do the Hilbert transform in real-time, one was mimicked using the normalized signal and its derivative to form a quadrature signal. The phase then can be found using an arctangent. The signal and its derivative were normalized using a max-function with a relaxation parameter, as follows

$$p_{max,i} = \max\{p_i, \quad p_{max,i-1} - \epsilon_1\} \tag{4.1}$$

$$p_{min,i} = \min\{p_i, \quad p_{min,i-1} + \epsilon_1\} \tag{4.2}$$

$$p'_i = \frac{2p_i}{p_{max,i} - p_{min,i}} \tag{4.3}$$

$$\dot{p}_{max,i} = \max\{\dot{p}_i, \quad \dot{p}_{max,i-1} - \epsilon_1\} \tag{4.4}$$

$$\dot{p}_{min,i} = \min\{\dot{p}_i, \quad \dot{p}_{min,i-1} + \epsilon_1\} \tag{4.5}$$

$$\dot{p}'_i = \frac{\dot{p}_i}{2\dot{p}_{max,i} - \dot{p}_{min,i}} \tag{4.6}$$

$$\Gamma_i = \arctan\left(\frac{-\dot{p}'_i}{p'_i}\right) \tag{4.7}$$

where p_i is the filtered signal at time step i, p_{max} and p_{min} give the running estimate of the amplitude of p, ϵ_1 is the relaxation parameter, set to 0.00113 for these tests, p' is the normalized signal, $\dot{p}$ is the derivative of p, and Γ_i is the instantaneous phase of the normalized signal.

The relaxation parameter ϵ_1 in the normalization routine is an optimization between relaxing too much, resulting in a poor instantaneous estimate of the system amplitude, and relaxing too little, resulting in a poor adaptation to a changing signal amplitude. However, the system is not terribly sensitive to the choice, and the value given above was seen to work acceptably for all trials.

The normalization routine described above worked fine with little computation,

as seen in Figure 4-4. It should be noted that, while the relaxed p_{max} parameter runs into and moves up a new peak, the normalized signal is saturated with a 'flat-top' at one, as seen in the zoom-in in Figure 4-4. This discontinuity in the slope is easily removable with an additional filter, as described below.

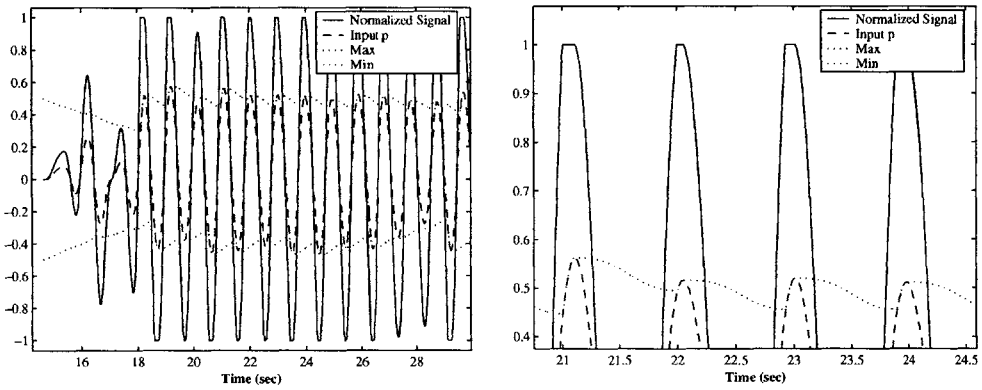

Figure 4-4: The normalization of the signal p, left, and a expanded view showing the 'flat-tops' created with the routine, right.

At this point the routine has filtered-out high frequency noise, and has calculated the phase of the incoming signal. If there were no inconsistencies in the cylinder shedding, this calculated phase could be directly applied to the foil heave and pitch commands, adding in any desired phase lag between the foil motion and the wake signal. This worked fine in the laboratory, where conditions are controlled, essentially giving rapid convergence to the desired phase and frequency (within two seconds). However, the response was erratic to wake inconsistencies, such as when the cylinder frequency was suddenly changed or even with just a bad shedding-cycle off of the cylinder. In any real application, this sort of inconsistency would likely be the rule, rather than the exception. Hence, two phase-following filters, which smooth the inconsistencies, were studied: Ermentrout's method, based on the flashing of fireflies, and the Stubborn Ramp Follower, a simple double integrator with a low bandwidth.

Ermentrout's Method

Fireflies exhibit the ability to synchronize their flashing to an external stimulus within a range of frequencies [48]. Some species will even do so with no phase loss, sometimes resulting in entire trees full of fireflies blinking together. A non-linear model for this synchronization was developed by Ermentrout [17].

These fireflies are able to synchronize, in frequency and phase, to an external stimulus within a small range of frequencies around the fireflies' internal-clock flashing frequency. Ermentrout's model basically sets up a system with a default flashing frequency. In the presence of an external forcing, it will begin to adapt its internal frequency towards that forcing frequency, as follows:

$$\begin{aligned} \frac{d\omega}{dt} &= \epsilon_2(\omega_{nat} - \omega) \quad + \quad P\Big\{ \max\Big(\sin(\gamma - \Gamma), 0\Big) \cdot (\omega_{min} - \omega) - \\ &\quad - \min\Big(\sin(\gamma - \Gamma), 0\Big) \cdot (\omega_{max} - \omega)\Big\} \end{aligned} \tag{4.8}$$

where ω is the output frequency, ϵ_2 is a relaxation parameter, P is a gain, γ is the output phase, Γ is the input phase from the filtered probe signal, and ω_{nat} is the default internal frequency. The output phase (γ) can then be used to control the position of the foil heave and pitch motions, plus or minus a desired phase lag for proper wake interaction.

This is a convenient solution for a few reasons. Its internal frequency gives it a default motion, which it relaxes back to even if the input stimulus disappears. Unlike most obvious solutions, this model doesn't utilize the input frequency, which is an inherently messy signal in practice. It ignores frequencies higher than ω_{max} and lower than ω_{min}, and will continue on with its default frequency if exposed to stimulus outside that range.

However, this model is not differentiable across the equilibrium ($\Gamma = \gamma$) due to the min and max functions, making the study of its particulars considerably more difficult.

For the following tests, $\epsilon_2 = 0.01$, $\omega_{max} = 4\pi$ radians/sec, $\omega_{min} = \pi$ radians/sec, $P = 1$, and $\omega_{nat} = 2.5\pi$ radians/sec.

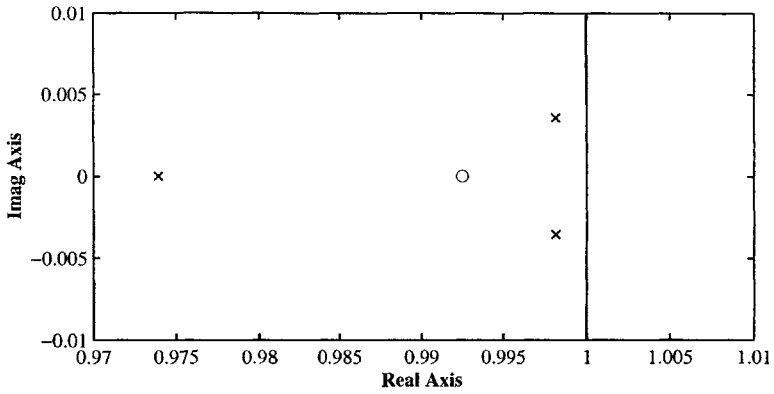

Figure 4-5: Pole-zero map of the closed-loop virtual system. The zero shown is a double zero. A zero also lies at z=-1 (not shown)

Stubborn Ramp Follower

A previous system was developed which used the phase of the filtered signal (Γ) directly as the input phase for the heave and pitch signals. While this worked to adequately synchronize foil motion to the wake, it was found to have poor robustness to imperfect wakes. That is, if the wake fell to noise for a few moments due to a sudden change in cylinder motion, the foil heave and pitch would follow the noise as well. Also, if the input signal was a poor sinusoid (whether because the wake was not centered on the probes or another reason), the output motion also suffered.

Hence, we desired to pass this input signal through a low-bandwidth virtual system which was capable of following a ramp with no lag (a 'stubborn ramp follower'). Since all that is required is a double-integrator (that is, a Type II system [38]), an open-loop system was invented consisting of the double integrator, one pole at $s = -3$, and a pair of zeros at $s = -1$ to encourage closed-loop poles to remain in the left half plane. The discrete closed loop system's pole-zero map, as seen in Figure 4-5, gives a feel for how the low-bandwidth system would ignore spontaneous wake inconsistencies, while still following the signal acceptably.

The discrete coefficients for the virtual system were read in by the control program before a run, and the input signal Γ was fed through the coefficients as a linear filter. As the filter was 3rd order, the current and last three values of the input and output

phases were stored.

Since, in its basic form, the system does not understand that $0 = 2\pi$, the SRF would continue to try to close a gap of several cycles unnecessarily, potentially reducing convergence time and unnecessarily working the system. In order to eliminate this problem, a phase-wrapping routine was set up, where if the difference between the input and output phase was greater than π or less than $-\pi$, all of the stored values for input and output phases were shifted by a multiple of 2π, so that the system is always trying to reduce the phase error reasonably, considering the periodic nature of the signals. Although this adds a non-linearity to the system, it is not near the equilibrium like it is for Ermentrout's method described above.

4.1.3 Results

The synchronization schema were run for three different steady-state cases. In Section 3.6, a matrix of tests determined the optimal foil parameters to run for the highest efficiency η available at a desired thrust. The synchronization method was tested at settings given for desired coefficients of thrust C_T of 0.5, 0.8, and 1.0 from Table 3.3, hereby referred to as Low, Mid, and High thrust coefficient, respectively. Five tests were performed for each treatment using each of Ermentrout's and the SRF methods, as well as forcing motion at the desired foil/cylinder heave phase ϕ for comparison. The forced motion tests were performed first, and the average phase between the foil heave and wake signal from the anemometers found during these tests was used as the desired phase lag for the subsequent synchronization schemes.

Both methods were seen to synchronize to the wake both quickly and smoothly, as can be seen in Figures 4-6 and 4-7.

The forced-motion C_T was approximately 0.1 higher than the previous tests discussed in Section 3.6, although η was similar within the scatter of data. This is likely due to the presence of the anemometer strut between the cylinder and the foil disrupting the flow and increasing the velocity deficit seen by the foil.

The thrust data shows decent agreeability between the synchronization methods and the forced motion, as seen in Figure 4-8, with Ermentrout and SRF averaging

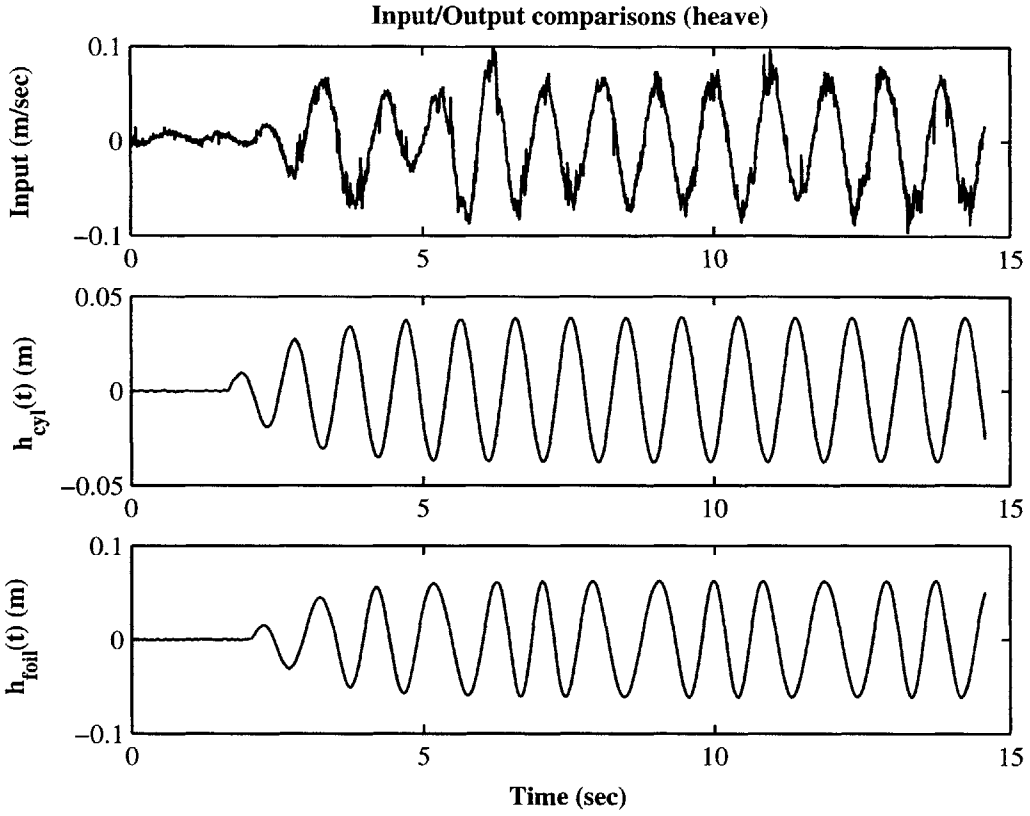

Figure 4-6: Ermentrout's method at the beginning of a run, showing rapid adjustment from the default frequency to the external stimulus

0.3% and 1.2% lower thrust than the forced-motion tests, respectively. The efficiency data show high variability from run-to-run for the low C_T (4-8) case for all three methods, but, in total, Ermentrout and SRF averaged 1.7% and 2.1% lower efficiency than the forced-motion trials. Efficiency may be more sensitive to variation in frequency during the run, and some runs may have had more variability than others, resulting in some 'poor' outliers and a scatter tending towards lower efficiency for the synchronization schema.

Both synchronization schema showed an excellent ability to find the correct phase (4-8), with Ermentrout off by only 0.05°, and SRF lagging by 5.2°. This error was likely caused by loss of digits in the virtual system coefficients during discretization or transferral of the coefficients to the control program from MATLAB, where they were created. Filters kept in coefficient form, for the numerator and denominator of

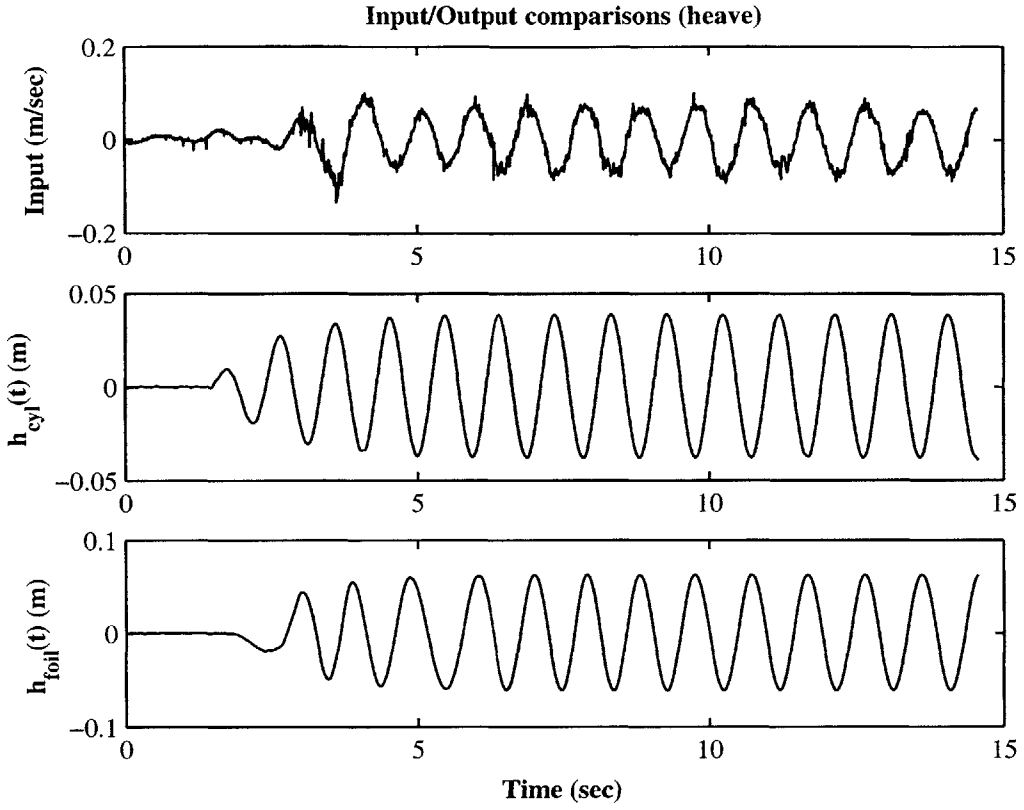

Figure 4-7: The Stubborn Ramp Follower at startup. Although these tests began with an initial output frequency of 0, the system rapidly converges to the input frequency

the transfer function, tend to be sensitive to numerical error, particularly at higher order. A potential solution would be to store and use the system in state-space form. This said, the error is not significant considering the broad performance peaks seen in Chapter 3, and is well within the phase accuracy necessary to take advantage of synchronization, so this alone would not be enough reason to disregard this method.

Ermentrout's method shows significant oscillations around the final frequency of 0.54 Hz standard deviation, as seen in Figure 4-9. These oscillations damp out slowly, if at all. Although audible, and disconcerting, this appears to have little effect on performance, and hence is not enough reason to disregard the method outright. Increasing the gain P in the method was seen to lead to faster convergence, but also reacts negatively to input noise, leading again to oscillations around the desired frequency, but in a less periodic fashion.

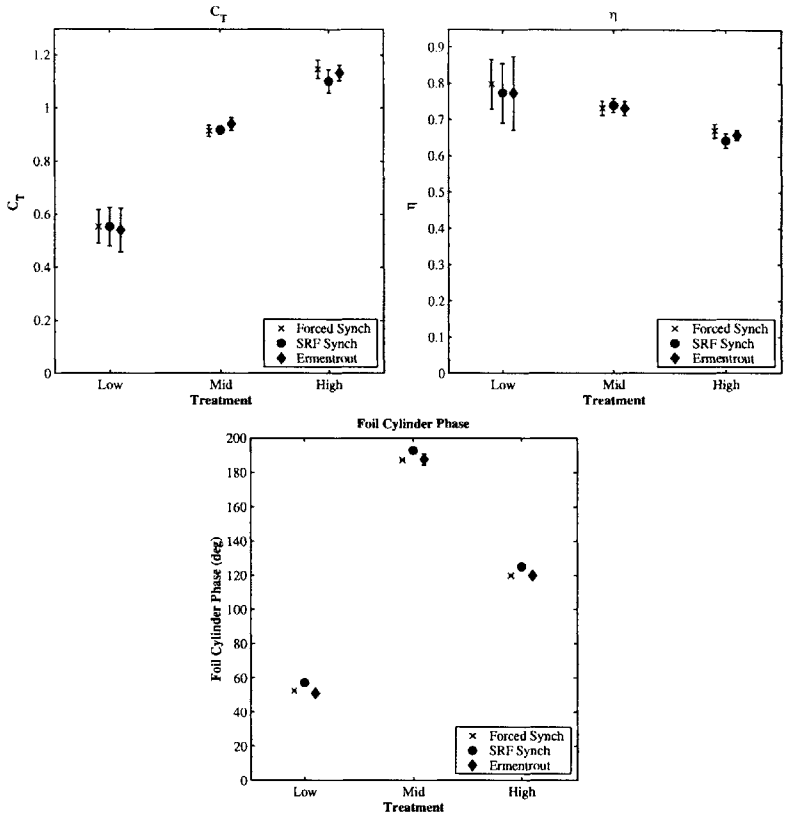

Figure 4-8: Coefficient of thrust, efficiency, and output foil/cylinder phase for the three treatments, shown for the three schema

The SRF method, however, matches frequency quickly and varies considerably less, with a standard deviation of 0.34 Hz, which was no longer audible. Similarly, Ermentrout's method oscillates around the desired phase, as seen in 4-9, whereas the SRF shows just noise after 5-10 seconds. However, the SRF shows a steady-state error of approximately 5 degrees, as previously discussed.

Ermentrout's method was found to converge within 45° of the desired phase in 5.6 ± 2.2 seconds, whereas SRF converged only slightly faster in 5.0 ± 1.4 seconds. Although Ermentrout's method converged to the correct phase, using an average over the run, the oscillation around that desired phase prevented us from calculating the convergence time using a value less than 45°, whereas SRF could use a much tighter bound.

Ermentrout's method converged to 20% of the cylinder frequency in 5.9 ± 2.4

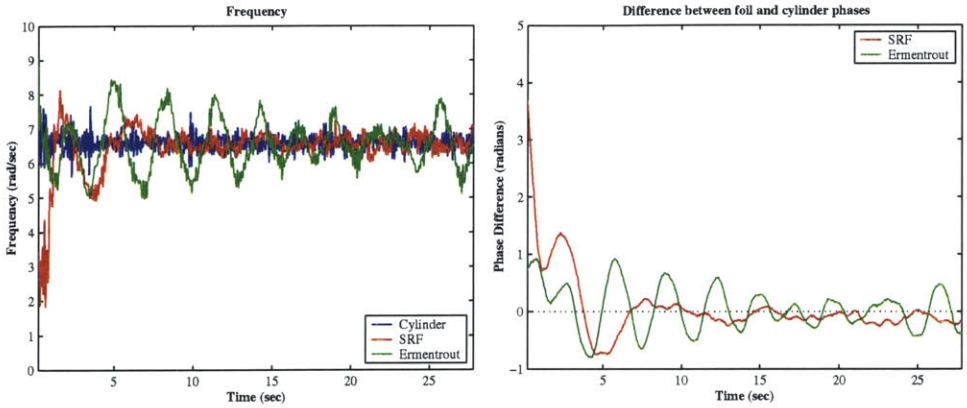

Figure 4-9: Instantaneous frequency (left) and phase (right) transients for both synchronization schemes. Runs shown are typical.

seconds, whereas the SRF did so in 4.0 ± 1.7 seconds. Again, the SRF could use a much tighter bounds, but the oscillations in Ermentrout's frequency would not allow it.

4.1.4 Robustness to Wake Variation

We then ran several experiments in order to test the robustness of the synchronization schema. This was done by suddenly changing the frequency and amplitude of the cylinder motion midway through the run. Tests were run with second-half frequencies of 0.75, 1.1, 1.2, and 1.5 Hz (whereas the first-half frequency was approximately 1 Hz for all runs). Switching cylinder frequencies suddenly often resulted in the complete loss of periodicity in the wake for a second or two, before rebuilding at the new frequency, as can be seen in Figure 4-10.

Both methods responded reasonably to this input, without sudden spikes in frequency or non-sinusoidal behavior, as in Figures 4-10 and 4-11. The frequencies understandably would ramp up or down to catch up to the new wake frequency and phase, as shown in Figure 4-12, in much the same way as during the startup transient.

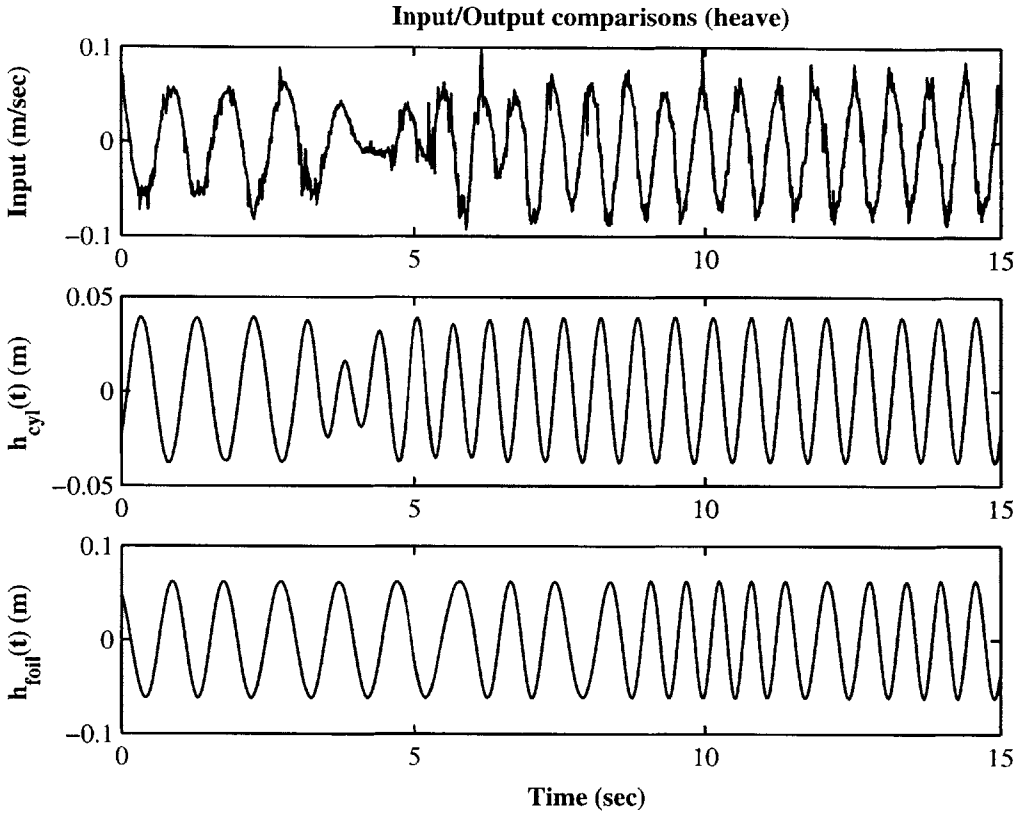

Figure 4-10: The transient response of Ermentrout's method to a sudden switch in the input frequency from 1 to 1.5 Hz

4.1.5 Discussion

Ermentrout's method has inherent advantages when it comes to ignoring input signals outside a desired range of frequencies, as well as having a default system frequency which the system can rely on when the wake disappears. That said, the SRF converges more quickly and has better noise rejection, and is a considerably easier system to study and understand, avoiding Ermentrout's strong non-linearities.

Either of these methods would work well in application. Some sort of gain scheduling would be required, as it is unlikely that a vehicle would spend all of its time within vortex wakes, and many wakes might be too weak to be bothered with. The anemometers could be replaced with many types of flow sensors without having to change the algorithms significantly, such as pressure sensors mounted on the vehicle

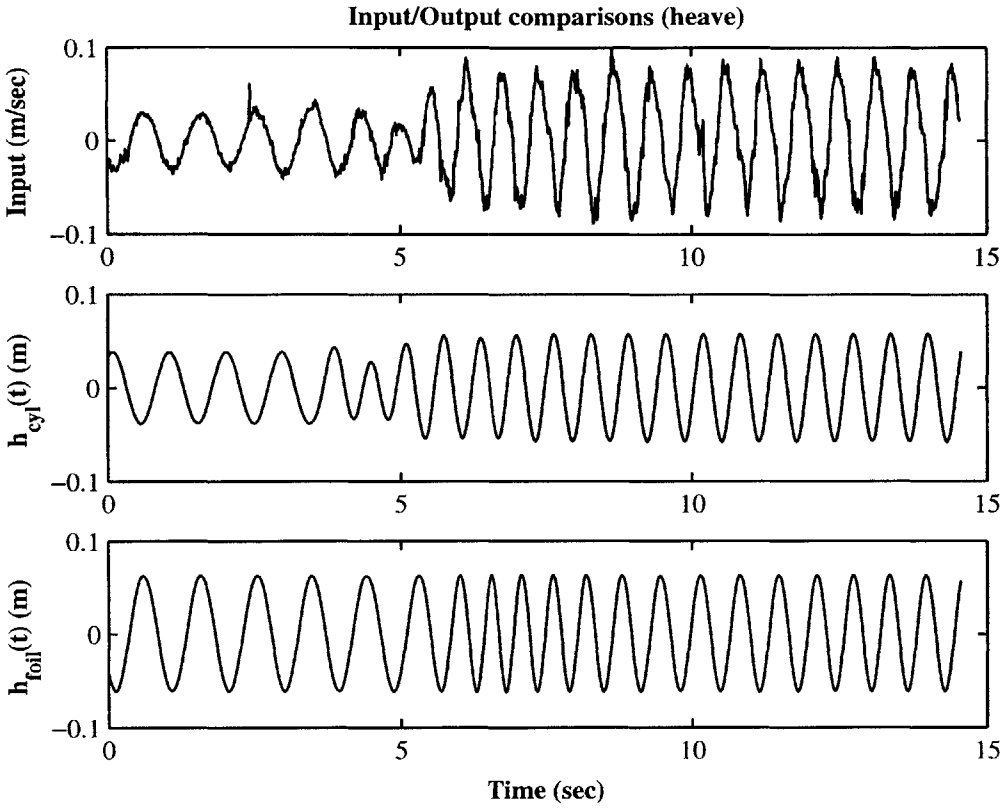

Figure 4-11: The transient response of the SRF to a sudden switch in the input frequency from 1 to 1.5 Hz

hull, or Doppler-velocimeters sensing the flow directly.

Both methods met the primary needs — a system that can follow a phase closely and robustly, with a performance similar to a forced system. Ermentrout's method oscillated around the desired frequency considerably. However, this did not appear to significantly effect the performance. The SRF was much better in this score.

4.2 Wake Centering

A vehicle would need to center itself within a wake in order to best take advantage of the velocity deficit to reduce its own body drag. A system was developed to center a vehicle within a wake, simply and quickly.

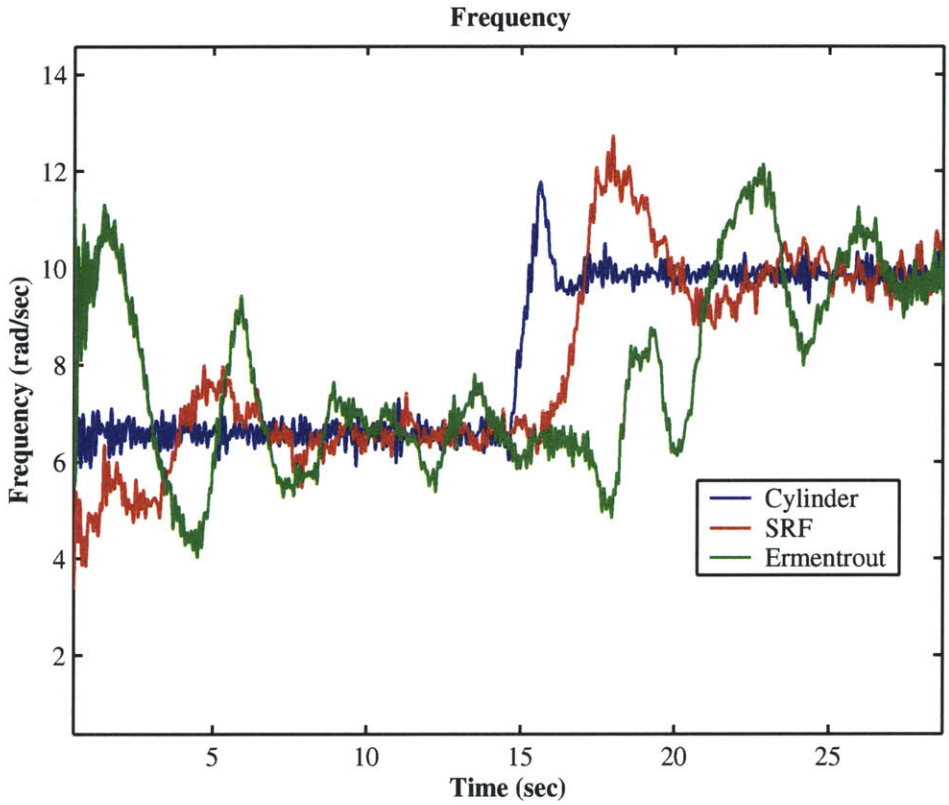

Figure 4-12: Transient frequency lock-in response for both synchronization methods. Cylinder frequency is changed suddenly once during the middle of the run, from 1 to 1.5 Hz, as a test of robustness to imperfect wakes.

4.2.1 Methods

In order to find the sensitivity of foil performance to an off-center position in the wake, some tests were performed at increasing offsets between the foil and cylinder mean positions. It was found that thrust and efficiency did not begin to degrade until the offset was greater than $0.5D$, for a $H_c = 0.5D$, $St_c = 0.20$ wake. However, the mean lift on the foil was non-zero, and grew with an increasing offset.

Two pairs of anemometers were mounted on the heaving linear slide usually reserved for the flapping foil, as seen in Figure 4-13. This allowed the control algorithm to move the probes so as to equalize the mean velocities seen by the upper probes with those of the lower probes.

The signal created by the difference of the sums of the bottom pair from the top

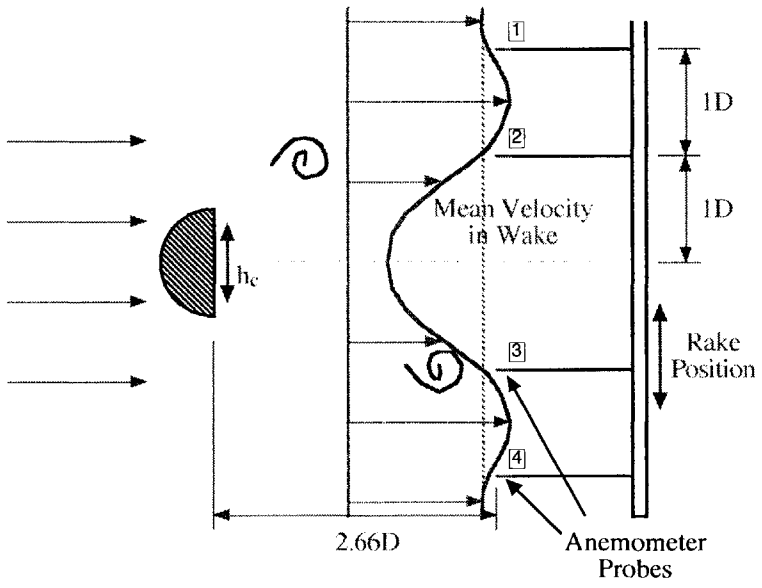

Figure 4-13: Four anemometer probes were used to center the anemometer rake within the cylinder wake

pair of sensors was passed through the normalization routine discussed in Section 4.1.2. The current measures of p_{max} and p_{min} were then used to find the mean of the merged signal, as seen in Figure 4-14. A proportional controller was then used to command the probe rake velocity in the direction of its equilibrium. Two pairs of probes are necessary to do this correctly; with one pair, the velocities can balance out off center if the wake happens to be a specific width relative to the probe separation.

Note that this method would not encourage a vehicle which is entirely outside of the wake to enter, as the system would never allow the vehicle to pass within the higher velocity 'humps' on either side of the velocity deficit 'well'. It is assumed that a vehicle which is tasked with station-holding within a strong current would first explore its environment to check if there are any regions with slower downstream flow, due to upstream obstacles or bottom conditions. If it finds a wake, it would then activate the wake centering algorithm, which fine-tunes the position of the vehicle, and the synchronization algorithm, which controls the frequency and phase of the foil

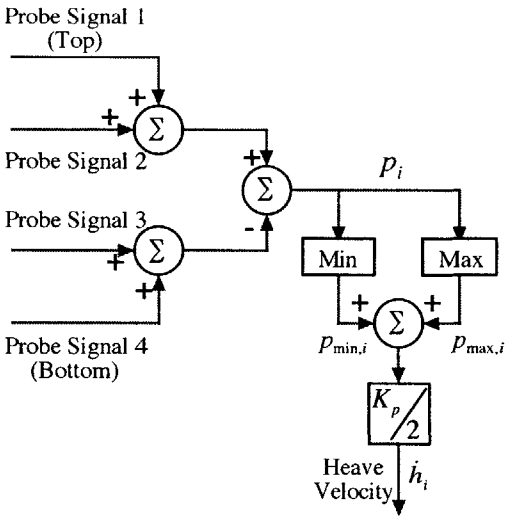

Figure 4-14: The wake centering algorithm. The mean difference in flow speeds seen by the top two probes relative to the bottom two is used to control the position of the probes within the wake.

propellors.

Tests were run within all three wakes studied in Chapter 3: $H_c = 0.5D$ with $St_c = 0.20$, $H_c = 0.75D$ with $St_c = 0.30$, and $H_c = 0.75D$ with $St_c = 0.33$. Tests were run with initial offsets of 0.5 and $1.0D$.

The anemometers used were TSI Model 1210-20W. A proportional gain of 10,000 counts/second, where the linear axis has 157,480 counts/meter, was used for all of these tests.

4.2.2 Results and Discussion

The wake centering routine properly centered the rake for all tests. The time of convergence to within $0.2D$ of the wake centerline averaged 5.8 ± 1.45 seconds, and the rake remained within $0.2D$ for the remainder of the run.

A typical centering run is shown in Figure 4-15. The system begins one diameter offset from the wake centerline, and converges to within 0.2 diameters of the center in approximately 6 seconds, and it stays within that band for the remainder of the run. The signals from all four probes for the same run are shown in Figure 4-16.

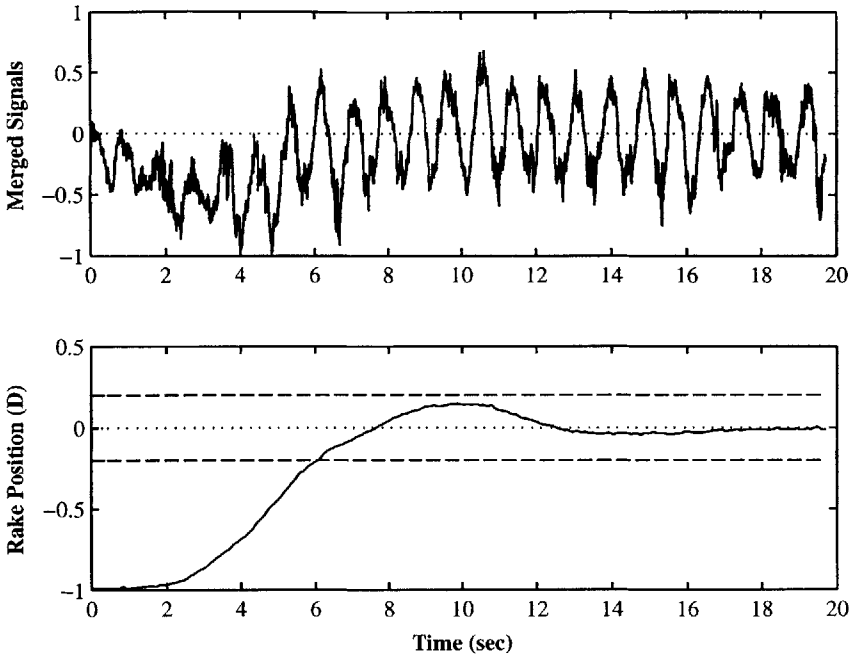

Figure 4-15: The position of the probe rake using the wake centering algorithm, for $H_c = 0.75D$ and $St_c = 0.33$ with a $1D$ initial offset. Dashed lines represent the $0.2D$ convergence band.

In application, the vehicle would center itself in the wake using this method, while simultaneously synchronizing its flapping foils to the wake frequency at the desired phase. By design, both controllers use a similar sensor setup as well as a similar controller programming structure, so a system with one could easily have both.

4.3 Summary

The foil synchronization algorithm was capable of locking-in the foil motion to any desired phase relative to the wake, and proved to be robust to brief losses of wake coherence and sudden changes in wake frequency. Using simple sensors and calculations, the system was capable of using information about the local flow in order to better the foil propellor's energy budget. As designed, the methods presented here would not be a significant burden in weight, space, or cost, enabling them to be easily added to vehicles for which wake synchronization may not be the primary consideration.

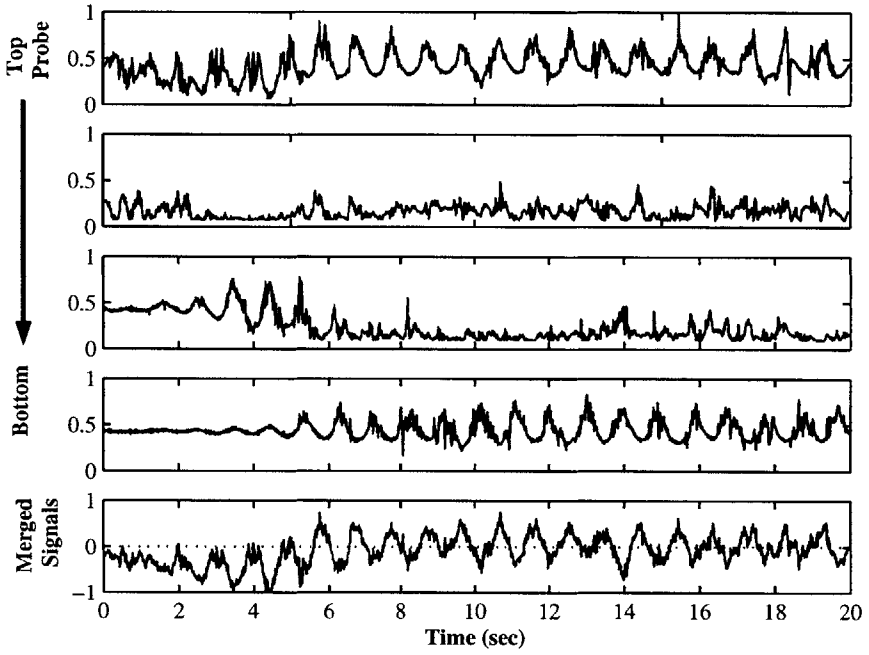

Figure 4-16: The individual probe signals, and the merged signal from all 4 probes, for $H_c = 0.75D$ and $St_c = 0.33$ with a $1D$ initial offset.

Chapter 5

Passive Energy Recovery in Wakes

A foil, through fluid-induced motion only, is capable of producing thrust with a negative hydrodynamic power input. This represents the energy extracting (and power generating) capability of the system. This was shown through the use of force-feedback to model the foil as if it were anchored to a passive spring-mass-damper, enabling the foil to produce a small amount of thrust as well as extract net power from the cylinder wake.

Although a body is incapable of extracting energy from a uniform stream without significant drag upon the body, as is the case of a windmill, Wu has shown that a foil heaving and pitching within a wavy stream is capable of producing thrust and extracting energy passively, through fluid-excited motion [57], as discussed in detail in the introduction to Section 2.4. Isshiki experimentally demonstrated passive thrust production with a foil in surface waves, compliantly mounted in heave and pitch [26].

Chapter 3 studied foils within a cylinder wake, where the foils were producing high thrust ($C_T \approx 1$), as would be the case for a foil propellor attached to a large or bluff body. In this case, a foil path where the lateral velocity of the flow opposed the foil heave motion, generally leading to a higher angle of attack, was found to be optimal. The lower thrust cases studied within Section 3.6 and with live fish in Chapter 2 both studied cases where the foil is only required to produce a small thrust ($C_T \approx 0.2$). In these cases, a path where the lateral motion of the body moved with the oscillating fluid was found to be optimal, allowing thrust production with low power input.

A third 'scenario' exists, where the foil produces only enough thrust to cancel its drag, while extracting energy from the oscillating flow. This represents a power generator, at the opposite end of the 'foil-in-wake' spectrum from the high-thrust cases studied. Whereas most generators which utilize flow streams have significant drag induced against them, a wavy-stream generator would be producing power utilizing the energy in the wake from the drag on a separate, upstream structure.

Although limited, this could realize an important subset of fluid-based power generators. Clearly it is not advantageous to build a 'wavy-stream' generator with low drag on the body if one needs to build a large bluff body with high drag upstream, as one could then just simply build a windmill or water turbine. However, if the drag producing body is already present, such as a rock in a stream, a building, or a ship, and some sensor or other machinery nearby is required to be portable and/or mobile, then being capable of extracting energy from the drag wake could be tremendously helpful. Examples of this could include a power supply for tiny sensors in streams, or to increase range on a vehicle designed to follow enemy ships or submarines.

5.1 Methods

We desired to test a passive foil moving forwards through an unsteady wake, with the foil motion in both heave and pitch modeled as if supported by a spring-mass-damper. All foil motion should be induced by the oscillating flow in the wake through the creation of an oscillating angle-of-attack across the foil, consequently inducing thrust production. Hence, the foil needs to extract sufficient energy to induce flapping of its body as well as create thrust and overcome resistance and losses.

Force-feedback enabled the use of the apparatus from Chapter 3 for the passive energy recovery tests. Using the measured forces on the sensors, the control system calculated the resulting velocities induced on the foil in heave and pitch, through a virtual spring-mass-damper, allowing easy alteration of the experimental system. Figure 5-1 illustrates the desired effect.

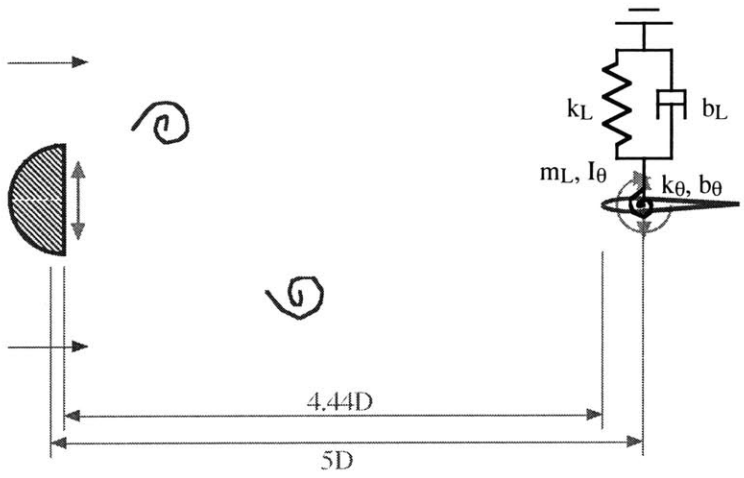

Figure 5-1: Through the use of force feedback, the foil is modeled as if supported by a spring-mass-damper in both heave and pitch

The desired virtual systems for the heave and pitch motions are as follows

$$L(t) = m_h\ddot{h}(t) + b_h\dot{h}(t) + k_h h(t) \tag{5.1}$$

$$\tau(t) = I_\theta\ddot{\theta}(t) + b_\theta\dot{\theta}(t) + k_\theta\theta(t) \tag{5.2}$$

where m_h, b_h, and k_h are the mass, damping, and stiffness of the heave virtual system, and I_θ, b_θ, and k_θ are the rotational inertia, damping and stiffness in the pitch direction. Equations 5.1 and 5.2 are coupled through the lift force and torque moment. For instance, moving in heave creates a torque about the foil pivot which induces motion in pitch, and vice versa.

In order to best model the virtual system presented above, the actual mass of the foil must be subtracted out and, since the pitch axis measures torque through the chain drive, the actual pitch damping and inertia should be subtracted out as well. The foil mass was measured as $m_{h,act} = .277\ kg$, but the sensor only sees half of that, as it measures force on only one side of the foil. The inertia and damping were measured by pitching the foil sinusoidally back-and-forth in air, at the desired frequency. The measured torque could then be broken down into components which

are in-phase with the position (which must be compliance or inertia) and components which are 90° out-of-phase with the position (which must be damping). Through this method, the pitch inertia and damping were estimated as $I_{\theta,act} = 0.000333\ kg\ m^2$ and $b_{\theta,act} = 0.00625\ \frac{kg\ m^2}{s}$, respectively.

Note that this value of $I_{\theta,act}$ will include the effect of the center-of-mass not being located at the foil pivot point. Additionally, the fact that the moment arm for the effects of gravity changes with pitch is not reflected in Equation 5.2 is also inconsequential, as the pitch angles measured in these experiments are small.

The state equations for heave and pitch, Equations 5.3 and 5.4 respectively, were developed in MATLAB in continuous time, discretized using a bilinear approximation, and then solved for the transfer functions relating the velocities $\dot{h}$ and $\dot{\theta}$ to the inputs L and τ before the coefficients were passed on to the C++ control code. The control code then solved for the current step's velocities using the current and last two values of lift and torque, and the last two values of the velocities, with a control-loop frequency of 250 Hz.

$$\begin{bmatrix} \dot{h}(t) \\ \ddot{h}(t) \end{bmatrix} = \begin{bmatrix} 0 & 1 \\ \frac{-k_h}{m_h - \frac{1}{2}m_{h,act}} & \frac{-b_h}{m_h - \frac{1}{2}m_{h,act}} \end{bmatrix} \begin{bmatrix} h(t) \\ \dot{h}(t) \end{bmatrix} + \begin{bmatrix} 0 \\ \frac{1}{m_h - \frac{1}{2}m_{h,act}} \end{bmatrix} L(t) \tag{5.3}$$

$$\begin{bmatrix} \dot{\theta}(t) \\ \ddot{\theta}(t) \end{bmatrix} = \begin{bmatrix} 0 & 1 \\ \frac{-k_\theta}{I_\theta - I_{\theta,act}} & \frac{-(b_\theta - b_{\theta,act})}{I_\theta - I_{\theta,act}} \end{bmatrix} \begin{bmatrix} \theta(t) \\ \dot{\theta}(t) \end{bmatrix} + \begin{bmatrix} 0 \\ \frac{1}{I_\theta - I_{\theta,act}} \end{bmatrix} \tau(t) \tag{5.4}$$

The system reacted poorly to low virtual masses (on the order of the actual foil mass), exhibiting a high frequency shaking that drowned-out the forces in the experiments. This is likely due to small time lags and backlash in the control system, actuators, and gearing, preventing the system from reacting instantaneously and in the proper phase to force-input, as an actual spring-mass-damper system would. By increasing the virtual mass, this effect disappeared, so that the system exhibited smooth motion and reacted intuitively to prodding and pushing.

The virtual system mass, stiffness, and damping coefficients were chosen in order to satisfy the desired resonant frequency, with a mass low enough that self-induced

motion had time to develop during the run in the tank yet high enough to avoid the chattering problems discussed above, and a damping low enough so that the system could resonate to the input forcing at a reasonable amplitude. The virtual parameters that were used for all tests presented here are listed in Table 5.1.

Heave	Pitch
$\omega_h = 13.193\ rad/sec$	$\omega_\theta = 13.193\ rad/sec$
$\zeta_h = 0.01$	$\zeta_\theta = 0.01$
$m_h = 14.71\ kg$	$I_\theta = 0.0263\ kg\ m^2$
$b_h = 3.88\ kg/s$	$b_\theta = 0.0069\ kg\ m^2/s$
$k_h = 2560\ kg/s^2$	$k_\theta = 4.5837\ kg\ m^2/s^2$

Table 5.1: Parameters used in the force-feedback experiments

As the forces measured in these experiments were small relative to the tests in Chapter 3, the apparatus was calibrated with a weight of 0.5 N, as a test of the system resolution. The calibration was within 3% of that with the usual weight of 4.273 N, as seen in Figure 5-2.

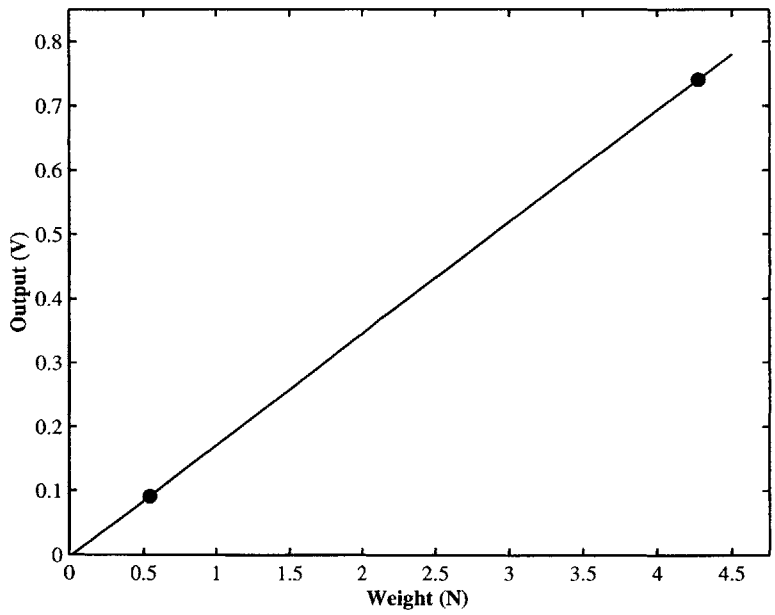

Figure 5-2: The thrust calibration at low forces correlated well with the normal calibration levels. The line is a best-fit to the data.

Since the amplitudes in the force-feedback experiments were quite low, we found that the forcing was stronger and the resulting foil amplitudes higher when the cylinder amplitude was also quite low. Additionally, energy in the wake and measured forces would be larger at a higher carriage velocity. Hence, all tests presented here used $H_c = 0.1\ D$, $St_c = 0.04$, with a carriage velocity $U = 0.8\ m/s$.

When conducting experiments, first the data collection was begun, in order to get zero-data when the carriage was not moving. Next, the carriage was begun. When at full speed, the control algorithm began moving both the cylinder and foil. Thrust and power coefficients were calculated as in Chapter 3. Results presented are averages of 5 tests.

5.2 Results and Discussion

The foil heave and pitch increased to a value near the maximum amplitude attained within a few cycles, as seen in Figure 5-3. The steady-state amplitudes and forces were low, relative to the tests performed in Chapters 3 and 4, reaching an average heave amplitude $h/D = 0.139 \pm 0.017$ and pitch amplitude $\theta_o = 0.107 \pm 0.021\ rad.$ The heave and pitch amplitudes were not necessarily steady over the course of the run, sometimes falling in amplitude before increasing again, but not in a way that would suggest beating. The lift and torque signals, however, would often be seen to degrade during the run, which was not seen when the foil was not heaving. The thrust tended towards positive, but low, and the power input tended towards negative, but low, but both were seen to switch signs, to negative and positive respectively, for portions of some cycles during the run.

The mean thrust and power coefficients were $C_T = 0.017 \pm 0.004$ and $C_P = -0.0071 \pm 0.001$, corresponding to thrusts of $0.27 \pm 0.06\ N$ and a power of $-0.090 \pm 0.012\ W$. The average phase between foil and cylinder heave motions was $\phi = 323 \pm 7°$, generally corresponding to phases where the foil heave velocity moves with, rather than opposing, the lateral flows.

The heave and pitch motions were approximately 90° out-of-phase, as seen in

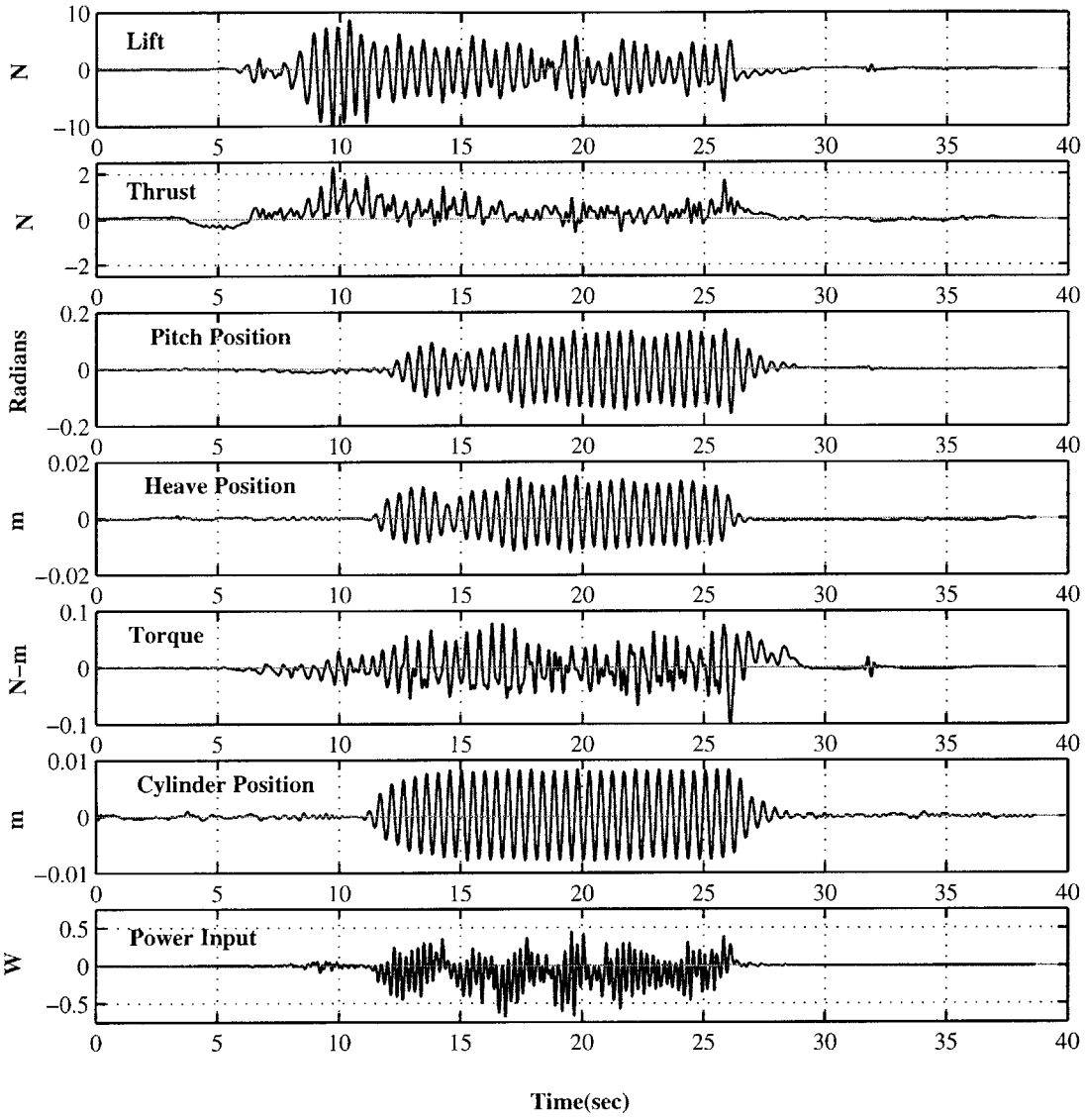

Figure 5-3: During this run, carriage motion was started at 4 seconds. The cylinder heaving and force-feedback algorithm were started at 11 seconds and ended at 26 seconds. This is run5. Data for other runs are shown in the Appendix.

Figure 5-4, which also compares several other output parameters from the force-feedback runs. Lift and heave weren't quite in phase, with the lift leading the heave position by $28.4° \pm 6.4°$, implying that most of the force was due to added mass. Similarly, the torque led the pitch position by $31.4° \pm 5.6°$. Since the added mass may have shifted the resonance peak, adjusting the virtual system's compliance may result in higher amplitude foil motion. It should be noted that the forced-motion runs in Chapter 3 revealed that the lift force was nearly in-phase with the heave velocity, implying that the effect of added mass was low relative to the damping losses to the fluid. Shifting the resonance peak so that the added mass effects are completely balanced by the system compliance could potentially do the same for the force-feedback system.

As seen in Figure 5-4, although two thrust peaks were seen (like during forced-motion runs), one thrust peak was significantly weaker than the other. Likely, with the low forces and amplitudes involved, some asymmetry was taking effect, like error in zeroing the pitch axis, or some slight difference in motion one way versus the other. If the second thrust peak was stronger, likely the thrust produced would be higher.

An example application for wake-energy extraction would be as a power generator for a sensor in a stream. Using a compliantly-mounted heaving and pitching foil, with the damping terms in the virtual system representing power generation devices which act as $P_{generated} = b_h\dot{h}(t) + b_\theta\dot{\theta}(t)$, the above system would have been averaging $44 \pm 12\ mW$ in power generation. For comparison, Onset Computer's Tattletale Model 8, a common low-power computer for applications such as these, has a power drain of "200 μA typical", at "7-15V", consuming approximately 3 mW [39], allowing surplus power to be stored for intermittent need.

Experiments were also run where the foil was set to have no heave or pitch motion within the wake. Although at a different velocity from the other runs in this Chapter ($U = 0.4\ m/s$), these tests show that the foil does indeed produce thrust in the wake solely due to the effect of the oscillating lateral flows across it, overcoming the foil's own drag and even producing excess, with a $C_T = 0.030 \pm 0.006$. The lift, thrust, and torque on the foil was considerably more regular than in the force-feedback cases,

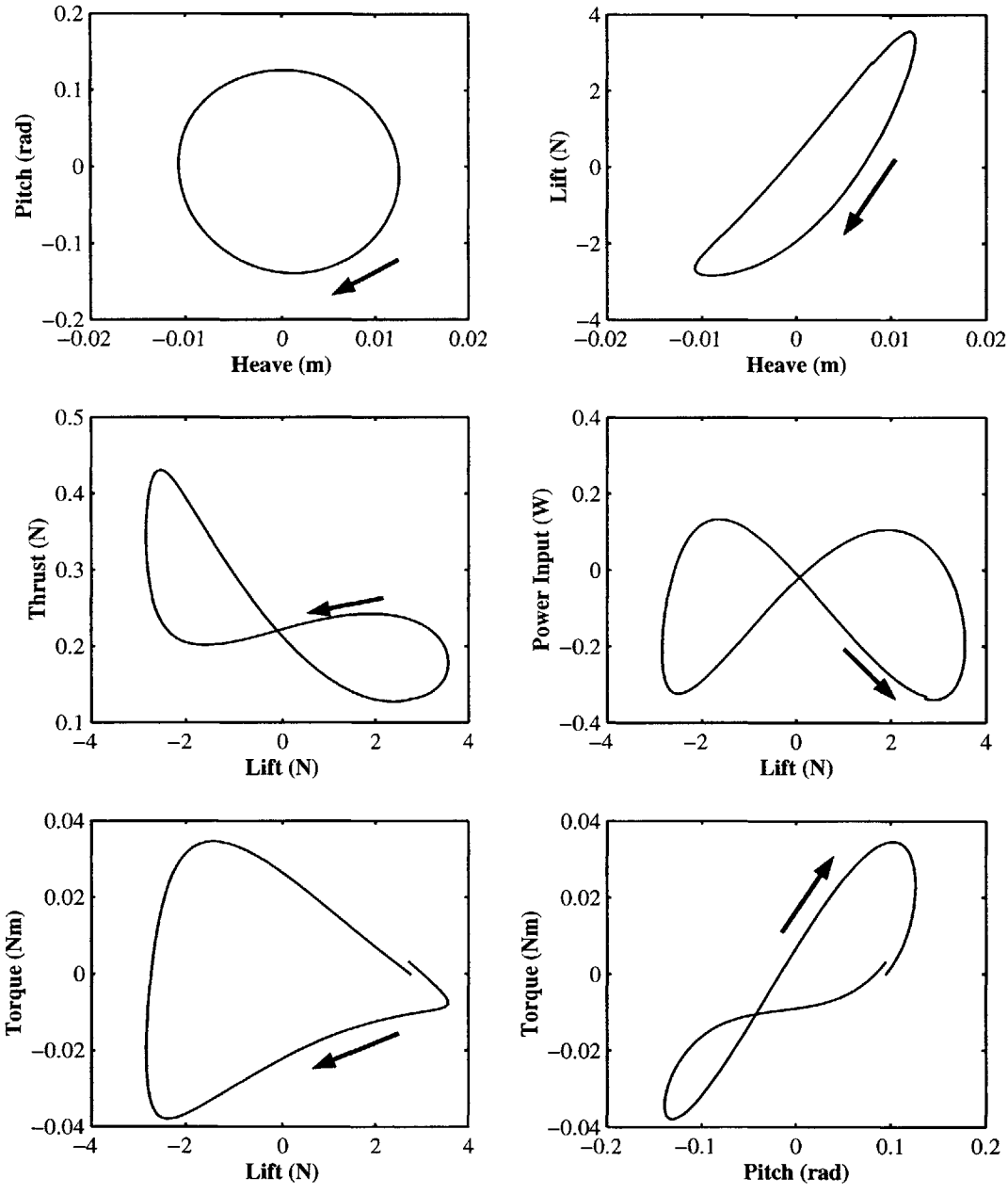

Figure 5-4: Comparison of phase-averaged signals for passive motion within the wake

although it did drift up and down during the run.

There appears to be a balance between the foil motion and the input stimulus forces. The lift forces are noticeably more regular when the foil is not moving, and once the foil starts its passive motion, the lift forces decrease in magnitude and periodicity. The oscillating fluid across the foil is inducing the foil to move with it, but once the foil is oscillating the stimulating flow across it is diminished (from the reference of the foil), implying that there is a maximum amplitude attainable within a wake for this particular setup, regardless of the values of stiffness, mass, and damping chosen. In the end, once the foil is moving with the fluid it no longer will have much flow across it, and the system will balance out at an amplitude where the mean input energy from the flow across the foil equals the mean output energy from thrust production, the virtual dampers, and the losses in the fluid.

This is supported by the fact that the passive foil setup created less thrust than the foil set to zero heave and pitch motion in the wake. Indeed, to create more thrust at these low amplitudes, one would likely have to heave the foil against the wake, increasing the angle-of-attack across it. This, however, would have a cost in power, unless the body pulling the foil across the flow was also in fluid-excited motion. For instance, if a whale or trout body was excited to lateral oscillations by the flow, it may pull the tail across the flow, increasing the thrust production. In this case the energy allowing the tail to move across the flow is coming from the body motion, which is receiving its energy in turn from the fluid.

In these tests we had not the opportunity to optimize the system for passive thrust production or energy recovery. Foils of a different size or shape may be more capable of extracting energy from this wake. Additionally, a flexible chord may create an effect not dissimilar from that of the whale or trout, where a more massive part of the foil moving with the flow pulls a less massive trailing edge across it. In conclusion, there is no reason to think that the power extracted here is near the maximum attainable.

Additionally, it is possible that through some internal stimulation the system could extract more net power. This stimulation may be in the form of either heave or torque motion, but would likely have to be in the proper phase with the incoming

flow in order to work properly.

The total percent of power recovered from the the cylinder wake is small, and it is uncertain what the maximum percent of power recoverable from a vortex would be. Work by Koochesfahani and Dimotakis using a pitching foil to cancel the vortex wake from an upstream pitching foil implies that at least all of the rotational energy in the wake is recoverable [28]. However, this does not imply that it can be done without considerable energy input on the part of the downstream foil, and a passive foil would be unlikely to be able to cancel the wake completely.

A system capable of extracting energy from vortex flows could be useful as a power supply or battery generator for small sensors mounted in turbulent environments. Although more power could likely be extracted by allowing a net drag on the system, certain design situations may require zero net drag, or even a small net thrust, at the cost of less, but still positive, power generation, as would be needed for a lightweight tidal-power generator, for instance.

Chapter 6

Conclusions

6.1 Summary of Main Results

Rainbow trout voluntarily synchronize with a cylinder wake in both frequency and phase. Using PIV, we compared the phase of the trout's lateral position with that of a wake function $W(x,t)$, defined as the lateral sum of the vorticity at a time t and position downstream from the cylinder x. If an object was in-phase with the wake function, by definition, its motion would oppose the lateral flow in the wake, and it would 'intercept' the vortices in a cylinder drag wake. The trout led the wake function by 100° for the head, 160° for the center-of-mass, and 240° for the tail, implying that the trout's mass was moving laterally with the flow in a low-power swimming mode. A euthanized trout synchronized with the wake and swam upstream against its drag solely due to fluid-induced motions, implying that trout entrain behind cylinders not just to draft, but to take additional advantage from the oscillating vortex wake.

Through experiments with a mechanical hydrofoil moving in heave and pitch, we found that thrust and power were generally higher when the foil leading-edge motion opposed that of the lateral flows in the wake, and both were lower when the leading-edge motion moved with the lateral flows in the wake. This is likely due to the change in the magnitude of the instantaneous angle-of-attack within the cross-flows, which would increase when the foil motion opposed the flow, increasing thrust, and vice versa.

The efficiency of the hydrofoil in a wake was more complicated. Although the sensitivity of efficiency to the wake interaction phase was low relative to thrust and power, when the foil was producing significant thrust ($C_T \approx 1.0$), efficiency was highest near the wake interaction phase resulting in peak thrust, where the phase of foil lateral position led the wake by 30° for the leading-edge and 120° for the trailing-edge. However, for lower thrust production ($C_T \approx 0.3$) the efficiency peak occurred at a wake interaction phase resulting in off-peak thrust production, where the phase of foil position led the wake by 125° for the leading-edge and 215° for the trailing-edge, qualitatively resembling the interaction strategy of the trout.

Since the characteristic frequency and phase of an incoming wake will not generally be known beforehand, I designed and tested a simple synchronization method which could synchronize to any desired phase relative to the wake within 6 seconds. The method was robust to brief wake variations.

Using force-feedback to model a passive system, I showed that a foil within a cylinder wake could produce thrust while also extracting net power from the wake. Although not optimized, this points the way towards future research into lightweight power systems in turbulent fluids.

This research spans a range of cases for foils synchronizing with cylinder wakes, from foils producing high thrust, as if a propellor for a large or bluff body, foils producing low thrust, as the propellor for a streamlined body like a fish, and foils passively producing near-zero net thrust while generating power from the oscillating flows in the wake. In the first case, the foil is producing power of the same order of magnitude as the cylinder wake. In the middle of the range, it's producing one or more orders of magnitude less, and in the last case, the power generator's power is negative.

In summary, both live fish and mechanical hydrofoils are capable of extracting energy from a vortex wake. As vehicles are developed with more maneuverability, and more capacity to sense the flow structures in their environment, they will be better able to utilize wakes for energy benefit as part of a system which also allows them to extract wave energy, sense other moving bodies, and react to unsteady currents. This

work supplies a basis for one part of the overall strategy, and perhaps could provide guidance and inspiration to those adapting a vehicle to react to its environment with the elegance and agility of nature's many creatures.

6.2 Recommended Future Work

The extensive experimentation with the flapping foil behind the cylinder presented here basically wrapped-up the work begun by Streitlien and Gopalkrishnan, and continued by Anderson, where the foil and fluid were all studied in a big-picture context. Numerical simulations would help flesh out the details, like the instantaneous pressures and smaller-scale vorticity induced on- or produced by- the foil.

The passive energy generator is one area that deserves considerable attention. Through optimization of the system, the power-output capacity of the technique needs to be identified. Additionally, application of the technology may be a challenge in itself. Near term uses include lightweight tidal generators and power generators for small, low-power sensors in streams, where they can be positioned near the surface waves or behind a shedding obstacle.

One could claim that an additional step should be added to the 'range' of cases with foils in wavy streams: that of a flapping foil optimized to extract as much energy as possible from the vortex wake regardless of the drag forces induced upon it. It is uncertain whether this system could out-perform a water turbine, but there may be many cases where it has advantages over one, such as environmental safety or surface wave-power extraction. The Engineering Business has developed and tested a prototype flapping foil tidal generator with a 30 meter span, but has not released any plans to use it in anything other than a uniform stream, making it an alternative system to a water turbine [37].

Work with the rainbow trout continues amongst my colleagues at Harvard University. The method of fish positioning needs to be worked out, both in synchronization and the upstream-downstream 'sweet-spot' location. Are fish capable of maintaining their position without a lateral line? The dead fish can synchronize and take advan-

tage of the wake, but they certainly are not capable of holding position behind the cylinder, as they are always either going forwards into the cylinder, or flailing back on the taut string.

The information in this thesis may be of considerable use to those studying the interactions of a fin with the wake produced by an upstream body-part, such as that seen by a caudal fin behind a dorsal fin, or the aft dragonfly wing behind the fore. Most important would be the idea of the wake function, where the phase of the oscillating lateral flow is of prime importance, rather than the proximity of the vortices as described as interception or slaloming by Anderson. The ideas behind the wake function hold whether in a drag wake, inline wake, or thrust wake: in each case it is directly and similarly related to the phase and sign of the local lateral flow.

The ability to sense and identify flow structures around a vehicle has several other promising characteristics, many taken from biological inspirations. A vehicle in the surf would need to optimize its power expenditure between fighting the back-and-forth nature of the surf in order to stay on its desired path and avoid obstacles, and to allow itself to move with the surf, keeping only the mean motion in the direction of the desired path while avoiding unnecessary power consumption.

Fish have been shown to use their lateral lines for rheotaxis, prey detection, and schooling. Rheotaxis is the nature of fish to align themselves with the current, an absolute must for a vehicle in strong but changing flows. The ability to detect other schooling fish, and detect prey insects thrashing on the surface, leads one to believe that an artificial lateral line may have potential as an alternative method for detecting objects in the water, without requiring the use of sonar.

Using an oscillating flow for energy benefit is certainly not the only important technique that needs to be developed for highly maneuverable vehicles, and it is probably not even the most crucial to a vehicle's survival. It was seen as a good starting point, with a limited amount of information necessary to describe the flow and make the system work, and being of the size and nature optimal for study in a laboratory setting in a world where flapping foil vehicles are only now in the prototype stage. This thesis is ahead of the curve, trying to identify the methods for biomimetic

vehicles to best utilize their impressive maneuverability while they are still in their infancy, in order to decrease the time necessary to implement these ideas on working machines.

Appendix A

Additional Foil Plots

A.1 Foil Performance within Varying Wakes

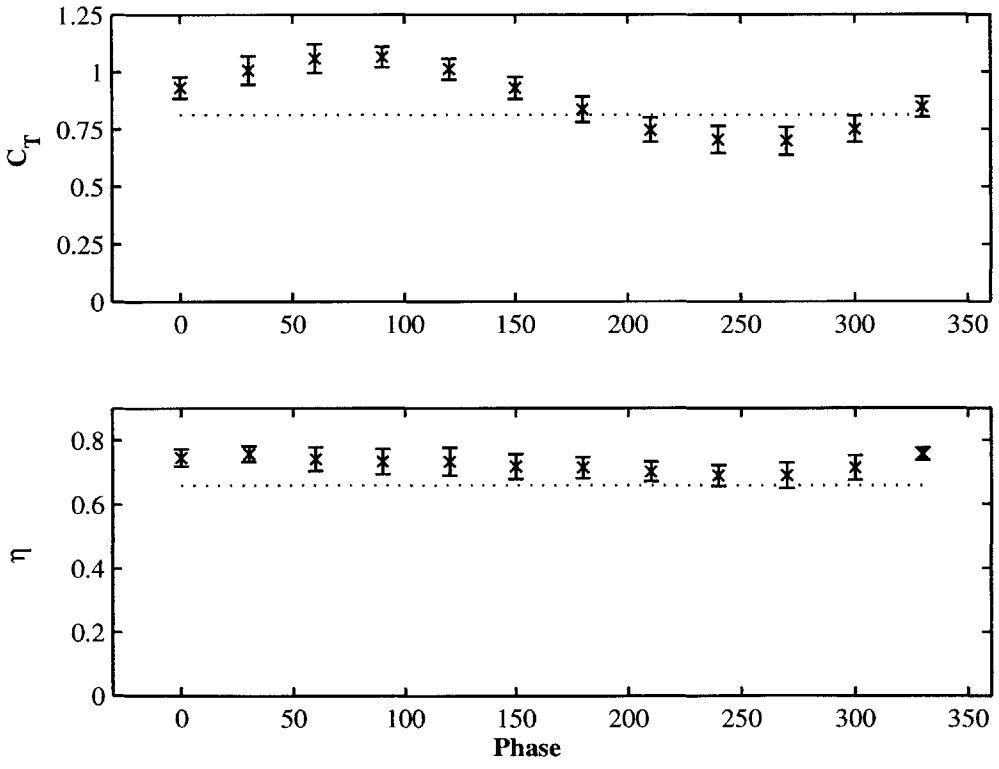

Figure A-1: Coefficients of thrust and efficiency for $H_c = 0.75D$, $St_c = .30$, $H_f = 1.0D$, $\theta_0 = 52.2°$, $\psi = 90°$. The dashed line represents the baseline drafting performance.

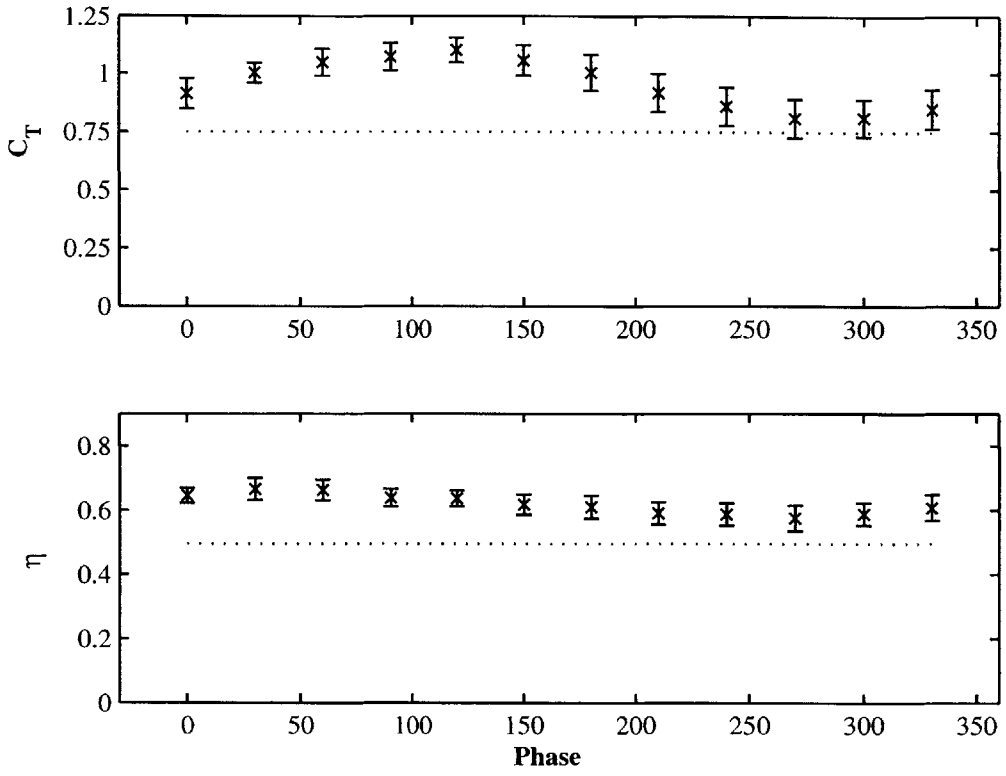

Figure A-2: Coefficients of thrust and efficiency for $H_c = 0.75D$, $St_c = .33$, $H_f = 1.0D$, $\theta_0 = 52.2°$, $\psi = 90°$. The dashed line represents the baseline drafting performance.

A.2 Dye Visualization

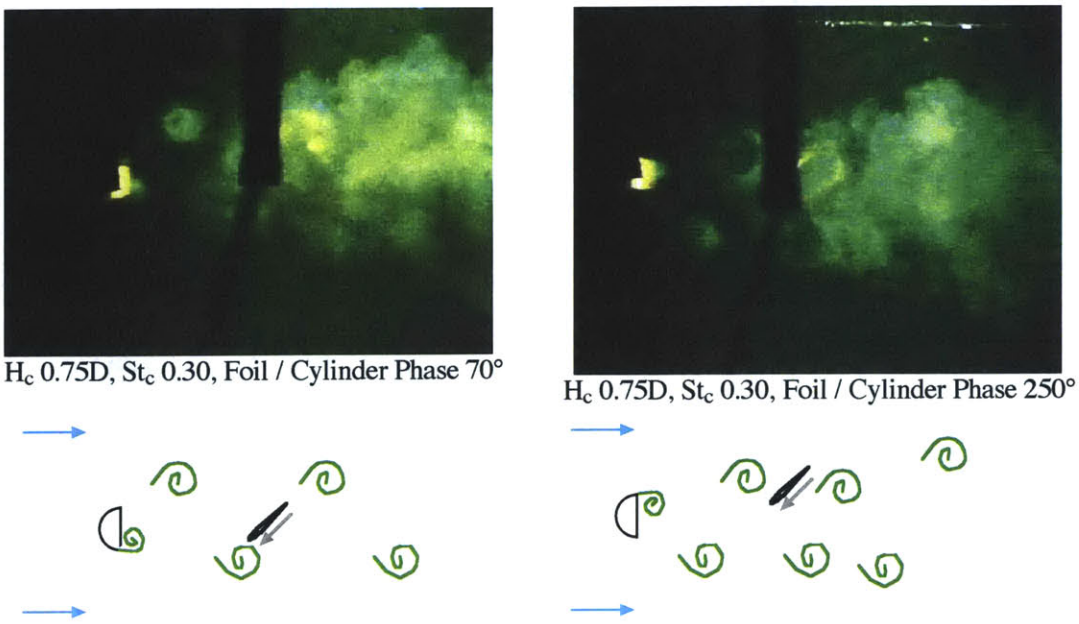

Figure A-3: Dye visualization showing leading-edge interception for high thrust and efficiency (left) and slaloming for low (right)

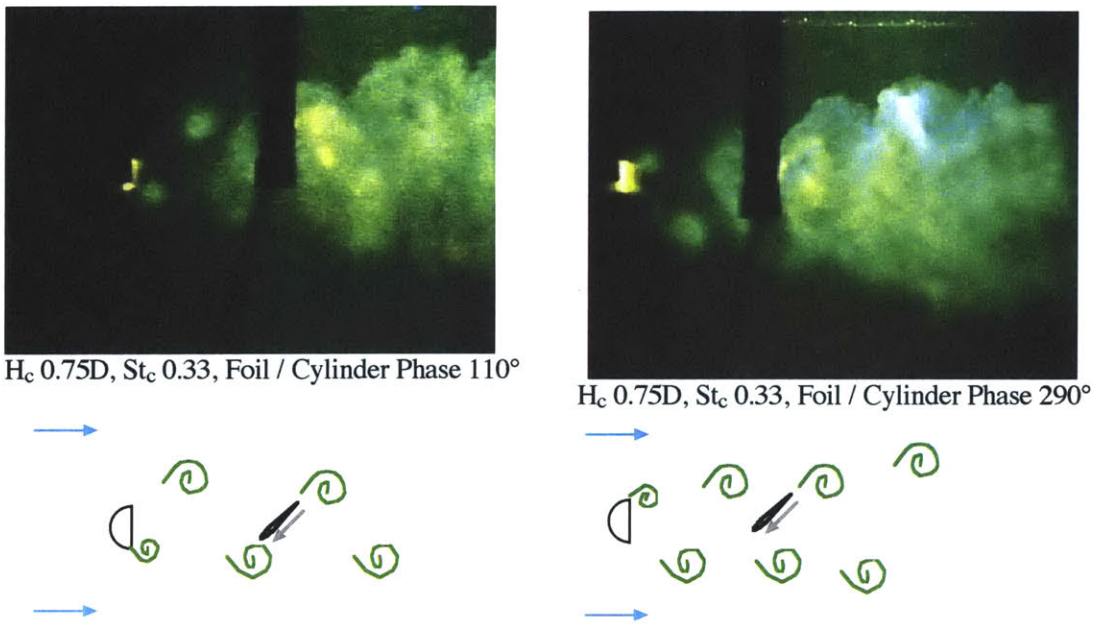

Figure A-4: Dye visualization showing leading-edge interception for high thrust and efficiency (left) and slaloming for low (right)

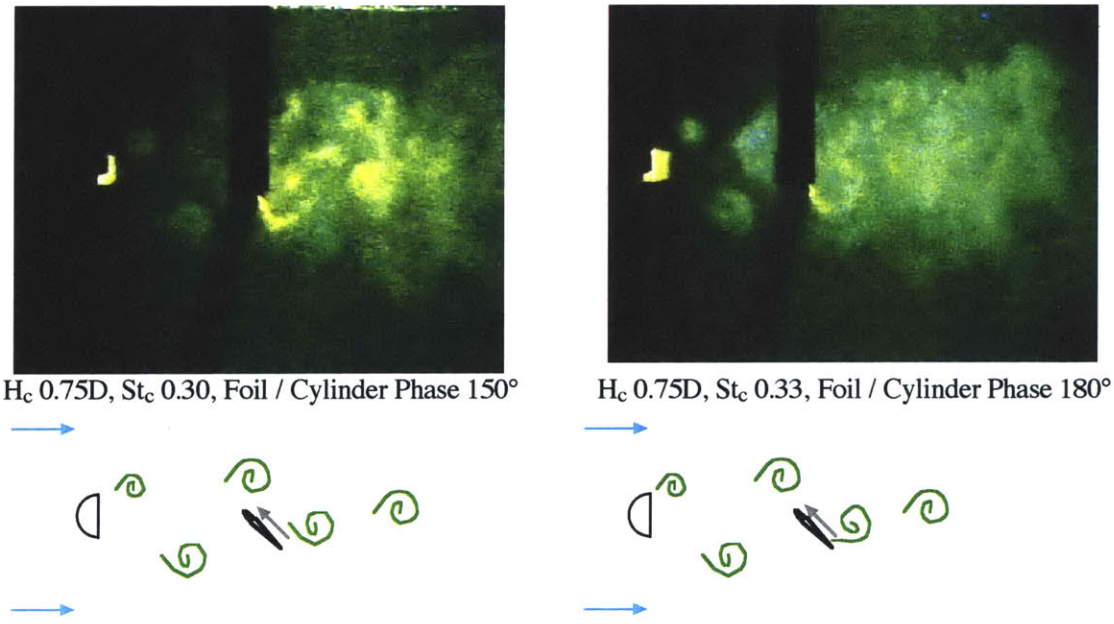

Figure A-5: Dye visualization showing interception near the mid-chord, at a foil/cylinder phase resulting combined wake vortices near the centerline.

A.3 Combined Wake

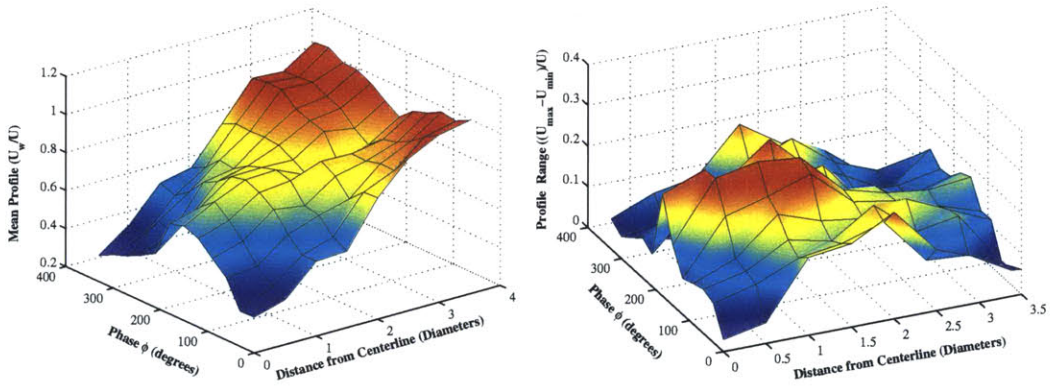

Figure A-6: The mean velocity profile seen within the combined wake, left, and the range of velocities seen in a period, right, as a function of foil / cylinder heave phase ϕ, for for $H_c = 0.75D$, $St_c = .30$

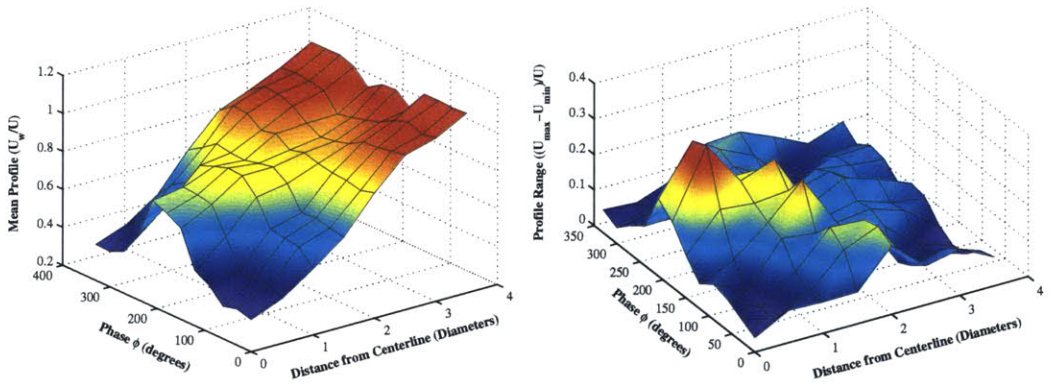

Figure A-7: The mean velocity profile seen within the combined wake, left, and the range of velocities seen in a period, right, as a function of foil / cylinder heave phase ϕ, for for $H_c = 0.75D$, $St_c = .33$

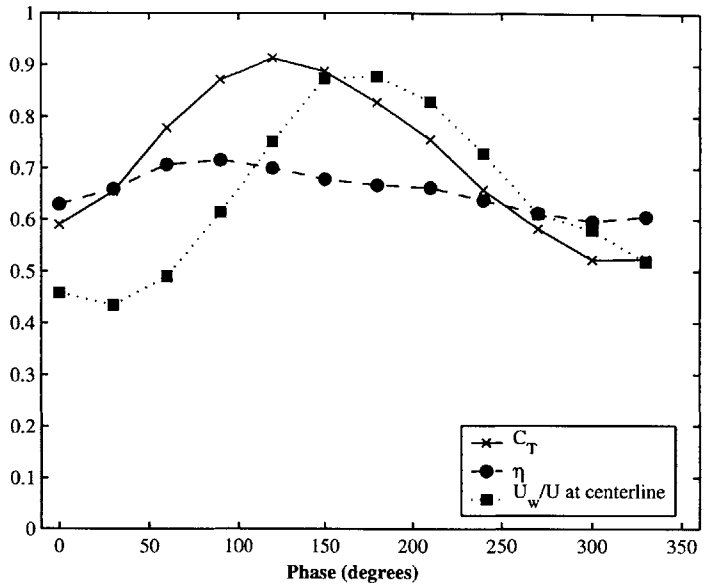

Figure A-8: The mean centerline velocity in the combined wake, with C_T and η, for $H_c = 0.50D$, $St_c = .20$

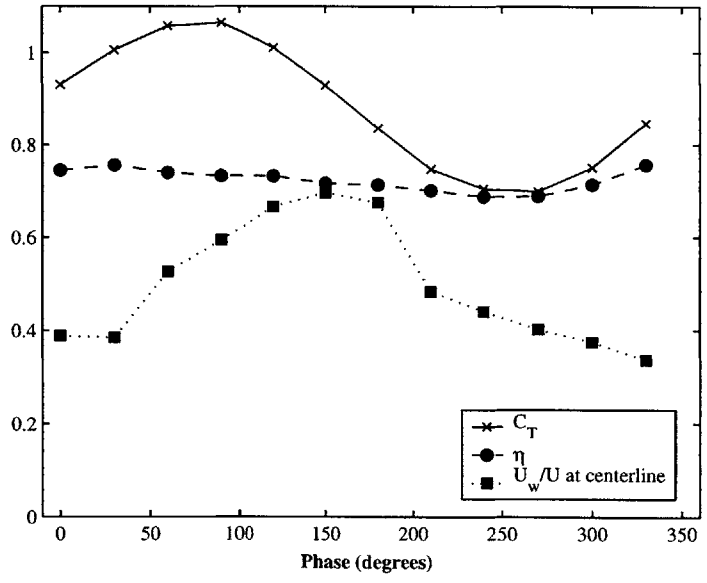

Figure A-9: The mean centerline velocity in the combined wake, with C_T and η, for $H_c = 0.75D$, $St_c = .30$

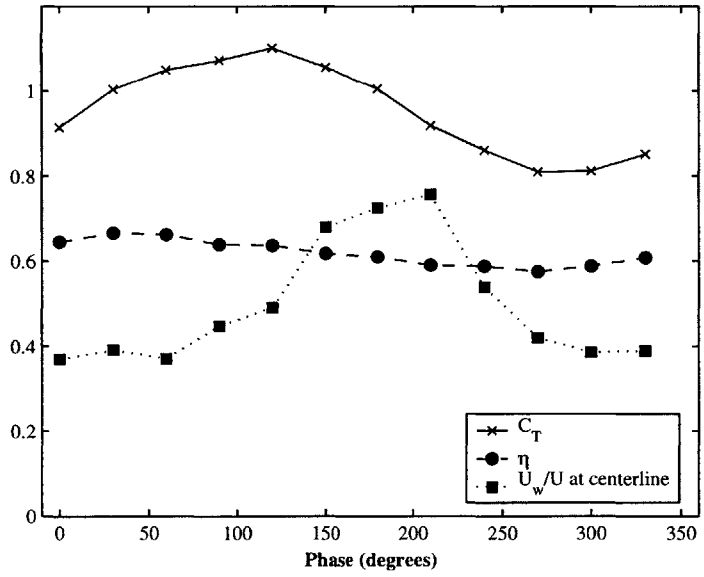

Figure A-10: The mean centerline velocity in the combined wake, with C_T and η, for $H_c = 0.75D$, $St_c = .33$

A.4 Varying Foil Parameters Within a Wake

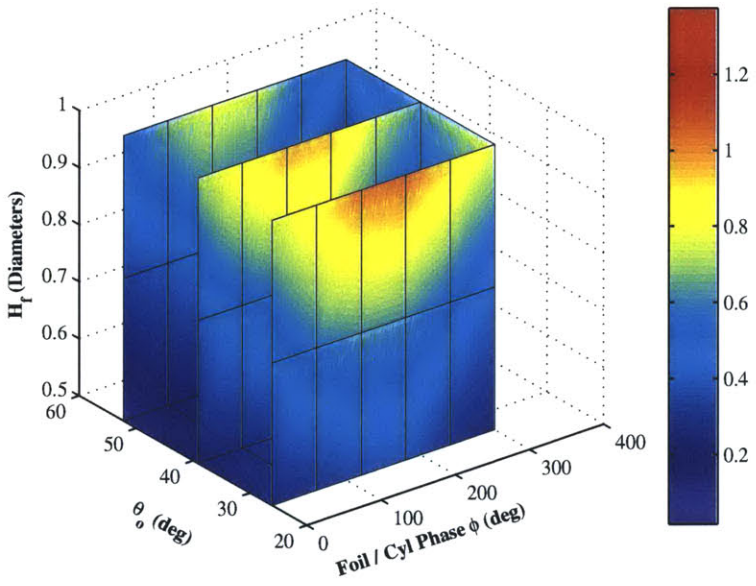

Figure A-11: Thrust coefficient as a function of ϕ, H_f, θ_o for $\psi = 80°$

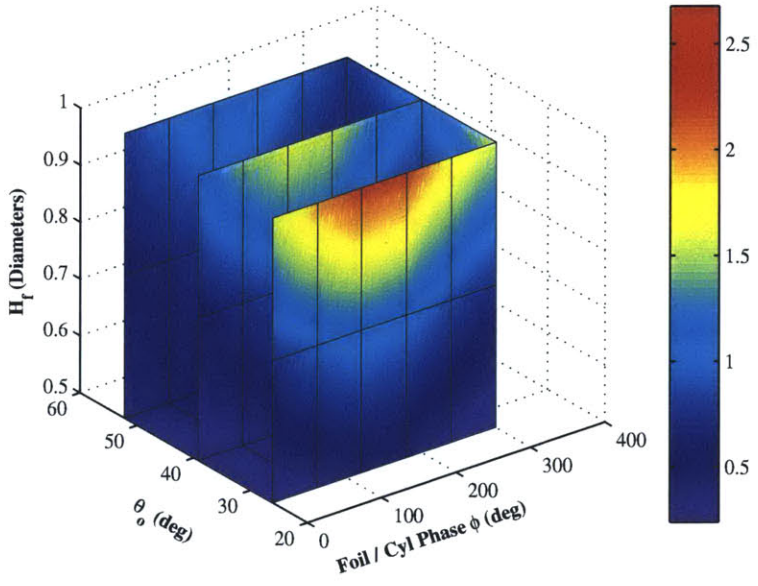

Figure A-12: Power coefficient as a function of ϕ, H_f, θ_o for $\psi = 80°$

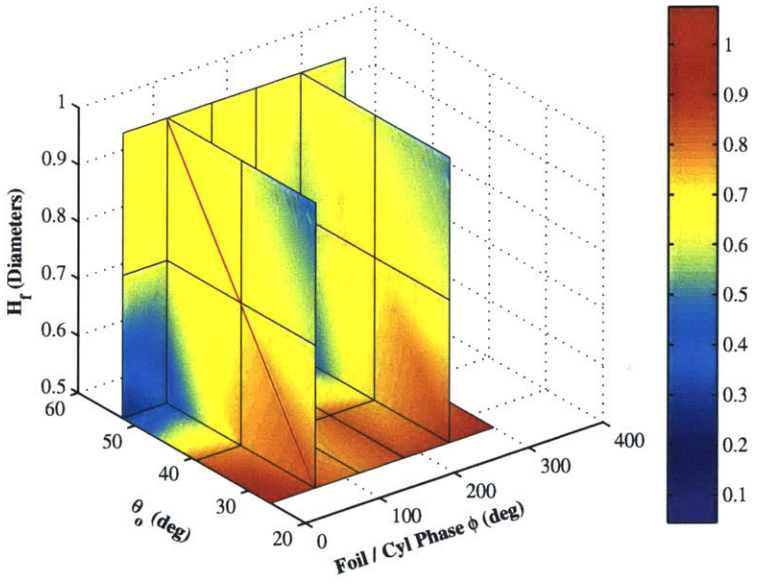

Figure A-13: Efficiency as a function of ϕ, H_f, θ_0 for $\psi = 80°$. The magenta line demarks $\alpha_{max} = 6°$.

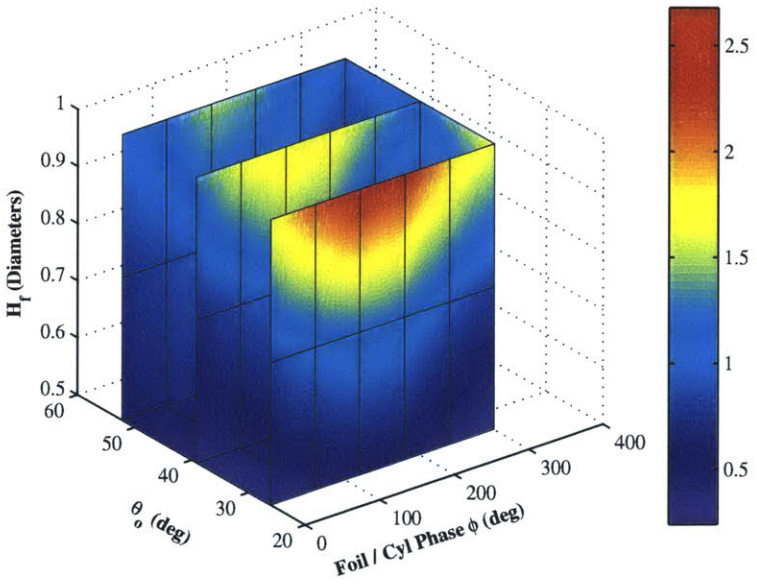

Figure A-14: Power coefficient as a function of ϕ, H_f, θ_o for $\psi = 90°$

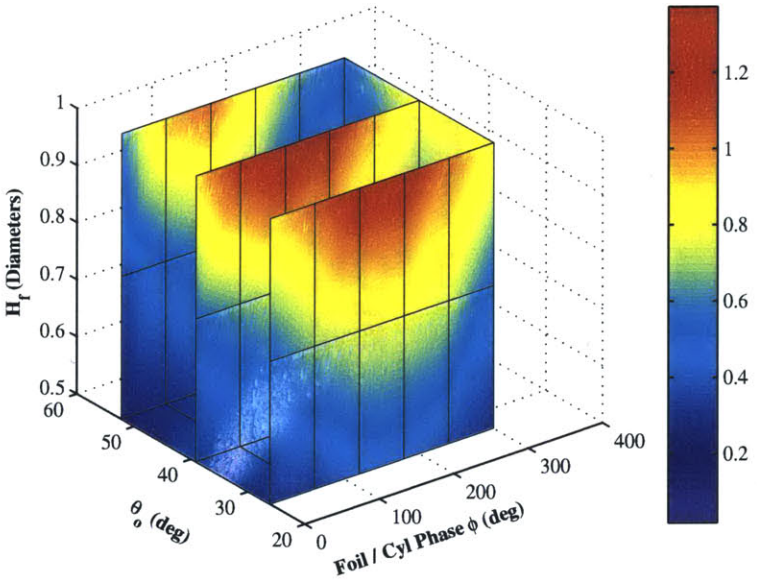

Figure A-15: Thrust coefficient as a function of ϕ, H_f, θ_o for $\psi = 100°$

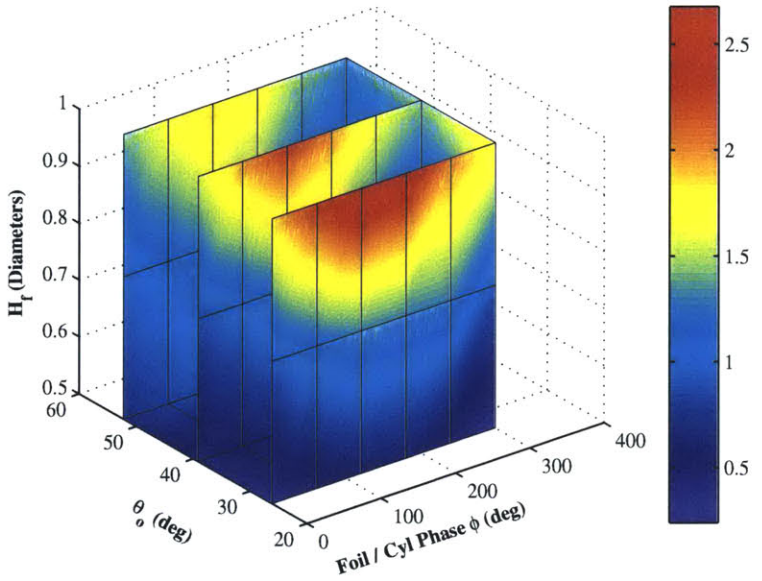

Figure A-16: Power coefficient as a function of ϕ, H_f, θ_o for $\psi = 100°$

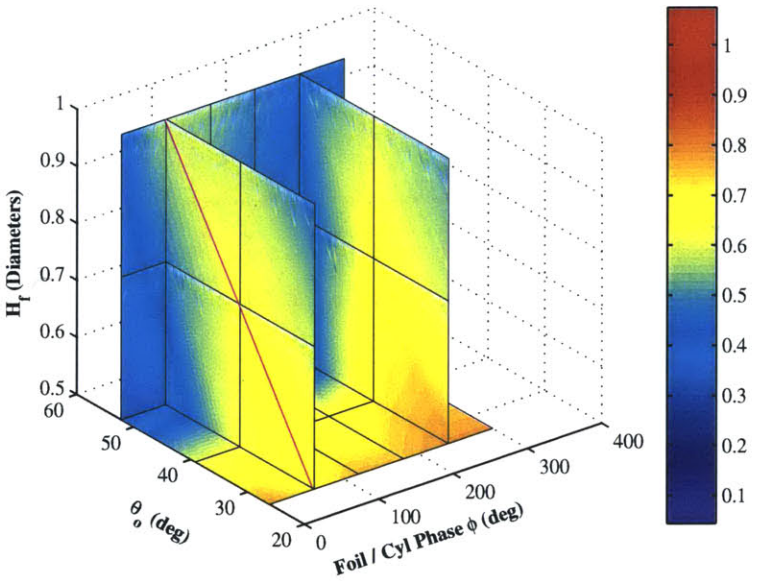

Figure A-17: Efficiency as a function of ϕ, H_f, θ_0 for $\psi = 100°$. The magenta line demarks $\alpha_{max} = 6°$.

A.5 Additional Passive Energy Recovery Runs

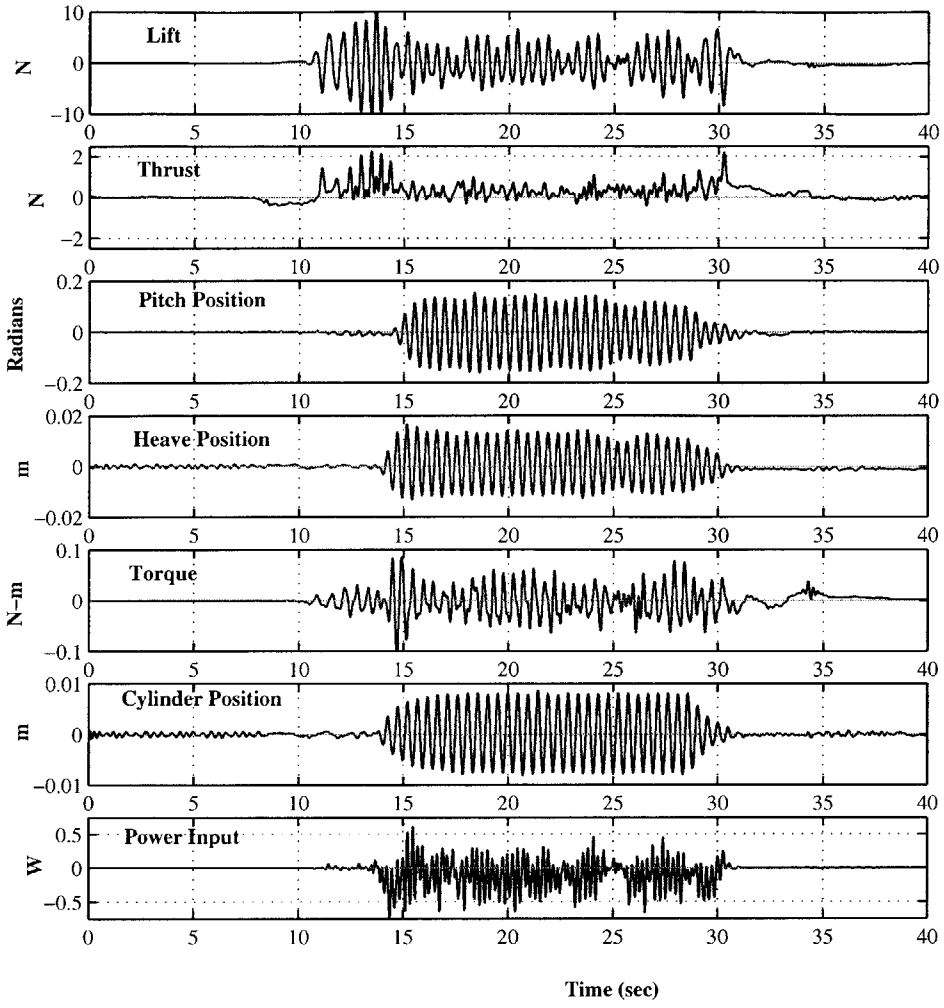

Figure A-18: During this run, carriage motion was started at 8 seconds. The cylinder heaving and force-feedback algorithm were started at 14 seconds and ended at 29 seconds. This is run1.

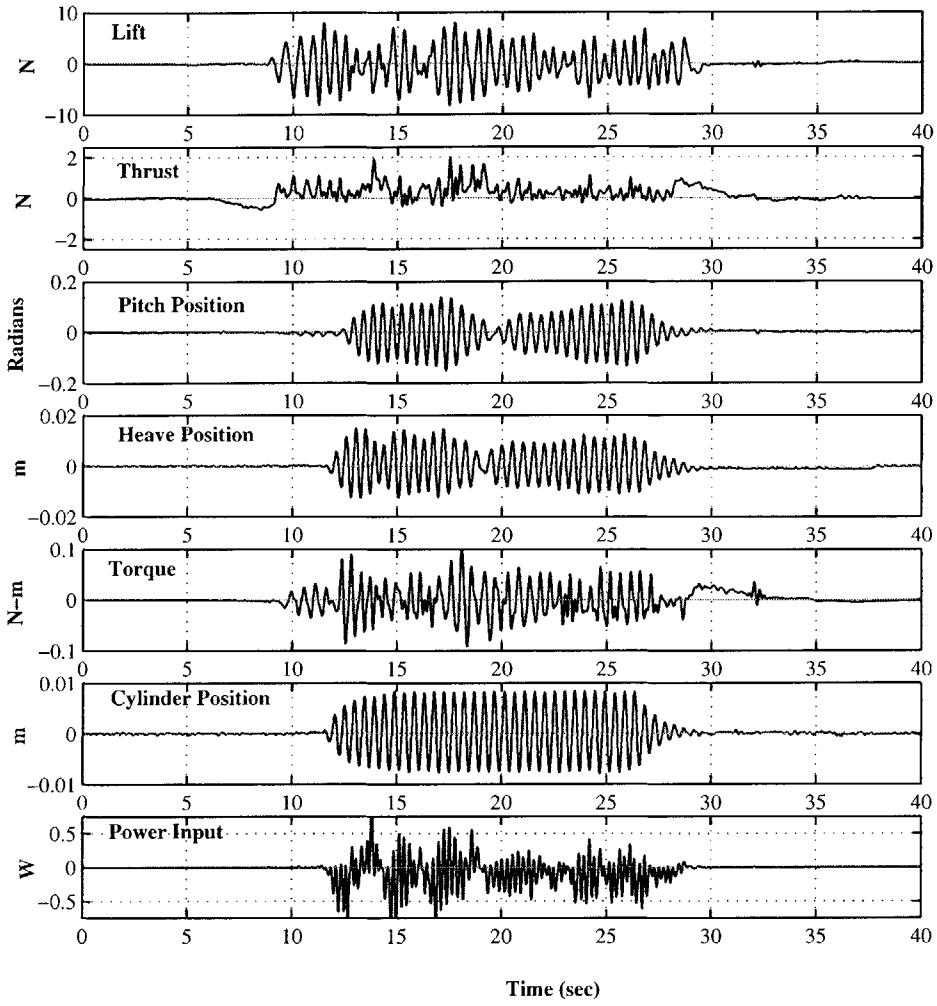

Figure A-19: During this run, carriage motion was started at 6 seconds. The cylinder heaving and force-feedback algorithm were started at 12 seconds and ended at 27 seconds. This is run2.

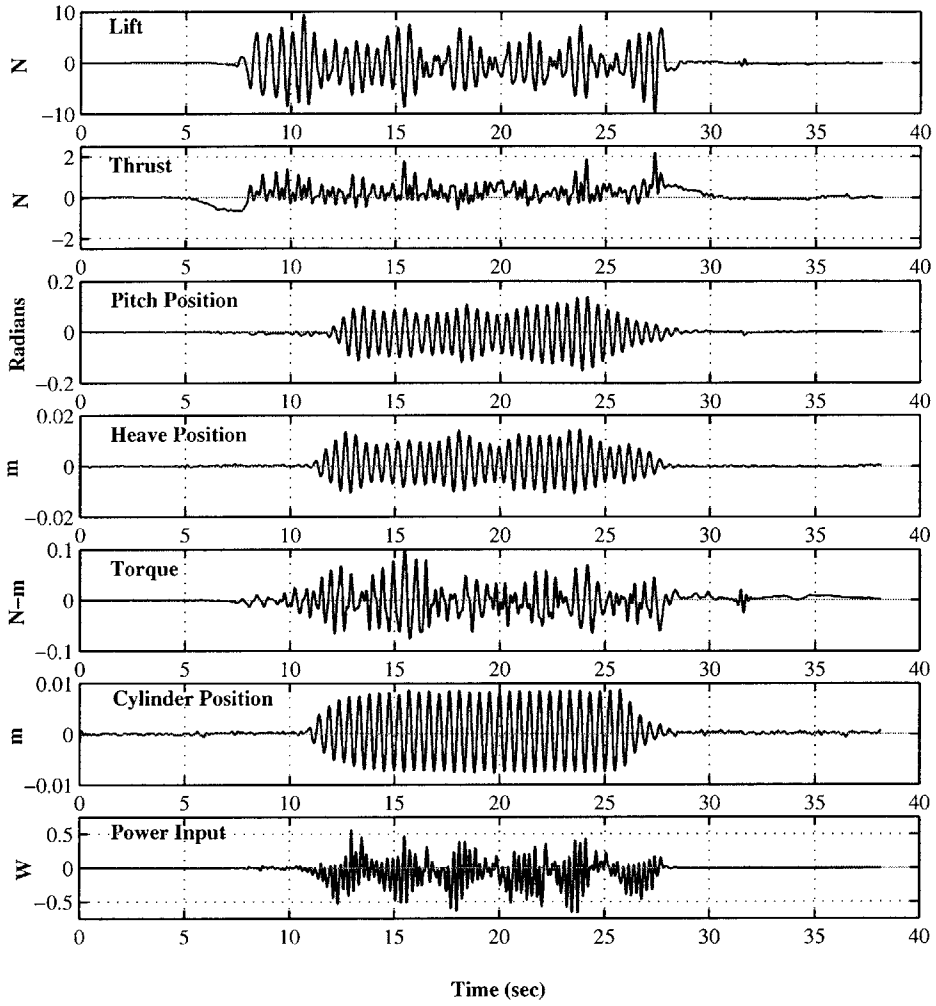

Figure A-20: During this run, carriage motion was started at 5 seconds. The cylinder heaving and force-feedback algorithm were started at 11 seconds and ended at 26 seconds. This is run3.

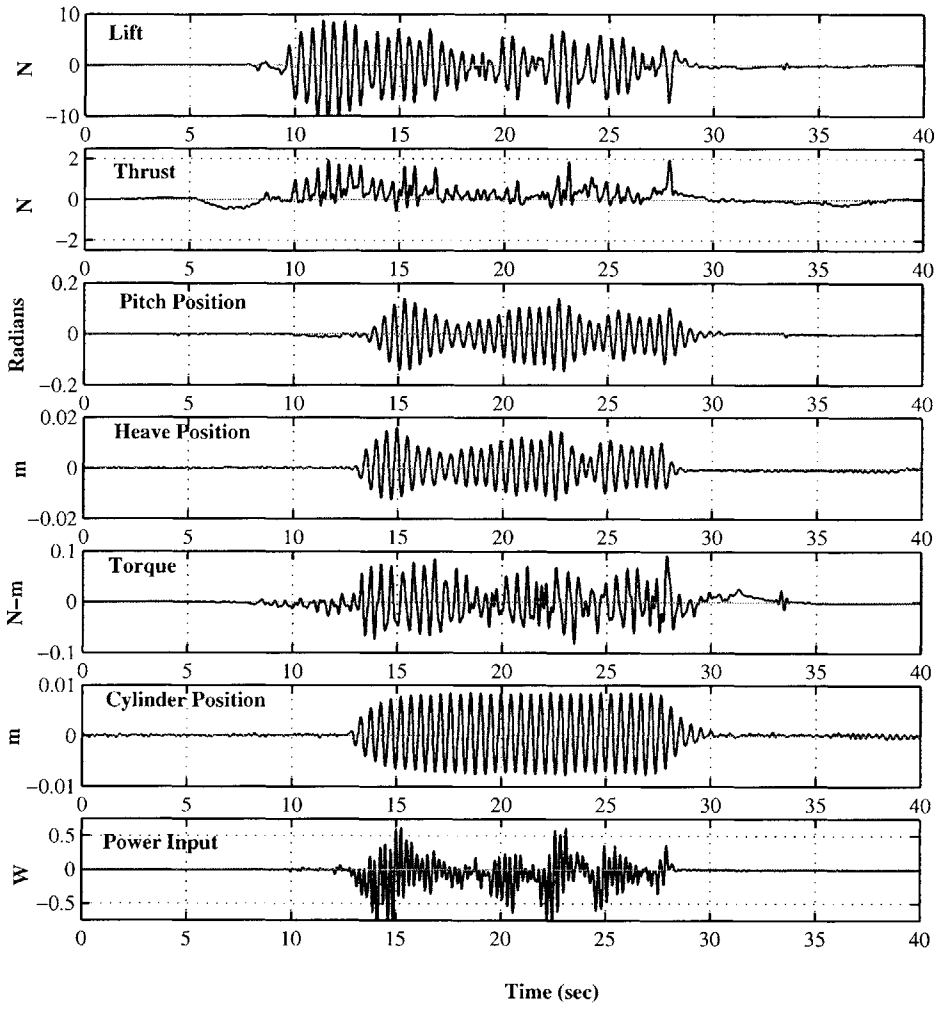

Figure A-21: During this run, carriage motion was started at 5 seconds. The cylinder heaving and force-feedback algorithm were started at 13 seconds and ended at 28 seconds. This is run4.

Bibliography

[1] Ira H. Abbott and Albert E. Von Doenhoff. *Theory of Wing Sections.* Dover Publications Inc., New York, 1959.

[2] D. E. Alexander. Unusual phase relationships between the forewings and hindwings in flying dragonflies. *Journal of Experimental Biology*, 109, 1984.

[3] D. E. Alexander. Wind tunnel studies of turns by flying dragonflies. *Journal of Experimental Biology*, 122, 1986.

[4] Alpharma Animal Health Limited, Fordingbridge, Hampshire, UK. *MS222 (Tricaine Methane Sulphonate) Technical Bulletin*, 2001.

[5] J. M. Anderson. *Vorticity Control for Efficient Propulsion.* PhD thesis, M.I.T., Cambridge, MA, 1996.

[6] J. M. Anderson and N. K. Chhabra. Maneuvering and stability performance of a robotic tuna. *American Zoologist*, 40, December 2000.

[7] J. M. Anderson, K. Streitlien, D. S. Barrett, and M. S. Triantafyllou. Oscillating foils of high propulsive efficiency. *Journal of Fluid Mechanics*, 360:41–72, 1998.

[8] D. S. Barrett. *Propulsive Efficiency of a Flexible Hull Underwater Vehicle.* PhD thesis, M.I.T., Cambridge, MA, 1996.

[9] Blevins. *Flow Induced Vibration, 2nd edition.* Krieger Publishing Company, Malabar, Florida, 1993.

[10] N. Bose and J. Lien. Energy absorption from ocean waves: a free ride for cetaceans. *Proceedings of the Royal Society of London*, 240:591–605, 1990.

[11] A. Brodsky. *Evolution of Insect Flight.* Oxford University Press, London, 1994.

[12] R. A. Conley and S. Coombs. Dipole source localization by mottle sculpin: Orientation after site-specific, unilateral denervation of the lateral line. *Journal of Comparative Physiology*, 183:335–344, 1998.

[13] Joshua T. Davis. Velocity characteristics in the wake of an oscillating cylinder. Master's thesis, M.I.T., Cambridge, MA, 2001.

[14] P. Domenici and R. W. Blake. The kinematics and performance of fish fast-start swimming. *The Journal of Experimental Biology*, 200:1165–1178, 1997.

[15] Eliot G. Drucker and George V. Lauder. Locomotor forces on a swimming fish: Three-dimensional vortex wake dynamics quantified using digital particle image velocimetry. *The Journal of Experimental Biology*, 202:2393–2412, 1999.

[16] Eliot G. Drucker and George V. Lauder. Locomotor function of the dorsal fin in teleost fishes: experimental analysis of wake forces in sunfish. *The Journal of Experimental Biology*, 204:2943–2958, 2001.

[17] B. Ermentrout. An adaptive model for synchrony in the firefly pteroptyx malaccae. *Journal of Mathematical Biology*, 29:571–585, 1991.

[18] Kurt D. Fausch. Profitable stream positions for salmonids: relating specific growth rate to net energy gain. *Canadian Journal of Zoology*, 62:441–451, 1984.

[19] A. A. Fejer. Porpoises and the bow-riding of ships under way. *Nature*, 188:700–703, 1960.

[20] F. E. Fish. Energetics of swimming and flying in formation. *Comments Theoretical Biology*, 5:283–304, 1999.

[21] P. Freymuth. Propulsive vortical signature of plunging and pitching airfoils. *AIAA*, 26:881–882, 1988.

[22] J. H. Gerrard. Formation region of vortices behind bluff bodies. *Journal of Fluid Mechanics*, 25:401–413, 1966.

[23] R. Gopalkrishnan, M. S. Triantafyllou, G. S. Triantafyllou, and D. Barrett. Active vorticity control in a shear flow using a flapping foil. *Journal of Fluid Mechanics*, 274:1–21, 1994.

[24] James Gray. *Animal Locomotion.* Weidenfeld and Nicolson, London, 1968.

[25] Øyvind Haugsdal. Motion control of oscillating foils for steady propulsion and starting maneuvers. Master's thesis, M.I.T., Cambridge, MA, 2000.

[26] H. Isshiki and M. Murakami. A theory of wave devouring propulsion (4th report). *Journal of The Society of Naval Architects of Japan*, 156:102–114, 1984.

[27] M. M. Koochesfahani. Vortical patterns in the wake of an oscillating airfoil. *AIAA Journal*, 27(9), 1989.

[28] M. M. Koochesfahani and P. E. Dimotakis. A cancellation experiment in a forced turbulent shear layer. *AIAA Journal*, 88:3713+, 1988.

[29] G. V. Lauder. Function of the caudal fin during locomotion in fishes: Kinematics, flow visualization, and evolutionary patterns. *American Zoologist*, 2000.

[30] James C. Liao, 2002. Unpublished personal communication.

[31] James C. Liao, David N. Beal, George V. Lauder, and Michael S. Triantafyllou. The Kármán gait: novel body kinematics of rainbow trout swimming in a vortex street. *Journal of Experimental Biology*, 206:1059–1073, 2003.

[32] M. J. Lighthill. Aquatic animal propulsion of high hydromechanical efficiency. *J. Fluid Mechanics*, 44:265–301, 1970.

[33] J. I. Martin, L. E. Howle, and M. M. Murray. Optimization of undulatory flap propulsors. *Proc. 12th International Symposium on Unmanned Untethered Submersible Technology*, 2001.

[34] J. C. Montgomery, C. F. Baker, and A. G. Carton. The lateral line can mediate rheotaxis in fish. *Nature*, 389:960–963, 1997.

[35] U. K. Müller, B. L. E. Van Den Heuvel, E. J. Stamhuis, and J. J. Videler. Fish foot prints: Morphology and energetics of the wake behind a continuously swimming mullet. *Journal of Experimental Biology*, 200:2893–2906, 1997.

[36] R. G. Northcutt. Swimming against the current. *Nature*, 389:915–916, 1997.

[37] Ocean News and Technology. *Renewable Energy from the Ocean*, March/April 2003.

[38] Katsuhiko Ogata. *Modern Control Engineering.* Prentice Hall, Englewood Cliffs, NJ, 1990.

[39] Onset Computer Corporation, Pocasset, MA. *Tattletale Model 8: Data Logger / Controller Engine.*

[40] T. J. Pitcher, B. L. Partridge, and C. S. Wardle. A blind fish can school. *Science*, 194:963–965, 1976.

[41] V. Polidoro. Flapping foil propulsion for cruising and hovering autonomous underwater vehicles. Master's thesis, M.I.T., Cambridge, MA, 2003.

[42] D. A. Read. Oscillating foils for propulsion and maneuvering of ships and underwater vehicles. Master's thesis, M.I.T., Cambridge, MA, 2000.

[43] D. A. Read, F.S. Hover, and M.S. Triantafyllou. Forces on oscillating foils for propulsion and maneuvering. *Journal of Fluids and Structures*, 17:163–183, 2003.

[44] M. Sachinis. The design and testing of a biologically inspired underwater robotic mechanism. Master's thesis, M.I.T., Cambridge, MA, 2000.

[45] R. M. C. So, I. Jadic, and M. P. Mignolet. Fluid-structure resonance produced by oncoming alternating vortices. *Journal of Fluids and Structures*, 13:519–548, 1999.

[46] C. Somps and M. Luttges. Dragonfly flight: novel uses of unsteady separated flows. *Nature*, 228:1326–1329, 1985.

[47] K. Streitlien, G. S. Triantafyllou, and M. S. Triantafyllou. Efficient foil propulsion through vortex control. *AIAA Journal*, 34(11), 1996.

[48] Steven H. Strogatz. *Nonlinear Dynamics and Chaos.* Addison-Wesley, Reading, MA, 1994.

[49] A. M. Sutterlin and S. Waddy. Possible role of the posterior lateral line in obstacle entrainment by brook trout. *J. of Fish. Res. Board Can.*, 32:2441–2446, 1975.

[50] G. S. Triantafyllou, M. S. Triantafyllou, and M. A. Grosenbaugh. Optimal thrust development in oscillating foils and application to fish propulsion. *Journal of Fluids and Structures*, 7:205–224, 1993.

[51] M. S. Triantafyllou and G. S. Triantafyllou. An efficient swimming machine. *Scientific American*, 272(3):64–70, March 1995.

[52] John J. Videler. *Fish Swimming.* Chapman & Hall, London, 1993.

[53] J.M. Wakeling and C.P. Ellington. Dragonfly flight (parts i, ii, and iii). *The Journal of Experimental Biology*, 200, 1997.

[54] P. W. Webb, P. T. Kostecki, and E. Don Stevens. The effect of size and swimming speed on locomotor kinematics of rainbow trout. *Journal of Experimental Biology*, 109:77–95, 1984.

[55] P[aul] W. Webb. Entrainment by river chub nocomis micropogon and smallmouth bass micropterus dolomieu on cylinders. *The Journal of Experimental Biology*, 201:2403–2412, 1998.

[56] M. J. Wolfgang, J. M. Anderson, M. A. Grosenbaugh, D. K. P. Yue, and M. S. Triantafyllou. Near-body flow dynamics in swimming fish. *The Journal of Experimental Biology*, 202:2303–2327, 1999.

[57] T. Y. Wu. Extraction of flow energy by a wing oscillating in waves. *The Journal of Ship Research*, pages 66–78, March 1972.

[58] T. Y. Wu and A. T. Chwang. Extraction of flow energy by fish and birds in a wavy stream. In T. Y. T. Wu, C. J. Brokaw, and C. Brennan, editors, *Proceedings of the symposium on swimming and flying in nature*, pages 687–702, New York, 1974. Plenum Press.